Redox Regulation of *Plasmodium falciparum* Methionine Adenosyltransferase and *Mycetinis scorodonius* DyP-type Peroxidase 1

A dissertation submitted to the
Faculty of Biology and Chemistry of
Justus Liebig University Giessen

in fulfillment of the requirements for a
Doctor of Natural Sciences (Dr. rer. nat.)
by

Jette Pretzel
born in Malchin

July 2016

This dissertation was prepared at the Interdisciplinary Research Center of Justus Liebig University Giessen, at the Chair of Biochemistry and Molecular Biology, under the supervision of Prof. Dr. med. Katja Becker.

1st supervisor and member of the reading committee:

Prof. Dr. Katja Becker, Biochemistry and Molecular Biology, Interdisciplinary Research Center, Justus Liebig University Giessen, Heinrich-Buff-Ring 26-32, 35392 Giessen

2nd supervisor and member of the reading committee:

Prof. Dr. Gabriele Klug, Microbiology and Molecular Biology, Interdisciplinary Research Center, Justus Liebig University Giessen, Heinrich-Buff-Ring 26-32, 35392 Giessen

Further members of the reading committee:

Prof. Dr. Christoph Grevelding, Department of Parasitology, Biomedical Research Center Seltersberg, Justus Liebig University Giessen, Schubertstrasse 81, 35392 Giessen

Prof. Dr. Michael Kracht, Rudolf Buchheim Institute of Pharmacology, Biomedical Research Center Seltersberg, Justus Liebig University Giessen, Schubertstrasse 81, 35392 Giessen

“Now, a living organism is nothing but a wonderful machine
endowed with the most marvellous properties
and set going by means of the most complex and delicate mechanism.”

(Bernard, 1865)

DECLARATION

I declare that this dissertation is my original work and sources of information have been properly quoted. This work has not been previously presented to obtain any other degree from any other university.

EIDESSTATTLICHE ERKLÄRUNG

Ich erkläre, ich habe diese vorgelegte Dissertation selbständig und ohne unerlaubte Hilfe und nur mit den angegebenen Hilfen angefertigt. Alle Textstellen, die wörtlich oder sinngemäß aus veröffentlichten Schriften entnommen sind, und alle Angaben, die auf mündlichen Auskünften beruhen, sind als solche kenntlich gemacht. Experimente die für mich und für diese Dissertation von anderen Personen als mir selbst durchgeführt wurden, wie z. B. in von mir mitbetreuten Masterarbeiten, sind als solche gekennzeichnet. Bei den von mir durchgeführten und in der Dissertation erwähnten Untersuchungen habe ich die Grundsätze guter wissenschaftlicher Praxis, wie sie in der ”Satzung der Justus-Liebig-Universität Gießen zur Sicherung guter wissenschaftlicher Praxis” niedergelegt sind, eingehalten.

Giessen, July 2016

_____

Jette Pretzel

ACKNOWLEDGEMENTS

This dissertation would not have been possible without the help of many people in many ways.

I am hugely indebted to my supervisor **Prof. Dr. Katja Becker** for trusting me with these projects and for giving me the opportunity to prepare this dissertation in her group. I am grateful to your professional guidance, support, and motivation and for the respectful, friendly and warm working atmosphere that you maintain in our group. Thank you for encouraging me to follow up my professional career in science and for sharing your passion for science with me. Thank you for giving me an insight into the 'hidden' politics behind the wheels of science and academics and for sharing your experiences with me. It was an honor and a great pleasure for me to work with you.

I am grateful to my second supervisor, **Prof. Dr. Gabriele Klug**, for her interest in my topic and for helpful discussions and hints during my dissertation, especially during planning and realization of antimicrobial susceptibility tests of my recombinant antimicrobial peptides and for kindly providing bacterial strains.

I am thankful to **Prof. Dr. Holger Zorn** for providing rMscDyP1 produced in *A. niger* and especially for initiation of our cooperation project regarding the crystallization of MscDyP1, his patience and trust. Likewise, I wish to thank **Katharina Schmidt** from the Zorn lab for lending me her experience with the ABTS and carotene assay.

I wish to express my sincere gratitude to **Dr. Esther Jortzik.** Thank you for your humanity, your patience, your positive thinking and always helpful comments, hints and discussions in scientific and personal issues during the last five years since the start of my master thesis to the beginning and completion of my dissertation. I am grateful to **Dr. Karin Fritz-Wolf**, our crystallographer, for solving the crystal structure of MscDyP1, on which the second part of this dissertation is based, and for kindly providing the PDB file of crystal D for this dissertation. I am especially thankful for many helpful critical discussions. I am thankful to **Christina Brandstädter**, who was not only a colleague but became a good friend. I really enjoyed the time with you together in the lab, our four-hour walks through the nature, sitting at the Lahn River having a beer and analyzing the world, watching classical must-have-seen movies or just our daily chai at Coffee Bay before work. Thank you for your friendship. I wish to thank **Marina Fischer** for patient advices and hints whenever an assay caused problems. I always enjoyed working at the Beckman photometer next to you working at the Hitachi, and guiding the practical courses together with you. Furthermore, I wish to thank **Dr. Jochen Bathke** (the Sheldon among us Pennys), with whom I started my dissertation in March 2011 and spent several hours having long scientific discussions, and who always nicely decorated the labs and our shared office with his cheering up "Handschuh-Fanten". Many thanks to **Dr. Stefan Rahlfs** who had always an idea and a matching story about how to solve any kind of problem, not only in the field of molecular biology. I wish to thank **Michaela Stumpf** for her always patient mind and her excellent technical assistance and support with the crystallization experiments. You are able to bring the necessary calm and peace into the lab. Your organizing talent is amazing. I thank **Melissa Schmidt** our technical assistant with an outstanding engagement and always helping hand in the lab. I am thankful to

my Bachelor student **Mirjam Kratzer** and my Master students **Irina Rotfuss** and **Marina Gehr**, whose scientific results and excellent dedication in the lab contributed significantly to the ongoing of this dissertation. Many thanks to **Elisabeth Fischer** for introducing me into the basic techniques and maintenance of *Plasmodium falciparum* blood-stage cell culture. I never met someone as spiritual and as reflective as you. I really enjoyed the time together with you in cell culture. I wish to thank **Franziska Mohring** for her cooperation within the projects we worked on together, the analysis of the *Anopheles* and *Galleria* peptidome. We successfully completed our projects expediently in teamwork. I am thankful to **Dr. Lihui Wang** for his support and helpful hints for the biotin switch assay and other nitrosylation experiments for PfalMAT. Many thanks to **Dr. Rimma Iozef** for her help in cloning of the (*E. coli*) rMscDyP1 methionine double mutant. I wish to thank **Timothy Bostick** for his careful proof reading of all of my posters and manuscripts. I also thank all the other current and former members of the Becker lab who at some point supported me with my dissertation: **Mahsa**, **Siegrid**, **Christina**, **Kristina**, **Katharina**, **Beate**, **Helena**, **Uli**, and **Sina**.

Furthermore, I wish to thank all the people who were involved in other projects of my dissertation and are not included here: I wish to thank **Dr. Stephanie Blandin** and **Marie Staub**, and all other members of the Anopheles group in Strasbourg for hosting me in their insectary for five weeks in order to isolate the hemolymph of *Anopheles* mosquitos. Thank you for cultivating the thousands of mosquitos that I needed. Thank you for your kindness and openness. I really enjoyed my stays in your lab and the time spent in the fromagerie together with you. I thank **Dr. Gabriele Pradel** and **Che Julius Ngwa** from the Research Center for Infectious Diseases Wuerzburg for hosting me and Franziska in their insectary in order to learn how to isolate the hemolymph from *Anopheles* mosquitos. It was a very exciting experience to work in your S3 lab wearing a whole body protection suit and being, even if only a bit but nevertheless, thrilled. I am thankful for this unforgettable opportunity. Many thanks to **Dr. Jochen Wiesner**, **Anne Pöppel**, **Dr. Krishnendu Mukherjee**, and **Prof. Dr. Andreas Vilcinskas** from the Fraunhofer Institute of Molecular Biology and Applied Ecology for teaching me and Franziska how to cultivate and isolate hemolymph of *Galleria mellonell*a larvae and for purifying one of my recombinant antimicrobial peptides using cation exchange chromatography. I'd like to thank **Dr. Johannes Strauss** and **Prof. Dr. Reinhard Lakes-Harlan** for kindly providing me the possibility to collect and sex *Drosophila melanogaster* flies in their lab for one of my projects. I thank **Anne Gries** and **Prof. Dr. Peter Mayser** from the Clinic of Dermatology, University Clinic of Giessen-Marburg for the possibility to test the susceptibility of human pathogenic dermatophytes to my recombinant antimicrobial peptides. I thank **Dr. Stefanie Gläser** and **Prof. Dr. Peter Kämpfer** of the Department of Microbiology of Recycling Processes for providing bacterial strains for antimicrobial susceptibility tests of my recombinant antimicrobial peptides. I wish to thank **Dr. Ann-Kristin Müller** from the Department of Infectious Diseases, Parasitology Unit 3, Heidelberg and **Mirjam Ester** and **Dr. Friedrich Frischknecht** from the Department of Infectious Diseases, Parasitology Unit 2, Heidelberg, for dissecting and providing mouse livers for one of my side projects. I thank **Saleh M. Khalil**, **Dr. Andreas Römpp** and **Prof. Dr. Bernhard Spengler** for their cooperation within our imaging mass spectrometry projects and joint publications.

I want to thank **Dr. Oliver Koch**, Medicinal Chemistry Group, Faculty of Chemical Biology at TU Dortmund University for giving me time to finish writing my dissertation while holding a post-doc position in his lab and for providing access to MOE 2013 and Gold 5.2 software.
This dissertation was partly funded by the **LOEWE Research Focus "Insect Biotechnology**."
Last but not least, I wish to express my deepest gratitude to my beloved **family** and my best friend **Steffi** for their continuous support, patience, and understanding during the past years.

SUMMARY

Changes in the redox state of protein cysteines in response to dynamic alterations of the cellular redox state modulate the activity and structure of proteins. Therefore, several vital cellular processes are redox regulated, including nitric oxide production, apoptosis, immune response, and signaling processes. The aim of this dissertation was to characterize in detail the redox regulation of two interesting target proteins: methionine adenosyltransferase of the malaria parasite *Plasmodium falciparum* (PfalMAT) and the dye-decolorizing peroxidase 1 of the fungus *Mycetinis scorodonius* (MscDyP1).

PfalMAT is an attractive drug target since its product, S-adenosylmethionine, is the major biochemical methyl group donor and a precursor for crucial downstream pathways such as polyamine metabolism and DNA methylation. However, PfalMAT has so far been poorly characterized. This dissertation provides a detailed kinetic analysis, including inhibitor and oligomerization studies to expand the biochemical characterization of this enzyme. Furthermore, the dimeric human homolog hMATIII was characterized here using the same assay system to allow a direct comparison of both enzymes. Previous pull-down experiments identified PfalMAT as a target of the plasmodial redoxins thioredoxin 1, glutaredoxin, and plasmoredoxin and as part of the *S*-glutathionylome and *S*-nitrosylome of *P. falciparum*. A second aim of this dissertation was to characterize the interplay of PfalMAT with the plasmodial redoxins and study in detail the impact of *S*-glutathionylation and *S*-nitrosylation. In order to identify potential sites of these redox modifications in PfalMAT, a homology model was created since a crystal structure was not yet available. This model indicated that among the eight cysteines of PfalMAT, only Cys52, Cys113, and Cys187 were solvent accessible in the dimeric enzyme. Hence, these cysteines were conservatively mutated via site-directed mutagenesis into serines, and their kinetic and oligomerization behaviors were studied using a spectrophotometric assay and gel filtration experiments, respectively. As indicated before, PfalMAT activity was indeed affected by redox regulatory processes; reduction of cysteines by the reducing agent dithiothreitol and reduced glutathione activated PfalMAT, whereas enzyme inhibition followed oxidative events, i.e. *S*-glutathionylation and *S*-nitrosylation. Consequently, the impact of the selected cysteines on these redox regulatory processes was studied, showing that thioredoxin 1 and plasmoredoxin potently activated PfalMAT at subcellular concentrations by changing the oxidation state of Cys52, Cys113, and Cys187, whereas glutaredoxin did not alter PfalMAT activity. Protein-*S*-glutathionylation inhibited PfalMAT through the specific formation of mixed disulfides between glutathione and Cys113, which was indicated with Western blots using an anti-GSH antibody and less inhibition of the respective mutant upon GSSG treatment compared to the wildtype. Protein-S-glutathionylation of PfalMAT was reversible by thioredoxin 1 and plasmoredoxin, which restored the activity of PfalMAT at physiological concentrations, suggesting a likely *in vivo* regulation. Furthermore, PfalMAT was inhibited upon *S*-nitrosylation under NO-stress, which was mediated by several cysteines, including Cys52, Cys113, and Cys187. These results indicate a coupling of the *S*-adenosylmethionine status to the cellular redox state of *P. falciparum* via redox regulation of PfalMAT.

The second enzyme on which this dissertation focussed, is MscDyP1. This dye-decolorizing peroxidase (DypPrx) is a member of the recently identified eponymous novel class of heme peroxidases, which differ structurally from classic heme peroxidases. They possess remarkably high substrate versatility and are therefore of great interest to environmental biotechnology and the food industry. Interestingly, MscDyP1 is, according to current knowledge, the only DypPrx capable of degrading carotenoids, for which it has been previously patented and is currently beeing used industrially to bleach whey.

During this dissertation, upon systematic screening and optimization of different crystallization conditions, high resolution protein crystals of MscDyP1 were obtained, which made it possible to solve its three-dimensional structure. This structure revealed interesting features. Two surface-exposed methionine residues, Met302 and Met305, which are not conserved among DypPrx, appeared to play an important structural role. Furthermore, several substrate oxidation sites, despite the active site of MscDyP1, were identified, including a second heme accession channel and a cavity around the single conserved cysteine residue Cys360 at the proximal heme site. Although the conservation of Cys360 indicates it has an important role, it has not yet been investigated. The crystal structure indicated that it is accessible to small redox-active molecules and therefore might present a target of redox-regulatory processes. In order to study the role of Met302, Met305, and Cys360 for catalysis and their structural functionality, site-directed mutagenesis was performed, and both the wildtype and the mutants were heterologously overexpressed in *E. coli*. Their activity and kinetic behavior were studied in two assay systems, using either ABTS as an electron donor or β-carotene. Both mutants, the double mutant lacking the selected methionine residues and the protein variant lacking Cys360, displayed significantly decreased activity compared to the wildtype produced in *E. coli*. Furthermore, the cysteine deletion mutant showed decreased affinity to hydrogen peroxide. Moreover, the mutants appeared to be less susceptible to suicide inactivation caused by excess amounts of hydrogen peroxide. These results confirmed the important structural role of the methionines and suggested that Cys360 participates in the regulation of MscDyP1 via redox processes. Nevertheless, the native enzyme and the one used for crystallization, a recombinant MscDyP1 overexpressed in *A. niger*, are highly glycosylated, in contrast to the recombinant enzyme produced in *E. coli*, which was not glycosylated. Moreover, previous biochemical characterizations of the native enzyme indicated that MscDyP1 is a dimer, and the crystal structure pointed out that glycosylation relevantly contributes to dimerization. Therefore, the recombinant enzyme produced in *A. niger* was treated with the thiol-blocking agents methylmethanethiosulfonate and iodoacetamide to block all solvent-accessible, sulfur-containing amino acids. Whereas (*E. coli*) rMscDyP1 was inhibited by 40% following this treatment, the activity of (*A. niger*) rMscDyP1 was not affected. This indicated that glycosylation protected these redox-sensitive residues and suggested that in the native highly glycosylated MscDyP1, contrary to the findings for PfalMAT, Cys360 appears to have a structural rather than catalytic or regulatory function.

ZUSAMMENFASSUNG

Veränderungen des zellulären Redoxmillieus gehen mit Änderungen des Redoxstatus von Cysteinen zellulärer Proteine einher. Dies hat Auswirkungen auf ihre Aktivität und Struktur. Die Redoxregulation von Proteinen spielt deshalb eine wichtige Rolle in vielen lebenswichtigen zellulären Prozessen, wie Apoptose, Signaltransduktion oder Immunreaktionen. Im Fokus dieser Dissertation stand die Untersuchung der Redoxregulation von zwei unterschiedlichen, jedoch sehr interessanten Zielproteinen: Der Methioninadenosyltransferase des Malariaparasiten *Plasmodium falciparum* (PfalMAT) und der DyP-Peroxidase 1 (Dye-decolorizing) des Basidiomyceten *Mycetinis scorodonius* (MscDyP1).

PfalMAT stellt ein attraktives Ziel für die Medikamentenentwicklung dar. Aufgrund seiner hohen Wachstums- und Teilungsrate, ist der Malariaparasit in besonderem Maße abhängig von der *S*-Adenosylmethioninproduktion, da dieses, als wichtigster Methylgruppendonor der Zelle, eine Vorstufe für lebenswichtige Stoffwechselwege und zelluläre Prozesse, wie den Polyaminstoffwechsel und die DNA-Methylierung, darstellt. Das *S*-Adenosylmethionin-synthetisierende Enzym, PfalMAT, ist bisher nur unzureichend untersucht. Die vorliegende Dissertation erweitert das biochemische Verständnis für dieses Enzym durch detaillierte kinetische Analysen und Inhibitorstudien. Darüber hinaus wurde PfalMAT mit dem dimeren humanen Homolog hMATIII verglichen, welches dazu ebenfalls heterolog in *E. coli* exprimiert und im gleichen Assaysystem wie PfalMAT charakterisiert wurde. Bereits im Vorfeld dieser Dissertation lagen durch Pull-down-Experimente Hinweise auf eine mögliche Redoxregulation des Enzyms vor: PfalMAT stellte sich als Substrat der redoxaktiven Proteine Thioredoxin, Glutaredoxin und Plasmoredoxin heraus und wurde als Bestandteil des *S*-Glutathionylom und *S*-Nitrosylom von *P. falciparum* identifiziert. Deshalb war ein weiteres Ziel dieser Dissertation, die Interaktion der plasmodialen Redoxine mit PfalMAT sowie den Einfluss der genannten posttranslationalen Modifikationen im Hinblick auf Aktivität und Konformation zu charakterisieren. Um die redox-modifizierbaren Thiole zu identifizieren wurde ein Homologiemodell von PfalMAT erstellt, da bisher noch keine Kristallstruktur veröffentlicht wurde. Dieses Model ließ vermuten, dass von den acht Cysteinen von PfalMAT nur Cys52, Cys113 und Cys187 in der dimeren Konformation des Enzyms für redox-aktive Moleküle zugänglich sind. Darum wurden diese Cysteine durch gerichtete Mutagenese zu Serinen mutiert. Die entsprechenden Mutanten wurden mit Hilfe eines spektrophotometrischen Assays kinetisch charakterisiert und ihre Oligomerisierung wurde in Gelfiltrationsexperimenten untersucht. PfalMAT wurde redoxreguliert, dabei führten Reduktion durch Glutathion und Reduktionsmittel, wie Dithiothreitol, zur Aktivierung und Oxidationsvorgänge, wie *S*-Glutathionylierung und *S*-Nitrosylierung zur Inhibierung von PfalMAT. Auf diese Beobachtung hin wurde der Einfluss der selektierten Cysteine auf diese Prozesse untersucht. Subzelluläre Konzentrationen an Thioredoxin 1 und Plasmoredoxin erhöhten die enzymatische Aktivität von PfalMAT, ein Effekt, der auf eine Reduktion der drei genannten Cysteine zurückgeführt werden konnte. Protein-*S*-Glutathionylierung inhibierte PfalMAT durch die spezifische Bildung eines gemischten Disulfids zwischen Glutathion und Cys113, wobei die *S*-Glutathionylierung durch den Zusatz von Thioredoxin 1 und Plasmoredoxin in physiologischen Konzentrationen vollständig reversibel war. Dies lässt eine

Regulation von PfalMAT durch die beiden redoxaktiven Proteine auch *in vivo* vermuten. Auch die *S*-Nitrosylierung inhibierte PfalMAT, wurde jedoch durch die Modifikation mehrerer Cysteine, einschließlich Cys52, Cys113 und Cys187, vermittelt. Diese Ergebnisse deuten auf eine Kopplung des *S*-Adenosylmethioninspiegels an den zellulären Redoxstatus von *P. falciparum* hin, die über die Redoxregulation von PfalMAT vermittelt wird.

Das zweite Enzym, das im Fokus dieser Dissertation stand, war MscDyP1. Diese DyP-type Peroxidase zählt zu einer erst kürzlich entdeckten Klasse von Hämperoxidasen, die sich strukturell und katalytisch stark von den klassischen Hämperoxidasen unterscheidet. Im Rahmen dieser Dissertation konnten durch ein systematisches Screening von Kristallisationsbedingungen Proteinkristalle von MscDyP1 mit einer hohen Auflösung generiert werden. Diese ermöglichten die Auflösung der dreidimensionalen Struktur des Enzyms, die interessante strukturelle Besonderheiten offenbarte. Auffällig waren zwei nicht-konservierte oberflächenexponierte Methionine (Met302 und Met305), die eine wichtige strukturelle Rolle zu spielen schienen. Außerdem wurden neben dem aktiven Zentrum von MscDyP1 zwei weitere mögliche Stellen für die Substratoxidation identifiziert: ein zweiter Zugangskanal zum Hämzentralatom und eine Höhle, die das einzige und konservierte Cystein (Cys360) umschließt. Obwohl die Konservierung von Cys360 eine wichtige Bedeutung für das Protein vermuten lässt, wurde es zuvor noch nicht untersucht. Die Kristallstruktur deutet darauf hin, dass Cys360 für kleinere redoxaktive Moleküle zugänglich ist und es deshalb Redoxmodifikationen unterliegen könnte. Um eine mögliche katalytische oder funktionelle Rolle der beiden Methionine und des Cysteins zu untersuchen, wurden diese mutiert und die entsprechenden Mutanten sowie der Wildtyp in *E. coli* überexprimiert und in zwei Assaysystemen kinetisch charakterisiert. Beide Mutanten, die Doppelmutante ohne Met302 und Met305 sowie die Cysteindeletionsmutante, zeigten eine signifikant verringerte spezifische Aktivität im Vergleich zum in *E.coli* rekombinant erzeugten Wildtyp. Des Weiteren hatte die Cysteindeletionsmutante eine geringere Affinität zu Wasserstoffperoxid. Darüber hinaus schienen beide Mutanten weniger anfällig gegenüber der unter Hämperoxidasen häufig beobachteten Inhibierung durch hohe Wasserstoffperoxid-konzentrationen zu sein. Diese Ergebnisse bestätigten die strukturelle Bedeutung der beiden Methionine und ließen eine Redoxregulation von MscDyP1 über Cys360 vermuten. Im Gegensatz zum in *E. coli* rekombinant hergestellten Enzym, das nicht glykosyliert ist, sind das native Enzym sowie das für die Kristallisationsexperimente genutzte in *Aspergillus niger* rekombinant hergestellte Enzym stark glykosyliert. Außerdem wurde durch eine biochemische Charakterisierung des nativen Enzyms im Vorfeld gezeigt, dass MscDyP1 als Dimer vorliegt. Die Kristallstruktur deutet auf eine entscheidende Rolle der Glykosylreste bei der Dimerisierung des Enzmys hin. Das in *A. niger* rekombinant hergestellte MscDyP1 wurde aus diesem Grund mit den thiolblockierenden Agentien Methylmethanthiosulfonat und Iodoazetamid behandelt, um alle lösungsmittelzugänglichen schwefelhaltigen Aminosäuren zu blockieren. Während die Aktivität des in *E. coli* hergestellten Enzyms um 40% sank, variierte die Aktivität des in *A. niger* produzierten Enzyms nicht. Dies lässt den Schluss zu, dass die Glykosylierung vermutlich die redoxsensitiven Reste schützt und dass im nativen stark glykosylierten Enzym, im Gegensatz zu den Beobachtungen der PfalMAT, Cys360 eher eine strukturelle als eine katalytische oder regulatorische Funktion einnimmt.

PUBLICATIONS

Peer-reviewed research articles

Pretzel J., Gehr M., Eisenkolb M., Wang L., Fritz-Wolf K., Rahlfs S., Becker K., Jortzik E.: Characterization and redox regulation of *Plasmodium falciparum* methionine adenosyltransferase. J Biochem accepted 14th June 2016

Khalil S. M., Pömpp A., **Pretzel J**., Becker K., Spengler B. (2015): Phospholipid Topography of Whole-Body Sections of *Anopheles stephensi* Mosquito, Characterized by High-Resolution Atmospheric-Pressure Scanning Microprobe Matrix-Assisted Laser Desorption/Ionization Mass Spectrometry Imaging. Anal Chem 87(22):11309-11316

Koch O., Jäger T., Heller K., Khandavalli P., **Pretzel J.**, Becker K., Flohé L., Selzer P. M. (2013): Identification of *M. tuberculosis* thioredoxin reductase inhibitors based on high-throughput docking using constraints. J Med Chem 56(12):4849-4859

Peer-reviewed review articles

Mohring F.*, **Pretzel J.***, Jortzik E., Becker K. (2014): The redox systems of *Plasmodium falciparum* and *Plasmodium vivax*: comparison, *in silico* analysis and inhibitor studies. Curr Med Chem 21(15):1728-1756

Pretzel J.*, Mohring F.*, Rahlfs S., Becker K. (2013): Antiparasitic peptides. Adv Biochem Eng Biotechnol 135:157-192

***shared co-authorship**

Manuscripts in preparation

Fritz-Wolf K.*, **Pretzel J.***, Schmidt K., Szweda R., Stumpf M., Rahlfs S., Zorn H., Becker K.: Crystal structure of *Mycetinis scorodonius* DyP-type peroxidase 1. (In preparation)

Pretzel J.*, Mohring F.*, Prieto Judith H., Wiesner J., Kollewe C., Vilcinskas A., Koncarevic S., Rahlfs S., Becker K.: Relative quantification, recombinant production and functional analysis of *Galleria mellonella* antimicrobial peptides. (In preparation)

Mohring F.*, **Pretzel J.*,** Prieto H., Koncarevic S., Becker K.: Quantification of *Anopheles* immune response peptides in response to *Plasmodium berghei* infection. (In preparation)

Khalil S. M., **Pretzel J.**, Pömpp A., Becker K., Spengler B.: Spatial distribution of lipids and pheromones in *Drosophila melanogaster* analyzed by AP-SMALDI imaging mass spectrometry. (In preparation)

Khalil S. M., Pömpp A., **Pretzel J.**, Becker K., Spengler B.: Mass spectrometry imaging for characterizing parasite host cell interactions in malaria research. (In preparation)

CONFERENCE CONTRIBUTIONS

Pretzel J., Fritz-Wolf K., Schmidt K, Szweda R., Stumpf M., Rahlfs S., Jortzik E., Zorn H., Becker K.: Crystal structure of *Mycetinis scorodonius* DyP-type peroxidase 1. Gordon Research Conference on Thiol-based Redox Regulation and Signaling, Girona, 2014, Poster

Pretzel J., Mohring F., Prieto H., Wiesner J., Kollewe C., Vilcinskas A., Koncarevic S., Rahlfs S., Becker K.: Relative quantification, recombinant production and functional analysis of *Galleria mellonella* antimicrobial peptides. 14th Drug Design and Development Seminar, Würzburg, 2013, Presented by Mohring F., Talk

Pretzel J., Rahlfs S., Mohring F., Vilcinskas A., Becker K.: Defense against pathogens–nature shows how: Insects as sources of novel chemotherapeutic compounds. 6th Annual Conference of the Giessen Graduate School for the Life Sciences. Giessen, 2013, Poster

Pretzel J., Fritz-Wolf K., Schmidt K., Szweda R., Stumpf M., Rahlfs Stefan, Zorn H., Becker K.: Crystallization and mutagenesis of *Mycetinis scorodonius* peroxidase-1. 5th Annual Conference of the Giessen Graduate School for the Life Sciences. Giessen, 2012, Poster

Pretzel J., Jortzik E., Becker K.: Redox regulation of *S*-adenosylmethionine synthetase of *Plasmodium falciparum*. 4th Annual Conference of the Giessen Graduate School for the Life Sciences. Giessen, 2011, Poster

TABLE OF CONTENTS

TABLES

FIGURES

ABBREVIATIONS

Å	ångström
A_x	absorption at x nm
AauDyP	*Auricularia auricula-judae* Dye-decolorizing peroxidase
ABTS	2,2'-azino-bis(3-ethylbenzothiazoline-6-sulphonic acid
AdoMet	*S*-adenosylmethionine
AdoMetDC	*S*-adenosylmethionine decarboxylase
APS	ammonium persulfate
ATP	adenosine triphosphate
bp	base pair
BadDyP	*Bjerkandera adusta* Dye-decolorizing peroxidase
BCR	β-carotene
BMA	β-D-mannose
BSA	bovine serum albumin
CAT	catalase
CBS	cystathionine-β-synthase
CHP	cumene hydroperoxide
cMAT	*E. coli* methionine adenosyltransferase
chMAT	*Cryptosporidium hominis* methionine adenosyltransferase
dcSAM	decarboxylated *S*-adenosylmethionine
DMSO	dimethyl sulfoxide
DNA	deoxyribonucleic acid
DNase	deoxyribonuclease
dNTP	deoxyribonucleotide triphosphate
DTNB	5,5‘-dithio-bis-(-2-nitrobenzoeic acid)
DTT	1,4-dithiothreitol
DyP	dye-decolorizing peroxidase
DypPrx	dye-decolorizing peroxidase
ε	absorption coefficient
E. coli	*Escherichia coli*
EDTA	ethylenediaminetetraacetic acid
EglDyP	*Exidia glandulosa* dye-decolorizing peroxidase
FAD	flavine adenine dinucleotide
FPLC	fast protein liquid chromatography
G6PDH	glucose-6-phosphate dehydrogenase
Glp	thioredoxin-dependent gluredoxin-like protein
GPx	glutathione peroxidase
GR	glutathione reductase
Grx	glutaredoxin
GSH	glutathione
GSNO	nitrosoglutathione
GSSG	glutathione disulfide
GST	glutathione-*S*-transferase

H_2O_2	hydrogen peroxide
hMAT	human methionine adenosyltransferase
HRP	horse radish peroxidase
IAA	iodoacetamide
IC_{50}	half maximal inhibitory concentration
iNOS	inducible nitric oxide synthase
IPTG	isopropyl-β-D-thiogalactopyranoside
kDa	kilodalton
k_{cat}	turnover number
K_i	inhibitory constant
K_M	Michaelis constant
LB	lysogeny broth medium
LRET	long-range electron transfer
MAT	methionine adenosyltransferase
MepDyP	*Mycena epipterygia* dye-decolorizing peroxidase
MMTS	methyl methanethiosulfonate
Msr	methionine sulfoxide reductase
MS	Methionine synthase
Msc	*Mycetinis scorodonius*
MscDyP1	*Mycetinis scorodonius* DyP-type peroxidase 1
MTA	5'-methylthioadenosine
NaAsc	sodium ascorbate
NADPH	nicotinamide adenine dinucleotide phosphate
NAG	N-acetyl glucosamine
NEM	N-ethylmaleimide
Ni-NTA	nickel nitrilotriacetic acid
NO	nitric oxide
NOS	nitric oxide synthase
OD	optical density
ODC	ornithine decarboxylase
PCR	polymerase chain reaction
PEG	polyethylene glycol
Pf	*Plasmodium falciparum*
Pfal	*Plasmodium falciparum*
PfalMAT	*Plasmodium falciparum* methionine adenosyltransferase
P_i	inorganic phosphate
PLP	piecewise linear potential fitnessfunction
Plrx	plasmoredoxin
PMSF	phenylmethylsulfonylfluoride
PP_i	pyrophosphate
PPP_i	tripolyphosphate
Prx	peroxiredoxin
PTM	post-translational modification
PVDF	polyvinyl difluoride

rlMAT	rat liver methionine adenosyltransferase
RNS	reactive nitrogen species
ROS	reactive oxygen species
RZ	Reinheitszahl value
SAH	*S*-adenosyl-homocysteine
SAHH	*S*-adenosyl-homocysteine hydrolase
SAM	*S*-adenosylmethionine
SAMS	*S*-adenosylmethionine synthetase
SDS	sodium dodecyl sulfate
SDS-PAGE	sodium dodecyl sulfate-polyacrylamide gel electrophoresis
SH	thiol
SOD	superoxide dismutase
TB	terrific broth medium
tBOOH	tert-bytyl hydroperoxide
TEMED	N,N,N',N'-tetramethylethylenediamine
Tris	tris-(hydroxymethyl)-aminomethane
Trx	thioredoxin
TrxR	thioredoxin reductase
U	international unit (µmol*min^{-1})
Vmax	maximal reaction velocity
3MD	2,6-dimethoxyphenol

Abbreviations of amino acids

amino acid	**3 letter code**	**1 letter code**
alanine	Ala	A
arginine	Arg	R
asparagine	Asn	N
aspartic acid	Asp	D
cysteine	Cys	C
glutamic acid	Glu	E
glutamine	Gln	Q
glycine	Gly	G
histidine	His	H
isoleucine	Ile	I
leucine	Leu	L
lysine	Lys	K
methionine	Met	M
phenylalanine	Phe	F
proline	Pro	P
serine	Ser	S
threonine	Thr	T
tryptophan	Trp	W
tyrosine	Tyr	Y
valine	Val	V

Abbreviations of nucleotides

nucleotide	**abbreviation**
adenine	A
thymine	T
cytosine	C
guanine	G
uracil	U

1 INTRODUCTION

The development of living organisms required the presence of oxygen, and most organisms rely on it. But to live in an aerobic environment under oxidative conditions also means they must combat oxygen-derived radicals, which requires a fine, tight, and complex regulation of processes involved in maintaining the cellular redox state.

1.1 Redox regulation

The cellular redox state, which depends on the level of oxidants and antioxidants, affects proteins and lipids and thereby regulates cellular processes and functions. A number of vital physiological processes are redox regulated, including nitric oxide (NO) production, vascular tone, cell adhesion, apoptosis, immune responses, and signaling processes (reviewed in Valko *et al.*, 2007).

1.1.1 Oxidative stress and radicals in cell metabolism

Oxidative stress is a condition of imbalance in the cellular redox homeostasis due to a deficient antioxidant defense and/or an excessive overproduction of reactive oxygen and/or nitrogen species (ROS and RNS) (Finkel *et al.*, 2000), which leads to decreased cellular glutathione and NADPH levels (Lewis, 2002).
The cell is confronted with approximately 1.5 x 10^5 oxidative adducts per day (Nakajima *et al.*, 1996; Beckman *et al.*, 1997), generated endogenously under basal physiological conditions as byproducts during cellular metabolism or derived from exogenous sources. The main sources of intracellular ROS are complex I (NADH:ubiquinone oxidoreductase) and complex III (ubiquinone-cytochrome c reductase) of the mitochondrial electron transport chain during oxidative phosphorylation in aerobic energy metabolism (Turrens *et al.*, 1980; Turrens *et al.*, 1985; Lewis, 2002). Peroxisomal enzymes, e.g. acyl-CoA oxidases, xanthine oxidase, polyamine oxidase, or inducible nitric oxide synthase (iNOS), generate ROS and RNS during their catalytic activity (Fransen *et al.*, 2012). Cytochrome P_{450} enzyme systems required for cellular detoxification contribute to ROS formation (Ekstrom *et al.*, 1989). Additionally, the immune system is a site of excessive ROS formation, especially during the oxidative burst, catalyzed by NADPH oxidase in macrophages and neutrophil granulocytes during phagocytosis. Exogenous sources such as irradiation by UV light, x-rays and gamma-rays, thermal stress, drugs (e.g. cyclosporine (Mun *et al.*, 2008) or gentamicin (Martinez-Salgado *et al.*, 2002)), environmental toxins (e.g. alcohol or cigarette smoke), or metal-catalyzed reactions (e.g. by iron, arsenic, copper, cobalt or vanadium) during Fenton reaction (Finkel *et al.*, 2000; Valko *et al.*, 2006; Pham-Huy *et al.*, 2008) contribute to the formation of oxidative or nitrosative agents that the cell has to cope with.
Redox homeostasis is maintained by enzymatic and non-enzymatic antioxidant systems. Enzymatic antioxidant defense is mediated mainly by superoxide dismutase (SOD), catalase (CAT), glutathione peroxidase (GPx), and peroxiredoxins. Furthermore, a number of non-enzymatic, low molecular weight molecules such as glutathione (GSH), ascorbate, pyruvate, flavonoids, and carotenoids contribute to intracellular ROS detoxification (Finkel *et al.*,

2000). Under physiological conditions at low and moderate cellular levels, ROS and RNS play a central role in cell growth, signaling processes, metabolism, and cell cycle regulation. A reducing cellular environment stimulates cell proliferation, whereas a more oxidizing cellular environment stimulates cell differentiation (reviewed in Valko *et al.*, 2007). An imbalance in the cellular redox state towards either too low or too high ROS or RNS levels impairs physiological processes. Numerous diseases are linked to oxidative or nitrosative stress, including cardiovascular diseases, diabetes, neurological disorders, age-related diseases, and cancer (reviewed in Dalle-Donne *et al.*, 2006; Valko *et al.*, 2007), due to oxidative damage of DNA (Ayala *et al.*, 2014), e.g. deamination and nitration of purines (Dalle-Donne *et al.*, 2006), and oxidation of proteins, altering their biological properties. Additionally, lipid peroxidation affects biological membranes by modifying fluidity, cell permeability, and membrane-associated receptors (Stocker *et al.*, 2004; Dalle-Donne *et al.*, 2006).

1.1.2 Oxidative protein modifications

Proteins are particularly sensitive to oxidative modifications in response to alterations of the cellular redox state. Cysteine, methionine, tryptophan, tyrosine, and histidine are the most susceptible amino acids (reviewed in Valderrama *et al.*, 2002).

2.3.2.1 Methionine oxidation and reduction in protein redox regulation

Although methionine residues can be oxidized, the reaction is slower compared to cysteine oxidation and is rapidly reversed by methionine sulfoxide reductases (MrsA and MrsB) (Wani *et al.*, 2014). Therefore, methionine oxidation plays a minor role under physiological conditions, e.g. in cellular redox signaling. However, research focused on the role of methionine oxidation in signaling is increasing. Due to their close proximity to serine, tyrosine, and threonine residues, three known protein phosphorylation sites, a possible role for methionine residues in phosphorylation-mediated signaling is suggested (Czernik *et al.*, 1987; Rao *et al.*, 2013). Methionine oxidation and reduction has been suggested to present a possible mechanism to regulate protein function because the site chain of methionine is flexible and non-polar, whereas the one in methionine sulfoxide is stiffer and more polar (Hoshi *et al.*, 2001). Therefore, methionine oxidation can change the physical and chemical properties of proteins, which might lead to dysfunctional proteins or contribute to the regulation of cell function (Hoshi *et al.*, 2001). Reversible methionine oxidation to methionine sulfoxide (MetO) is suggested to exert a scavenger function to protect other amino acids from irreversible overoxidation in order to maintain protein functionality, similar to cysteine redox modifications. Therefore, methionines can act as antioxidants, protecting proteins under conditions of oxidative stress (reviewed in Rao *et al.*, 2015). However, overoxidation by excess ROS leads to irreversible formation of methionine sulfone ($MetO_2$), which can irreversibly damage proteins. The reverse reaction of methionine sulfoxide to methionine via thioredoxin-dependent methionine sulfoxide reductase (MrsA) is linked to the cellular redox state via thioredoxin reductase and NADPH (Hoshi *et al.*, 2001). This suggests a possible contribution of methionine residues to redox regulation of protein function or an alteration of the structure, depending on the cellular redox state.

2.3.2.2 Cysteines, key players in redox regulation

Cysteines represent one of the least prominent amino acids within proteins (Jones, 2008). Nevertheless, they are the most conserved residues and are often located at functionally or structurally important protein sites (Fomenko *et al.*, 2008). Cysteine content increases with the complexity of organisms from 0.4-0.5% in archaea to 2.26% of the total encoded amino acids in mammals, indicating that increased cysteine content was advantageous during evolution (Miseta *et al.*, 2000). Cysteines inherit important functions in proteins varying from catalytic, redox active, regulatory, or structural cysteines to cysteines participating in metal coordination, as sites of post-translational modifications (PTMs), or participation in substrate binding or protein-protein interaction (Fomenko *et al.*, 2008; Jacob *et al.*, 2012). Cysteine is unique among the encoded amino acids since it carries a reactive sulfhydryl group, or thiol group, that readily reacts with another sulfhydryl group, resulting in the formation of a disulfide bridge (Wani *et al.*, 2014). Due to their thiol group, which can adapt multiple oxidation states ranging from -2 to +6, cysteines are highly susceptible to redox modifications (Wani *et al.*, 2014); therefore, they play a crucial role in the redox regulation of proteins. Susceptibility of cysteines to redox modifications is known to depend on different factors such as the cysteine redox state, proximity to metal centers, its accessibility, electrostatic interactions, and its pK_a (which is normally ~8.5) (Jacob *et al.*, 2012; Cremers *et al.*, 2013), which might be affected by surrounding amino acids, e.g. positively charged residues. Furthermore, the environmental pH and intracellular redox state affect redox modifications of cysteines (Xiong *et al.*, 2011; Roos *et al.*, 2013). An overview of oxidative cysteine modifications is provided in Figure 1.

Oxidation of a cysteine thiol by ROS or RNS leads to formation of the highly reactive sulfenic acid, which due to instability readily reacts with another thiol to form an intra- or intermolecular disulfide bond or reacts with RNS or GSSG and is thus *S*-nitrosylated or *S*-glutathionylated, respectively (Cremers *et al.*, 2013). These modifications are reversible. Persisting oxidative conditions and oxidative stress can induce overoxidation of sulfenic acid to sulfinic acid and sulfonic acid, analogous to sulfoxidation of methionine. Formation of sulfinic and sulfonic acids had been considered irreversible; however, some studies were published showing sulfinic acids can be reduced enzymatically to thiols e.g. by ATP-dependent sulfiredoxin as shown for *Saccharomyces cerevisiae* (Biteau *et al.*, 2003) or as shown for peroxiredoxins (Woo *et al.*, 2003), whereas for the latter one, the responsible enzyme system has not yet been identified.

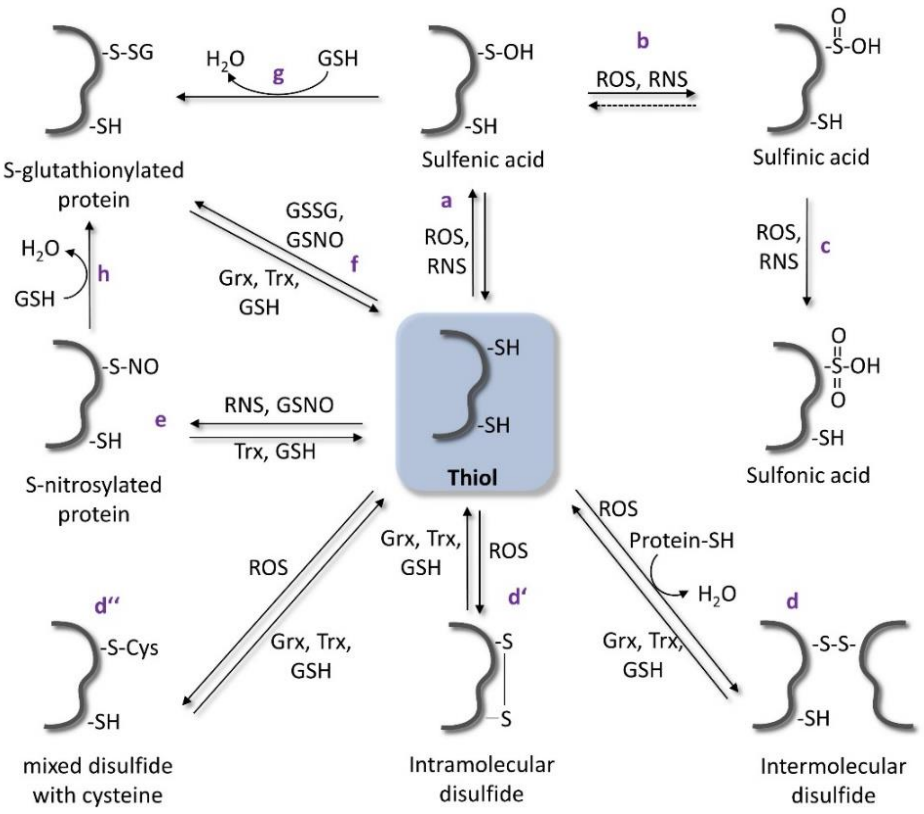

Figure 1: Cysteine modifications

Oxidation of a cysteine thiol leads to the formation of the highly reactive sulfenic acid (a), which readily reacts with another thiol to form either an intramolecular (d') or an intermolecular disulfide bond (d), a mixed disulfide with a free cysteine (d''), or it can react with RNS e.g. *S*-nitrosoglutathione (GSNO) (e) or GSSG (f) and is thus *S*-nitrosylated or *S*-glutathionylated, respectively. These modifications are reversible by glutathione (GSH) or the redox-active proteins thioredoxin (Trx) and glutaredoxin (Grx). High levels of oxidative stress can induce overoxidation of sulfenic acid to sulfinic acid (b) and sulfonic acid (c). This figure was modified from (Jortzik *et al.*, 2012) and (Dalle-Donne *et al.*, 2009).

Reversible switches of cysteine redox states in response to dynamic alterations in the cellular redox state serve as molecular redox sensors via formation or cleavage of disulfide bonds, followed by a direct or indirect modulation of protein function by modulating functionally important cysteines or inducing conformational changes that affect critical cysteine residues (Nagahara, 2011). These thiol switches are suggested to play a role in regulating cell signaling through different compartments or subcellular localizations via redox-sensitive catalytic cysteines of signaling enzymes, e.g. protein-tyrosine kinases (Ostman *et al.*, 2011). Furthermore, redox-sensing thiol switches participate in regulation of protein expression via redox regulation of transcription factor activity, as shown for CprK (Pop *et al.*, 2004) and OxyR (Lee *et al.*, 2004), and thereby link protein expression to the cellular redox state (Nagahara, 2011).

2.3.2.3 Protein-*S*-glutathionylation

Protein-*S*-glutathionylation, a post-translational modification and the most abundant oxidative thiol modification, is the reversible formation of mixed disulfides between a protein cysteine-sulfhydryl moiety and the cysteine-sulfhydryl moiety of the tripeptide glutathione (Dalle-Donne *et al.*, 2007). Under physiological cellular conditions, glutathione is present mostly in

its reduced form GSH in millimolar concentrations (1-10 mM) (Meister *et al.*, 1983), with a molecular ratio of the glutathione redox couple GSH/GSSG of 10,000:1 (Morgan *et al.*, 2013) (a ratio of 100:1 was suggested for a long time (Hwang 1992 Science 257:1496)). GSH is the major redox thiol in cells and maintains the reduced state of the cell (Muller, 2015). Protein-*S*-glutathionylation occurs under conditions of oxidative and nitrosative stress as well as in unstressed cells under physiological conditions (Dalle-Donne *et al.*, 2007).
Several reactions can mediate protein-*S*-glutathionylation (according to (Dalle-Donne *et al.*, 2009). GSH can react directly with cysteines that were previously oxidized by e.g. hydroxyl radicals, i.e. sulfenic acids or thiyl radicals, leading to formation of protein-glutathione mixed disulfides (PSSG). Protein-*S*-glutathionylation can occur via thiol-disulfide exchange between GSSG and a protein thiol in response to a shift in the GSH/GSSG ratio towards GSSG, i.e. under conditions of oxidative stress. Furthermore, reaction of a protein thiol and nitrosothiol, i.e. *S*-nitrosoglutathione, can result in protein-*S*-glutathionylation and the reaction of *S*-nitrosylated proteins with GSH. Furthermore, protein-*S*-glutathionylation can be catalyzed enzymatically by glutaredoxin (Grx) (Lind *et al.*, 1998) and glutathione-*S*-transferase (GST) (Townsend *et al.*, 2009). However, the exact *in vivo* mechanism of protein-*S*-glutathionylation is not yet fully understood.
The cellular level of *S*-glutathionylated proteins increases within cells under conditions of oxidative stress compared to physiological conditions (Lind *et al.*, 2002); therefore, protein-*S*-glutathionylation is suggested to prevent cysteine residues from irreversible overoxidation. Moreover, protein-*S*-glutathionylation functions as an intracellular storage form of glutathione in order to prevent GSSG export from the cell under oxidative stress (Sies *et al.*, 1984; Dalle-Donne *et al.*, 2009). A prerequisite for its cysteine-protecting and glutathione storage functions is the reversibility of protein-*S*-glutathionylation. The reverse process is called deglutathionylation and is catalyzed enzymatically by Grx (Jensen *et al.*, 2014) via a monothiol mechanism (Shelton *et al.*, 2005), thioredoxin (Trx) (Greetham *et al.*, 2010; Kehr *et al.*, 2011), sulfiredoxin (Findlay *et al.*, 2006), and plasmoredoxin, a redox-active protein unique to *Plasmodium falciparum* (Kehr *et al.*, 2011). The reversibility of protein-*S*-glutathionylation suggests a potential role in redox signaling. However, specificity is a requirement for a potential role in signaling processes. Although some cysteines are more sensitive to *S*-glutathionylation than others, a specific glutathionylation motif has not yet been observed, and the exact parameters facilitating protein-*S*-glutathionylation specificity are still unclear. The cysteine's accessibility and the pK_a, surrounding amino acids which can affect the cysteine's pK_a, and therefore its reactivity are still uder debate (Dalle-Donne *et al.*, 2009).

2.3.2.4 Protein-*S*-nitrosylation

$NO^{\cdot}$ is an important messenger molecule in cell signaling processes that participates in numerous physiological processes (Moncada *et al.*, 1991) such as cardiovascular function, blood vessel dilatation, muscle relaxation, neurotransmission, and immune defense mechanisms (reviewed in Knott *et al.*, 2010). It reacts with a wide variety of target molecules, e.g. DNA (Tamir *et al.*, 1996), proteins, ROS, and metals (McCleverty, 1979), affecting numerous downstream mechanisms. NO can lead to the formation of *S*-nitrosoglutathione (GSNO) in the presence of GSH. Under aerobic conditions NO undergoes autoxidation to dinitrogen trioxide (N_2O_3) (Gardner *et al.*, 2004; Toledo *et al.*, 2012) or forms higher nitrogen

oxides, e.g. $ONOO^-$, with harmful cellular effects (Sun *et al.*, 2006). N_2O_3 is a key mediator of protein-*S*-nitrosylation, a reversible post-translational modification occurring under physiological conditions and during nitrosative stress, with effects on protein function, conformation, and stability (Kim *et al.*, 2004; Hess *et al.*, 2005). It is the covalent attachment of a nitroso group (-NO) to a protein thiol, resulting in the formation of an *S*-nitrosothiol (Hess *et al.*, 2005). Under oxidative stress conditions, protein-*S*-nitrosylation might have a protective function for protein thiols in order to prevent overoxidation and loss of protein function (reviewed in Sun *et al.*, 2006), similar to protein-*S*-glutathionylation. Protein-*S*-nitrosylation can occur either directly via interaction of a protein thiol with RNS or via transfer of an NO-group from another *S*-nitrosothiol e.g. GSNO, a process called transnitrosylation (Hess *et al.*, 2005). Analogous to protein-*S*-glutathionylation, which is suggested to have a GSH storage function under oxidative stress conditions, protein-*S*-nitrosylation is believed to have an NO-storage function due to the longer half-life of RSNO compared to NO (Broillet, 1999). However, the NO half-life is supposed to be concentration dependent (Wink *et al.*, 1998); under physiological (nanomolar) concentrations, NO has a relatively long half-life enabling an interaction of NO with target molecules, whereas under pathophysiological (micromolar) concentrations, NO rapidly reacts with ROS or RNS and facilitates nitrosative stress (Toledo *et al.*, 2012). Similar to protein-*S*-glutathionylation, not every cysteine undergoes *S*-nitrosylation. It has been suggested that the specificity of protein-*S*-nitrosylation depends on the pK_a of the cysteine, its accessibility, a hydrophobic environment (Liu *et al.*, 1998; Sun *et al.*, 2006), and the subcellular colocalization of target proteins and NOS (Sun *et al.*, 2006). Furthermore, a consensus acid-base motif for *S*-nitrosylation has been proposed via database screenings (Stamler *et al.*, 1997; Broillet, 1999) and is suggested to control the pK_a and nucleophilicity of the target thiol (Sun *et al.*, 2006). This motif is composed of XYCZ, with X presenting a polar, uncharged, or nonpolar amino acid, Y being either a basic or an acidic amino acid, and Z being an acidic amino acid (Stamler *et al.*, 1997; Broillet, 1999). Besides its specificity and spatiotemporal restriction, *S*-nitrosylation fulfills another criterion for its role in NO signaling processes: reversibility (denitrosylation) (Derakhshan *et al.*, 2007). Denitrosylation, the removal of an NO group from a thiol, can either be non-enzymatically driven or enzymatically catalyzed by denitrosylases, e.g. by Trx (Benhar *et al.*, 2008), GSH (Zaffagnini *et al.*, 2013), GSNO reductase (Liu *et al.*, 2001), superoxide dismutase (SOD) (Jourd'heuil *et al.*, 1999), protein disulfide isomerase (Sliskovic *et al.*, 2005), xanthine oxidase (Trujillo *et al.*, 1998), or carbonyl reductase (Bateman *et al.*, 2008). A wide variety of proteins are *S*-nitrosylated, including enzymes of energy metabolism (glycerine aldehyde-3-phosphate dehydrogenase (Hara *et al.*, 2005)), heat shock proteins (Hsp90 (Martinez-Ruiz *et al.*, 2005)), ion channels (L-type Ca^{2+} channel (Sun *et al.*, 2006)), and transcription factors (NF-κB (Reynaert *et al.*, 2004)) with regulatory downstream effects on cellular pathways. Furthermore, dysregulated *S*-nitrosylation (hypo- or hyper-*S*-nitrosylation) is linked to the pathogenesis of neurological diseases (e.g. Alzheimer's and Parkinson's diseases), cancer, cardiovascular diseases, pulmonary diseases (i.e. asthma), and diabetes (Foster *et al.*, 2009).

1.3 PfalMAT: a target of redox-regulatory processes

1.3.1 Malaria and *Plasmodium falciparum*

Malaria is a mosquito-borne infectious disease caused by protozoan apicomplexan parasites of the genus *Plasmodium* (CDC, 2015). Infected patients often suffer from cold- or flu-like symptoms such as fever, headache, chills, nausea, and vomiting. Left untreated malaria patients can develop severe complications and may die (CDC, 2015). Malaria is one of the most prevalent infectious diseases worldwide, with more than 40% of the world's population being at risk of malaria (WHO, 2008). In 2012, 207 million estimated malaria cases were reported. Each year, around 800,000 people die from malaria (WHO, 2010). The poorest and children under 5 years of age are affected the most, partly due to a weakened immune system and undernourishment, in tropical and subtropical areas of Africa, Mexico to South America, Southeast Asia, and Eastern Mediterranean regions.

Among the more than 100 *Plasmodium* species, five are human pathogenic, namely, *Plasmodium falciparum*, *P. vivax*, *P. ovale*, *P. malariae*, and *P. knowlesi* (Tuteja, 2007). *P. falciparum* is the most virulent species, causing severe tropical malaria. Typical features of a *P. falciparum* infection includes severe anemia, the sequestration of infected erythrocytes from the blood, and their accumulation in various organs e.g. lung, kidney, placenta, and brain. Due to antigenic variation on the surface of infected erythrocytes encoded by var genes, parasitized erythrocytes evade splenic elimination and host immune response (Chen *et al.*, 2000). Instead, parasitized erythrocytes are eliminated from the blood stream via enhanced adherence to the endothelium of blood vessels, resulting in vasoconstriction. This cytoadherence is caused by the expression of *Plasmodium*-derived adhesion molecules (PfEMP-1) on the surface of infected erythrocytes, which bind to host adhesion molecules (i.e. ICAM-1). These vascular constrictions are further aggravated by rosetting, an agglutination of infected and uninfected erythrocytes, and can lead to occlusions of small blood vessels, e.g. in the brain, which can cause severe cerebral malaria (Mackintosh *et al.*, 2004; Tuteja, 2007).

Plasmodium is transmitted by female *Anopheles* mosquitos. Among the approximately 400 *Anopheles* species, 60 serve as vectors under natural conditions and can transmit malaria (Tuteja, 2007). *Plasmodium* undergoes different developmental stages within its complex life cycle (Figure 2) in its human and mosquito hosts, which are characterized by different environmental conditions (Tuteja, 2007), that the parasite must adapt to.

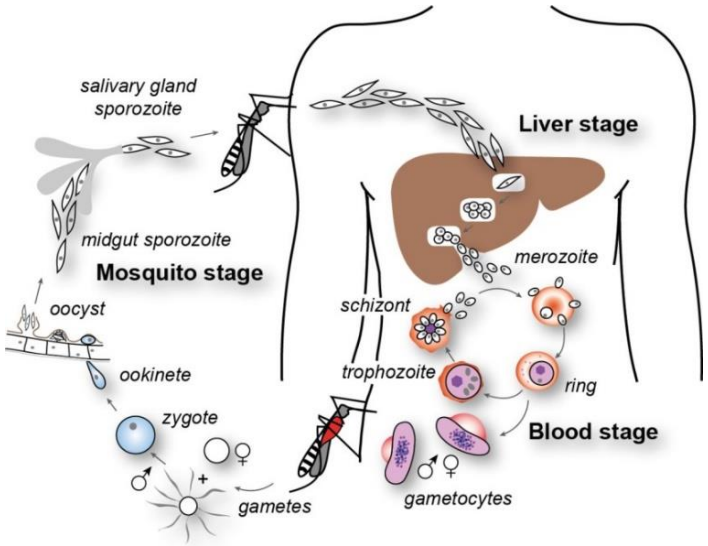

Figure 2: Life cycle of *Plasmodium falciparum*

Infective sporozoites are transmitted by the bite of an infected female *Anopheles* mosquito from her salivary glands to the human host, followed by release into the blood stream (Tuteja, 2007). Parasites reach the liver and penetrate the hepatocytes. Within hepatocytes (exo-erythrocytic cycle / liver cycle) *P. falciparum* undergoes asexual replication and develops into schizonts. Mature schizonts rupture and release merozoites, which enter erythrocytes and start the intraerythrocytic cycle (blood stage). Within the erythrocytic cycle merozoites develop asexually into a ring form, which matures into trophozoites. Trophozoites enlarge and develop into schizonts that almost completely fill the infected erythrocyte. The mature schizont ruptures and releases merozoites into the blood stream, which are able to infect more erythrocytes. This rupture of infected erythrocytes causes the typical repetitive fever of tropical malaria. The erythrocytic cycle of *P. falciparum*, (invasion, multiplication, release, invasion) takes 48 hours and occurs relatively synchronously (Tuteja, 2007). A few intraerythrocytic merozoites differentiate into the sexual forms, male and female gametocytes, which can be ingested by *Anopheles* mosquitos during blood meals on infected human hosts. Within the insect host (mosquito stage / sporogonic cycle), gametocytes reach the midgut, where they develop into micro- and macrogametes. After fertilization of the macrogamete by the microgamete, these sexual forms fuse to form a zygote, which transforms into an ookinete. The ookinete penetrates the midgut epithelial cell wall and differentiates into an oocyst. Oocysts in the midgut grow, rupture, and release sporozoites, which invade the salivary glands and can be transmitted to another human host via the next blood meal (CDC, 2015). This figure was taken from (Cowman *et al.*, 2012).

1.3.2 Redox metabolism of *P. falciparum*

Plasmodium is exposed to high levels of oxidative and nitrosative stress during its life cycle. The rapid growth, replication, and differentiation of *Plasmodium* requires a specialized protein expression and high metabolic rate, which are accompanied by the formation of reactive intermediates (Becker *et al.*, 2004). Furthermore, *Plasmodium* digests hemoglobin from the hosting infected erythrocyte because it is its main amino acid source. The degradation of hemoglobin in the acidic parasite food vacuole results in a spontaneous oxidation of Fe^{2+} to Fe^{3+} in hemoglobin, as well as the formation of toxic free heme (ferriprotoporphyrin IX, FP IX) and superoxide anion radicals ($O^{2-\cdot}$), which lead to the formation of hydrogen peroxide (H2O2) via superoxide dismutase (SOD) and hydroxyl radicals ($OH^{\cdot}$) (Becker *et al.*, 2004; Muller, 2004). FP IX is detoxified via degradation to hemozoin. However, a small amount of FP IX is released into the cytosol and leads to radical formation, which causes oxidative stress and can damage membranes, proteins, DNA, and lipids (Atamna *et al.*, 1993; Becker *et al.*, 2004; Muller, 2004). Furthermore, *Plasmodium* has to combat host-derived radicals from the oxidative burst as an immune response (Muller, 2004). *Plasmodium* superoxide dismutase (SOD) contributes to antioxidant defense. But

Plasmodium lacks the classic antioxidant enzymes catalase and glutathione peroxidase. Therefore, the two major antioxidant redox systems of *Plasmodium*, the thioredoxin system and the glutathione system, are more important in combating oxidative and nitrosative stress. Both systems rely on NADPH provided by the pentose phosphate pathway as an electron donor that provides reducing equivalents, and both systems closely interact in order to maintain cellular redox equilibrium (reviewed in Mohring, Pretzel *et al.*, 2014).

2.3.2.1 Thioredoxin system of *P. falciparum*

The thioredoxin system of *P. falciparum* comprises two NADPH-dependent thioredoxin reductases (PfTrxR) capable of reducing three thioredoxins (PfTrx 1-3), two thioredoxin-like proteins (PfTlp 1-2) that cannot be reduced by PfTrxR (Nickel *et al.*, 2006; Jortzik *et al.*, 2012), five thioredoxin-dependent peroxiredoxins (PfPrx1a, PfPrx1m, PfPrx5, PfPrx6, and PfPrxQ), and the parasite's unique plasmoredoxin (PfPlrx) (Becker *et al.*, 2003). Similar to human TrxR, the two FAD-dependent PfTrxRs belong to high molecular weight TrxRs. But unlike the human counterpart, whose C-terminal redox center is composed of a cysteine-selenocysteine motif, PfTrxR possesses a Cys-xxxx-Cys motif. The two PfTrxR isoforms exhibit similar kinetic properties (Nickel *et al.*, 2006), although they have different subcellular localizations (cytosolic and mitochondrial) (Kehr *et al.*, 2010). PfTrxR transfers electrons from NADPH via FAD to disulfide substrates, mainly Trx, which is subsequently reduced and able to reduce disulfides of low molecular weight (LMW) substrates, including glutathione disulfide (GSSG), hydrogen peroxide (H_2O_2), cumene hydroperoxide (CHP), tert-butyl hydroperoxide (tBOOH), and *S*-nitrosoglutathione (GSNO) (Kanzok *et al.*, 2000; Nickel *et al.*, 2006; Jortzik *et al.*, 2012). Furthermore, in its reduced state Trx can reduce disulfides of several target proteins, including Trx-dependent peroxidases (Rahlfs *et al.*, 2001), proteins involved in energy metabolism, protein biosynthesis, transcription, signal transduction, and *S*-adenosylmethionine (SAM) and polyamine metabolism (Sturm *et al.*, 2009).
Among the three PfTrxs, the cytosolic PfTrx1 plays the most important role in redox metabolism of *P. falciparum* (Kehr *et al.*, 2010). Its WCGPC active site motif forms a disulfide in the oxidized state and is kept in the reduced dithiol state by PfTrxR (Powis *et al.*, 2001). In the reduced state, PfTrx1 transfers reducing equivalents from one of the catalytic thiols to numerous target proteins of *P. falciparum* (Sturm *et al.*, 2009) and diverse low molecular weight substrates (Rahlfs *et al.*, 2001). Moreover, PfTrx1 is capable of catalyzing the deglutathionylation of *S*-glutathionylated proteins (Kehr *et al.*, 2011). *Plasmodium* species encode an additional member of the Trx-superfamily, the dithiol redox-active protein, plasmoredoxin (Plrx), which contains a Trx-fold and a putative WCKYC active site motif (Becker *et al.*, 2003; Jortzik *et al.*, 2012). Plrx shares common features with PfTrx and PfGrx, i.e. deglutathionylation of *S*-glutathionylated proteins (Kehr *et al.*, 2011; Jortzik *et al.*, 2012). However, Plrx is not a substrate of PfTrxR or *P. falciparum* glutathione reductase (PfGR) but can be reduced by PfTrx, glutaredoxin (PfGrx), and GSH, albeit less efficiently (Jortzik *et al.*, 2012). Plrx reduces disulfide substrates such as GSSG, peroxiredoxin PfPrx1a, ribonucleotide reductase, and insulin (Becker *et al.*, 2003). A total of 21 target proteins interacting with Plrx were identified in pull-down experiments, among them PfalMAT (Sturm *et al.*, 2009).

2.3.2.2 Glutathione system of *P. falciparum*

Glutathione is the major redox buffer that regulates cellular redox homeostasis (Muller, 2015) by switching between a reduced form (GSH) and an oxidized form (GSSG) (Jortzik *et al.*, 2012). Intracellular GSH concentration is approximately 2.4 mM, thus considerably higher than the concentration of NADPH (< 100 µM) and Trx (~ 10 µM), additional redox-active compounds contributing to cellular redox equilibrium (Jortzik *et al.*, 2012). *Plasmodium* synthesizes GSH *de novo* in an ATP-dependent manner in a two-step reaction catalyzed by γ-glutamylcysteine synthetase (γGCS) and glutathione synthetase (GS) (reviewed in Mohring, Pretzel *et al.*, 2014; Muller, 2015). The glutathione redox system of *P. falciparum* is composed of glutathione reductase (GR), glutathione-*S*-transferase (GST), glyoxalases, glutaredoxin (Grx), and three Trx-dependent glutaredoxin-like proteins (Glp 1-3). The FAD-dependent GR reduces GSSG to GSH upon consumption of NADPH (Jortzik *et al.*, 2012). GSH provides reducing equivalents for numerous GSH-dependent proteins of *P. falciparum*, including GST, glyoxalases, Grx, and Glps. Upon reduction by GSH, the thiol-disulfide oxidoreductase Grx can reduce disulfides of a variety of target proteins: 17 have been identified in *P. falciparum* using a proteomic approach, including proteins involved in glycolysis, protein-folding, and *S*-adenosylmethionine metabolism (PfalMAT) (Sturm *et al.*, 2009). The glutathione system of *P. falciparum* efficiently regulates the cellular redox state by recycling of GSSG to GSH, and it regulates protein-*S*-glutathionylation and deglutathionylation catalyzed by PfGrx (Kehr *et al.*, 2011).

2.3.2.3 Redox system of *P. falciparum* as a drug target

The X-chromosomal inherited glucose-6-phosphate dehydrogenase (G6PDH) deficiency can protect against malaria infections. G6PDH catalyzes the first step in the pentose phosphate pathway that converts $NADP^+$ into its reduced form, NADPH, which provides reduction equivalents for many downstream antioxidant processes and protects the erythrocyte from oxidative stress. A G6PDH deficiency is accompanied by reduced NADPH levels and therefore decreases protection against oxidative stress, leaving erythrocytes more susceptible to ROS and RNS, which can damage the red blood cells and cause hemolytic anemia. In G6PDH deficiency, *Plasmodium* has to face higher levels of oxidative stress within their hosting erythrocytes. This deficiency is highly prevalent in malaria-endemic regions, suggesting a selectivity-based protective function against malaria, and highlights the importance of oxidative stress when defending against *Plasmodium* (Ginsburg *et al.*, 1996). The susceptibility of *Plasmodium* to oxidative stress and the vital role of its antioxidant defense mechanism make its redox systems an attractive drug target to combat malaria. Therefore, many antimalarial drugs in current clinical use lead to oxidative stress by releasing ROS itself (methylene blue, pyocyanine, synthetic peroxides, artemisinin and derivatives), by preventing the scavenging of pro-oxidant metabolic byproducts e.g. toxic free heme (quinolines e.g. mefloquine, azoles, isonitriles, xanthones; and their derivatives), or by inhibiting enzymes of the antioxidant defense systems of *Plasmodium* i.e. PfGR, PfGST, or PfTrxR (dehydroepiandrosterone, phenolic Mannich bases, ellagic acid, naphthoquinones, artemisinin and its derivatives, methylene blue, and isoalloxazine derivatives) (Pal *et al.*, 2012); (Mohring, Pretzel *et al.*, 2014).

However, a spread of resistance is observable in *Plasmodium* species against all classes of currently used antimalarial drugs: amodiaquine, chloroquine, mefloquine, quinine, sulfadoxine-pyrimethamine, and artemisinin (WHO, 2010). Furthermore, resistances of *Anopheles* mosquitos against insecticides are spreading (WHO, 2012). The best way to combat malaria infection would be a long-term prophylaxis via vaccination (MMV, 2015). However, development of vaccines against malaria is challenging due to the complexity of the parasite, its life cycle, and its antigenic variation. The WHO currently lists 27 malaria vaccine candidates in clinical trials. However, the only one in late-stage drug development, i.e. most advanced vaccine candidate, is RTS,S/AS01 (Mosquirix). It finished phase III clinical trials in 2014 and WHO could possibly recommend and approve it in 2016 (MMV, 2015; PATH, 2015; WHO, 2015). However, this vaccine is not completely protective; it reduces the clinical cases of severe infant malaria by 26-36%. Furthermore, it requires a booster dose after 18 months, because efficacy decreases over time (PATH, 2015). A completely effective vaccine against malaria is still missing.
Altogether, this threatens our progress in disease control and the partial eradication achieved during the last ten years, which were based on vector control using insecticides, efforts to block transmission, draining of marshlands, the use of insecticide-treated bed nets, indoor residual spraying, and antimalarial drugs (WHO, 2010; 2012). The spread of resistance against antimalarial drugs necessitates novel therapeutic approaches. Novel targets and drugs against malaria, with modes of action distinct from currently available drugs, are urgently needed.

2.3.2.4 *S*-adenosylmethionine metabolism as a drug target

"[…] SAM can be considered as a spider in a biochemical web." (Loenen, 2006).

S-adenosylmethionine (SAM, also known as AdoMet), is the major biological methyl group donor for methyltransferase-catalyzed reactions and is present in all living organisms. Its importance in living cells is based on three downstream key pathways (Figure 3): transsulfuration, transmethylation and polyamine biosynthesis (Lu, 2000). SAM serves as a precursor of GSH via the transsulfuration pathway, i.e. the conversion to cysteine. The *S*-methyl group of SAM is transferred to a variety of substrates including nucleic acids, phospholipids, amines, small molecules such as arsenic, and numerous proteins in transmethylation reactions (reviewed in Lu, 2000; Loenen, 2006). Therefore, SAM metabolism is linked to regulation of gene expression via DNA methylation and influences membrane fluidity and receptor mobility (Fontecave *et al.*, 2004). Moreover, SAM is one of the most frequently used enzyme substrates after ATP (Loenen, 2006). Furthermore, SAM is a precursor for polyamine synthesis, which is essential for cell growth (Thomas *et al.*, 2001). Besides, the generation of SAM radicals (5-deoxyadenosyl radical) is necessary for SAM radical enzymes, which are involved in DNA repair and biosynthesis of vitamins and coenzymes (Tabor *et al.*, 1984; Lu, 2000). SAM is synthesized in the cytosol of each cell, mainly in hepatocytes. 85% of all methylation reactions occur in the liver (Hoffman *et al.*, 1980). Orally administered SAM has been shown, both in animal and man, to have beneficial effects in alcoholic liver disease, it prevents the development of liver cancer in rodents, and it is well tolerated (Mato *et al.*, 1999).

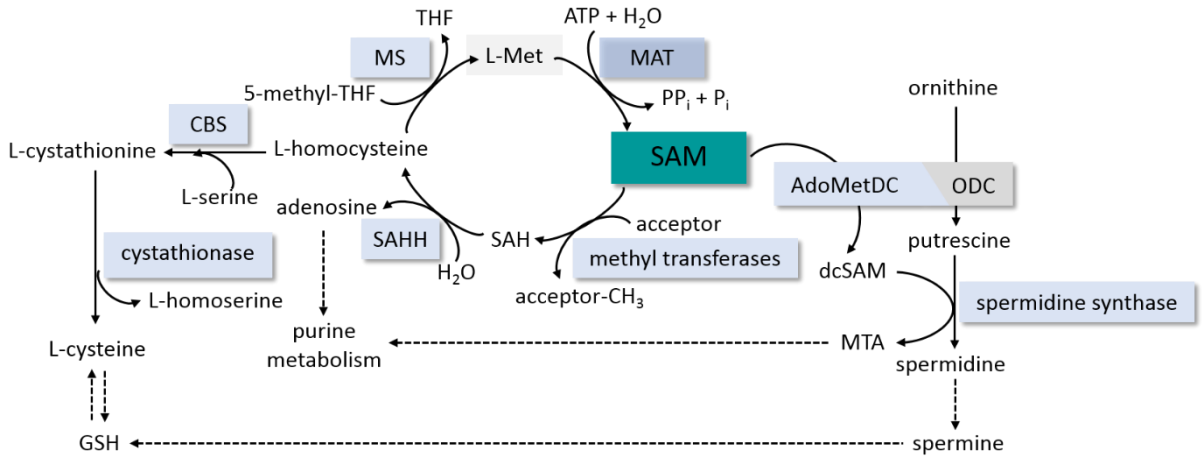

Figure 3: SAM metabolism

SAM synthesis is catalyzed via methionine adenosyltransferase (MAT) by using L-methionine and ATP. The *S*-adenosyl moiety of ATP is transferred to methionine, resulting in the formation of a sulfonium ion that readily transfers its methyl group to acceptor substrates (Lu, 2000). SAM is thereby converted to *S*-adenosyl-L-homocysteine (SAH), which is converted to adenosine for purine metabolism and homocysteine catalyzed by SAH hydrolase (SAHH). Homocysteine can be used by methionine synthase (MS) and betaine-homocysteine transferase in order to resynthesize methionine. Within the liver, the transsulfuration pathway, converts homocysteine to cystathionine, a reaction catalyzed by cystationine-β-synthase (CBS). Cystathionine is converted to cysteine, a precursor for GSH synthesis. Thereon, SAM metabolism is linked to redox metabolism and regulation of the cellular redox balance. However, in *P. falciparum* there is presumably no generation of cysteine from methionine via the transsulfuration reaction because the parasite lacks the respective cystathionine-β-synthase and cystathionine-γ-lyase genes (Gardner *et al.*, 2002) rather depending on cysteine import (Muller *et al.*, 2008). A further downstream pathway of SAM starts upon its decarboxylation via the *S*-adenosylmethionine decarboxylase (AdoMetDC), which is a bifunctional enzyme in *Plasmodium* (AdoMetDC fused to ornithine decarboxylase [ODC]). Decarboxylated SAM (dcSAM) is a precursor for the synthesis of the polyamines spermidine and spermine by providing the necessary aminopropyl moiety. This figure was modified from (Sturm *et al.*, 2009).

SAM synthesis is presumably crucial for life (Loenen, 2006), because even organisms lacking MAT, e.g. *Pneumocystis*, rely on SAM import from their hosts (Merali *et al.*, 2004). SAM depletion, e.g. from low folate levels, polymorphisms of the methylenetetrahydrofolate reductase receptor, and high homocysteine levels, is linked to numerous diseases including cancer, liver diseases, neural tube defect, and neurological disorders such as Alzheimer's disease and depression (Lu, 2000; Lieber *et al.*, 2002; Loenen, 2006). Due to the prominent role of SAM in cell metabolism and its ubiquity among all living organisms, inhibition of SAM synthesis affecting downstream pathways is considered as an attractive strategy to combat pathogenic organisms such as *Leishmania donovani* (Trager *et al.*, 1980; Messika *et al.*, 1990; Perez-Pertejo *et al.*, 2006), *Trypanosoma brucei* (Simo *et al.*, 2010), *Mycobacterium spp.* (Berger *et al.*, 2003), and *Plasmodium spp.* (Muller *et al.*, 2008). Inhibition of SAM downstream pathways has antiplasmodial effects, e.g. inhibition of the methylation cycle via SAHH, and inhibition of the polyamine synthesis route, which arrests growth at the trophozoite stage (Assaraf *et al.*, 1984; Bitonti *et al.*, 1989). Therefore, SAM depletion via inhibition of plasmodial MAT likely blocks parasite growth. A *P. falciparum* strain overexpressing this enzyme has been reported to be resistant to sinefungin, an adenine-containing nucleoside antibiotic with high similarity to SAM that inhibits the growth of *P. falciparum* and *L. donovani* (Trager *et al.*, 1980; Messika *et al.*, 1990; Perez-Pertejo *et al.*, 2006; Muller *et al.*, 2008) via depletion of polyamines (Messika *et al.*, 1990).

2.3.2.5 *P. falciparum* methionine adenosyltransferase

Methionine adenosyltransferases (EC 2.5.1.6) (systematic name: ATP:L-methionine *S*-adenosyltransferase [abbreviated as MAT], or synonymous *S*-adenosyl-L-methionine synthetase [SAMS]) catalyze the formation of *S*-adenosylmethionine from ATP and L-methionine and can be found in nearly every organism. A high level of conservation, typically 30%, can be observed among MATs from different species from bacteria to eukaryotes (Sanchez-Perez *et al.*, 2004; Markham *et al.*, 2009). According to the SCOP database MATs belong to the α/β-protein class. The classical MAT fold consists of three similar intertwined domains, each comprising a βαββαβ repeat (Murzin A. G., 1995; SCOP, 2009). The α-helices appear at the solvent exposed protein surface and the β-sheets are located in the monomer-monomer contact zone (Markham *et al.*, 2009). Resulting from the inverted assembly of two subunits, two cavities are formed in their interface and present the active sites. Interestingly, residues of both subunits contribute to the formation of each active site (Markham *et al.*, 2009). Conserved sequences of MAT comprise a P-loop signature (HGGGAFSGKD), which is in general supposed to contribute to triphosphate binding (e.g. ATP and PPP_i) (Deigner *et al.*, 1995; Markham *et al.*, 2009), and a preserved substrate-binding motif composed of GAGDQG. Furthermore, a flexible loop is located above the active site and acts as a gate or a lid that controls access to the active site (Takusagawa *et al.*, 1996; Taylor *et al.*, 2002). It has been suggested, that this loop participates in the SAM synthetase reaction rather than the tripolyphosphatase reaction, since the k_{cat} of cMAT is decreased upon mutation of this loop but the tripolyphosphatase rate is unaffected (Taylor *et al.*, 2002). All amino acids involved in the formation of the active site were found to be conserved among MATs of different organisms (Takusagawa *et al.*, 1996).

MATs are bifunctional enzymes demonstrating SAM synthetase activity (synthesis of SAM from ATP and L-methionine) and tripolyphosphatase activity (hydrolysis of tripolyphosphate into pyrophosphate and orthophosphate) (Mudd, 1963) with the following two reactions:

(1) ATP + L-methionine → SAM + PPP_i

(2) $PPP_i + H_2O \rightarrow PP_i + P_i$.

The catalytic reaction of MAT is assumed to proceed in a sequential mechanism containing four steps (reviewed in Markham *et al.*, 2009): (i) formation of the enzyme-ATP-methionine complex, (ii) formation of an intermediate enzyme-SAM-PPPi complex, (iii) subsequent hydrolysis of PPP_i to PP_i and P_i, then (iv) release of the products from the enzyme. A swinging movement of the flexible loop above the active site, which results in either opening or closing of the active site cavity, regulates substrate access (Taylor *et al.*, 2002; Taylor *et al.*, 2003). In the open conformation, substrates and the products can enter and leave the active site (Komoto *et al.*, 2004). After the substrate enters the active site, the tripolyphosphate chain of ATP is recognized by the basic amino acids Arg, Lys and His, of the active site and tightly bound to the enzyme via hydrogen bonds and ionic bonds (Komoto *et al.*, 2004). Afterwards, the adenosine moiety of ATP is bound to the enzyme via weak interactions including Gly and Lys (Takusagawa *et al.*, 1996), and the second substrate L-methionine is bound in a planar position, stacking against Phe, which is located on the gate loop (Gonzalez *et al.*, 2000; Markham *et al.*, 2009). After substrate binding, the flexible loop enters the active site, binds to the substrates via water-mediated hydrogen bonds, and closes the active site entrance (Komoto *et al.*, 2004). The catalytic mechanism of MATs is an S_N2 displacement mechanism,

a bifunctional mechanism occurring in one step, with a nucleophilic attack of the sulfur atom of L-methionine (S_D) on C5' of ATP and a simultaneous cleavage of the C5'-O5' bond of ATP, which occurs upon changing the ribose ring conformation from C4'-exo to C4'-endo (Komoto *et al.*, 2004). Thus the MAT reaction allows SAM formation via a nucleophilic attack of the sulfur atom of L-methionine and a displacement of the cleaved negatively charged PPP_i by the resulting sulfonium cation in a concerted manner (Markham *et al.*, 2009). Subsequently, the tripolyphosphate chain is hydrolyzed to pyrophosphate and orthophosphate. This requires Mg^{2+}, which is involved in the coordination of the phosphate groups (Markham *et al.*, 2009). Cleavage of PPP_i occurs from both sides of the tripolyphosphate chain, between ribose and α-phosphate and between β- and γ- phosphate (Komoto *et al.*, 2004), whereas, more than 95% of the inorganic phosphate (P_i) produced is derived from the γ-phosphoryl group of ATP (Markham *et al.*, 1980; Markham *et al.*, 2009). The MAT reaction is exergonic due to hydrolysis of PPP_i. The hydrolysis energy is assumed to be necessary for product release, because products are trapped inside the active site when the ATP analog AMPPNP is used instead of ATP, which cannot be hydrolyzed between the β- and γ-phosphate groups (Komoto *et al.*, 2004). Moreover, enzyme-PPP_i hydrolysis is the rate-limiting step (Markham *et al.*, 2009).

P. falciparum encodes one MAT isoform (PfalMAT; formerly PfSAMS, but renamed in context of this dissertation according to the consensus nomenclature for methionine adenosyltransferases suggested by (Kotb *et al.*, 1997) and in order to distinguish the plasmodial enzyme from the recently published respective enzyme of *Pyrococcus furiosus* [PfMAT] (Porcelli *et al.*, 2015)). The respective gene is located on chromosome 9 (reference assembly: NC_004330.1) (Gardner *et al.*, 2002). So far PfalMAT has been poorly studied, and a crystal structure is not yet available. It was studied on a molecular basis in 1999 by Chiang *et al.* Their homology model, based on the structure of cMAT, suggests a dimeric assembly of PfalMAT (Chiang *et al.*, 1999). PfalMAT displays high homology (~40-60%) to MAT from other organisms. Accordingly, all active site residues are preserved in PfalMAT, including the phosphate-binding P-loop (HGGGAFSGKD), the signature sequence motif of the MAT superfamily (GAGDQG), and amino acids for binding ADP, P_i, and metal ions (Chiang *et al.*, 1999). Furthermore, PfalMAT is weakly inhibited by the classic MAT inhibitor cycloleucine (K_i 17 mM), in a competitive manner with respect to the substrate L-methionine (Chiang *et al.*, 1999).

2.3.2.6 Indications for redox regulation of PfalMAT

Enzymatic activity of MAT from different organisms has been shown to be affected by oxidative modifications of different cysteine residues. Chemical cysteine modification of *E. coli* MAT (cMAT) and rat liver MAT (rlMAT) using the sulfhydryl alkylating agent N-ethylmaleimide (NEM) resulted in complete inactivation of the enzymes and induced a dissociation of the active tetramers into inactive dimers, suggesting a role for cysteines in enzyme activity and the presence of an intersubunit disulfide contributing to subunit association of MAT (Markham *et al.*, 1988; Corrales *et al.*, 1990; Pajares *et al.*, 1991). Furthermore, rlMAT has been shown to be *S*-nitrosylated specifically via Cys121, which is located on the gate loop above the active site, resulting in an inhibition of this enzyme (Avila *et al.*, 1997). Likewise, the respective loop of PfalMAT contains a cysteine residue (Cys113),

which might be regulated in a similar way. Previous experiments of our group demonstrated that PfalMAT undergoes redox-based thiol modifications, pointing towards a redox-dependent regulation of PfalMAT. In pull-down experiments, using affinity purification and mass-spectrometric identification of captured proteins from *P. falciparum* cell lysate, PfalMAT was identified as a target protein of PfTrx1, PfGrx, and PfPlrx, by using active site mutants of these thiol disulfide reductases lacking the resolving cysteine, resulting in the formation of stable, mixed disulfides with target proteins (Sturm *et al.*, 2009). In similar approaches PfalMAT was identified as a protein that is *S*-glutathionylated and *S*-nitrosylated by blocking free thiols of proteins within the parasite cell lysate using NEM or MMTS. Blocked *S*-glutathionylated proteins were reduced by recombinant PfGrx, and *S*-nitrosothiols were specifically reduced with sodium ascorbate. The reduced proteins were subsequently biotinylated and purified via avidin affinity chromatography (Kehr *et al.*, 2011; Wang *et al.*, 2014).

Redox regulation of PfalMAT, might have downstream effects on crucial cellular SAM-dependent pathways of *P. falciparum* such as polyamine metabolism and DNA-/histone-methylation reactions. One aim of this dissertation was to characterize in detail the interplay of PfalMAT with the plasmodial thiol disulfide reductases PfTrx1, PfGrx, and PfPlrx with respect to a potential regulation of the enzymatic activity of PfalMAT. Furthermore, the impact of the post-translational modifications *S*-glutathionylation and *S*-nitrosylation, two potential cysteine protective mechanisms under oxidative stress, on activity and oligomerization of PfalMAT should be addressed. Mutational studies of selected cysteine residues should be performed in order to identify the sites of these redox-based thiol modifications.

1.4 MscDyP1: a novel dye-decolorizing peroxidase

Heme proteins comprise a huge number of diverse proteins that play a crucial role in redox chemistry and multiple biochemical pathways (Singh *et al.*, 2015). Among them, heme peroxidases (EC 1.11.1.7) were originally classified into two superfamilies, the plant and animal peroxidases, but are nowadays subdivided into six superfamilies: catalases, non-animal peroxidases, animal peroxidases, haloperoxidases, di-heme cytochrom-c-peroxidases, and DyP-type peroxidases (Fawal *et al.*, 2013; PeroxiBase, 2015).

1.4.1 DyP-type peroxidases

Dye-decolorizing peroxidases (DyP-type peroxidases, DyP, DypPrxs, EC 1.11.1.19) represent a novel superfamily of heme peroxidases (Sugano, 2009). DypPrxs differ from other known peroxidases in their tertiary structure, catalytic residue, and pH optimum; they lack homology to other peroxidases; and they possess a particularly wide substrate specificity (Zubieta *et al.*, 2007; Yoshida *et al.*, 2015). The first and eponymous member of this enzyme family [DyP from *Thanatephorus cucumeris*, formerly *Geotrichum candidum* Dec 1, and nowadays *Bjerkandera adusta* DyP (BadDyP), due to reclassification of the strain (Ruiz-Duenas *et al.*, 2011)] was discovered in 1999 (Kim *et al.*, 1999) and later named based on its ability to efficiently oxidize and thereby decolorize various dyes (Sato *et al.*, 2004). According to the PeroxiBase database, DypPrxs were phylogenetically subdivided into four classes based on

their structural similarities, with classes A, B, and C comprising mostly members of bacterial origin and class D containing fungal DypPrx (Fawal *et al.*, 2013; PeroxiBase, 2015). However, a reclassification of the DypPrx family was recently proposed, based on structure-based sequence alignments, in response to the phenomenal number of novel members identified in recent years (Yoshida *et al.*, 2015), currently 5,723 members (Interpro, 2015; Mitchell *et al.*, 2015). Among those, are three DypPrxs of viral, 31of archaeal, 440 of eukaryotic, and more than 5,200 of bacterial origin. This is interesting since the first identified members of this family were fungal proteins and therefore DypPrxs were originally suggested to be restricted to basidiomycetous fungi. The new DypPrx classes comprise class I ("intermediate," formerly class A), class P ("primitive," formerly class B), and class V ("advanced," formerly classes C and D) (Yoshida *et al.*, 2015). Members of class P possess a short amino acid sequence, and more compact structure compared to classes I and V. Classes I and V contain extra sequences, I less than V, resulting in more complex structures than those of class P, as shown in Figure 4 (Yoshida *et al.*, 2015).

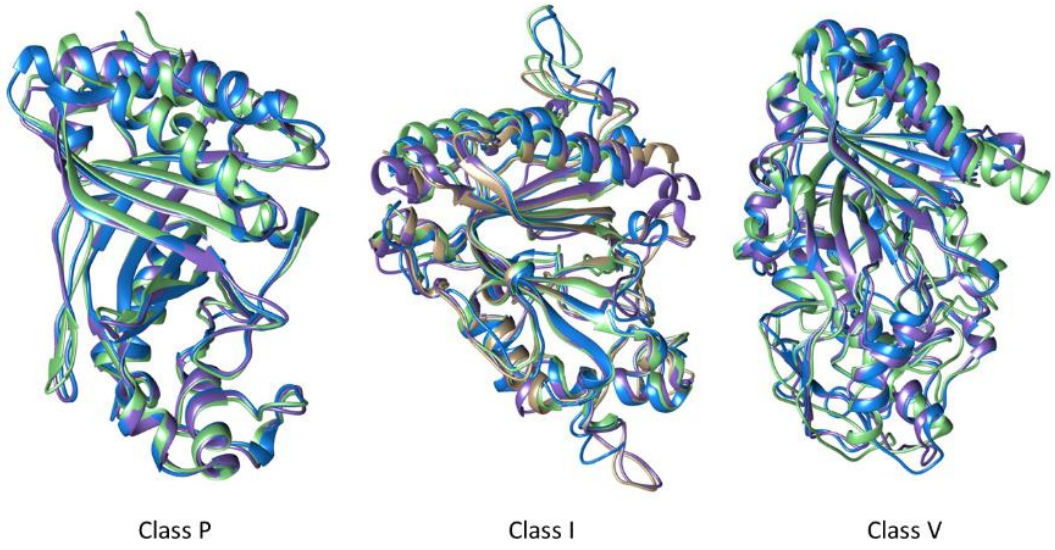

Figure 4: DyPrx classes

Structural superposition of members of the DypPrx classes P (2iiz, 3qns, 4gu7), I (PDB IDs: 4gs1, 4gt2, 3o72, 4grc) and V (PDB IDs: 4g2c, 4au9, 3afv). The UCSF Chimera program was used for superpositioning chain A of each structure using the Needleman-Wunsch algorithm and the BLOSUM 55 matrix. This figure was modified from (Yoshida *et al.*, 2015).

2.3.1.1 Structure of DypPrxs

Although this relatively young enzyme family currently comprises more than 5,000 members, the number of published protein crystal structures available in the PDB database is limited, and they are derived from only nine different DypPrx enzymes (Berman *et al.*, 2000; PDB, 2015). Among them, BadDyP and AauDyP (*Auricularia auricula-judae* DyPrx) are the best studied. The overall fold of DypPrxs contains an α/β-ferredoxin-like fold. Members of the DypPrx family possess a conserved GXXDG motif, which contains the catalytic aspartic acid. Furthermore, DypPrxs contain a conserved heme-binding pocket, with an architecture similar to that found in other heme peroxidases. A histidine represents the classic proximal fifth ligand of the heme iron. Interestingly, instead of the distal histidine, which contributes to

heme binding in classic heme peroxidases, in DypPrxs an asparagine and arginine residue assume this function. The conserved H_2O_2 binding pocket at the distal site of the heme cofactor is composed of the aforementioned Asp and Arg and furthermore contains leucine and phenylalanine residues. The prosthetic heme cofactor, a penta-coordinated ferriprotoporphyrin IX group, is buried within the protein but accessible through a narrowing channel leading to the heme plane (Strittmatter *et al.*, 2015).

2.3.1.2 Catalytic mechanism and substrate specificity of DypPrxs

"Peroxidases have more functions than a Swiss army knife." (Passardi *et al.*, 2005)
This is particularly true for DypPrxs (Figure 5).

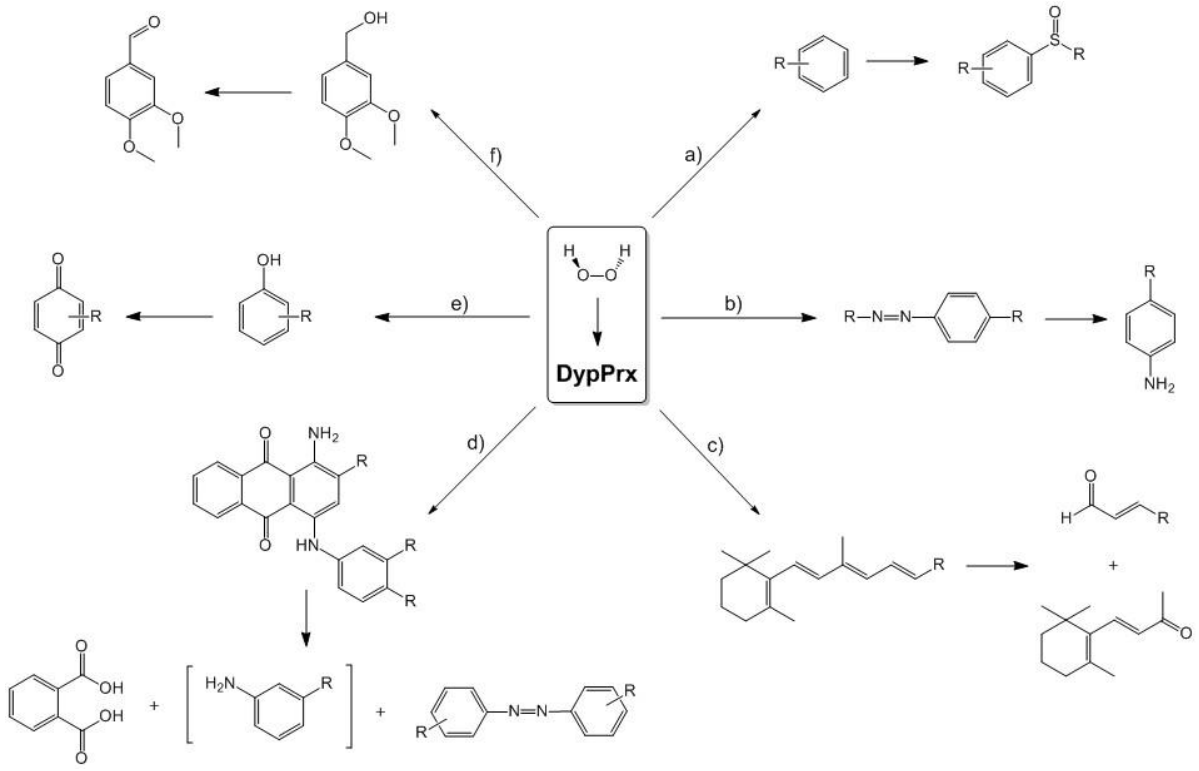

Figure 5: Substrate versatility of DypPrxs

a) Sulfoxidation of aromatic sulfides. b) Oxidative cleavage of azobenzenes. c) β-carotene oxidation to β-ionone and β-apo-10'-carotenal. d) Oxidation and thereby degradation of anthraquinone dyes to phthalic acid, aminobenzene derivatives and azobenzenes. e) Phenol oxidation to quinone. f) Oxidation of non-phenolic aromatics, e.g. veratryl alcohol to veratraldehyde. This figure was created using ChemDraw 15.0, modified from (Hofrichter *et al.*, 2010).

They are capable of oxidizing typical peroxidase substrates, e.g. 2,2'-azino-bis(3-ethylbenzothiazoline-6-sulphonic acid (ABTS) and 2,6-dimethoxyphenol, but also recalcitrant anthraquinone dyes, e.g. Reactive Blue 5 (Sugano *et al.*, 2000). Furthermore, DypPrxs are active at a lower pH range (pH~1-4.5) than plant peroxidases (Zubieta *et al.*, 2007; Liers *et al.*, 2013). Some DypPrxs share functional properties with lignin peroxidases and oxidize high-redox-potential non-phenolic methoxylated aromatics, e.g. veratryl alcohol and non-phenolic β-O-4 lignin model dimers (Liers *et al.*, 2010), although to a lesser extent than lignin peroxidases (Liers *et al.*, 2013). AauDyP has been shown to oxidize *ortho*-, *meta*-, and *para*-nitrophenols (Buttner *et al.*, 2015). A redox potential ranging from 1.1 to 1.2 V was determined for fungal DypPrx, including AauDyP, *Mycetinis scorodonius* DypPrx

(MscDyP1), *Exidia glandulosa* DypPrx (EglDyP), and *Mycena epipterygia* DypPrx (MepDyP), using a phenol oxidation method (Liers, 2014). This redox potential is slightly lower than that of high-redox potential lignin peroxidases (1.26 V) but higher than that of low-redox potential plant (0.93 V for soybean peroxidase, SBP) and fungal (1.06 V for *Coprinopsis cinerea* peroxidase, CiP) peroxidases (Liers, 2014).

This exceptionally broad substrate specificity distinguishes DypPrxs from classic plant or animal peroxidases and makes them highly interesting for biotechnological applications.

The catalytic cycle of heme peroxidases consists of a three-step reaction, initiated by a two-electron transfer from heme protein ($PorFe^{III}$) to H_2O_2, resulting in the formation of compound I (equation 1), a higher oxidation state of the enzyme containing an oxoferryl center, and an organic π-cation radical ($^{\cdot+}PorFe^{IV}=O$). Upon substrate oxidation, compound I is subsequently reduced by two one-electron reductions via formation of compound II ($PorFe^{IV}=O$) (equation 2) back to the native resting iron (III) state of the enzyme (equation 3) (Banci, 1997; Liers, 2014):

(1) $PorFe^{III} + H_2O_2 \rightarrow {}^{\cdot+}PorFe^{IV}=O + H_2O$

(2) $^{\cdot+}PorFe^{IV}=O + AH_2 \rightarrow PorFe^{IV}=O + AH^{\cdot}$

(3) $PorFe^{IV}=O + AH_2 \rightarrow PorFe^{III} + AH^{\cdot} + H_2O$.

As mentioned before, classic heme peroxidases contain a proximal histidine as an axial heme ligand, contributing to heme stabilization, and a distal histidine presenting the acid-base catalytic residue necessary for compound I formation (Yoshida *et al.*, 2011) (Figure 6).

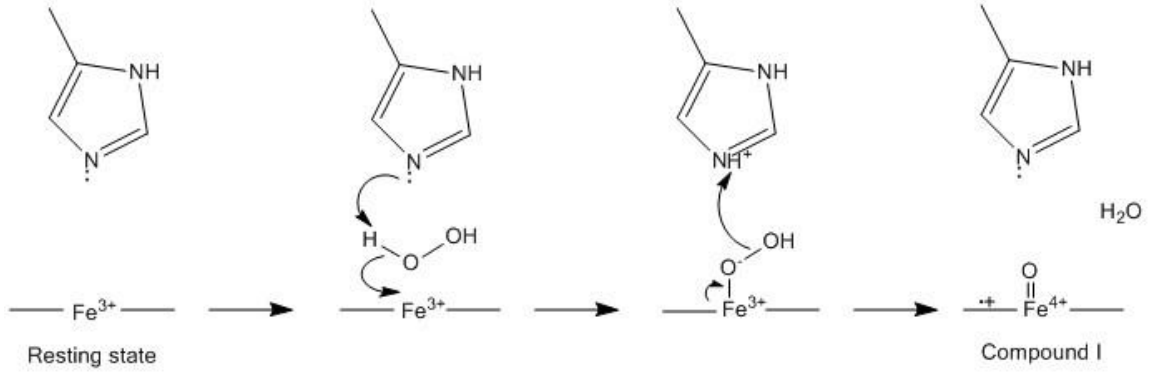

Figure 6: Compound I formation by classic heme peroxidases

Upon reaction of the resting state enzyme with H_2O_2, electrons are transferred from the heme molecule to the substrate H_2O_2, resulting in compound I formation, a higher oxidation state of the heme molecule characterized by the porphyrin ring cation radical ($^{\bullet+}$). The heme plane is indicated as lines enclosing an iron atom. The acid-base catalytic histidine is indicated via its imidazole group. This figure was created using ChemDraw 15.0 according to (Yoshida *et al.*, 2011).

An important difference between DypPrxs and other heme peroxidases is that DypPrxs lack the catalytic histidine that participates in compound I formation in classic heme peroxidases. Instead, an aspartic acid replaces the catalytic function of this distal histidine (Sugano *et al.*, 2007). In detail, the catalytic reaction of DypPrxs requires a swinging movement of this Asp towards the heme plane after the enzyme reacts with H_2O_2 to form compound I (Yoshida *et al.*, 2011) (Figure 7).

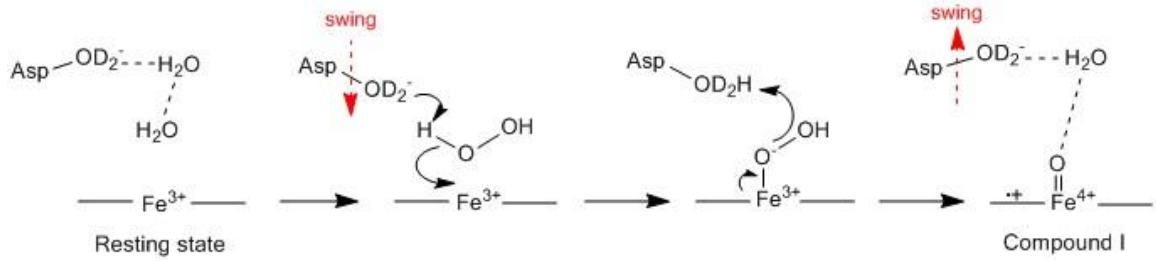

Figure 7: Compound I formation by DypPrxs

Compound I formation in the catalytic reaction of DypPrxs requires a swinging movement of the oxygen OD2 of the catalytic aspartic acid towards the heme plane in order to react with H_2O_2, followed by electron transfer from the heme molecule to H_2O_2 resulting in compound I formation, a higher oxidation state of the heme molecule characterized by the porphyrin ring cation radical ($^{\bullet}$+). The heme plane is indicated as lines enclosing an iron atom. This figure was created using ChemDraw 15.0, modified from (Yoshida *et al.*, 2011).

The exact physiological role of DypPrxs is still unclear. They could possess a biocatalytic function in lignin oxidation, due to the secretion of class V (former class D) DypPrxs from *Basidiomycota* and their lignin-degrading activity (Yoshida *et al.*, 2015). They might play a role for the fungal detoxification of toxic aromatic compounds (Liers *et al.*, 2013). Furthermore, it has been suggested that DypPrxs could have a protective function under oxidative stress since transcription of a putative DypPrx (VNG0798H) of *Halobacterium salinarum* is induced in response to H_2O_2 and paraquat (forms radicals after electron acceptance) treatment (Kaur *et al.*, 2010). Besides, DypPrxs provide interesting biotechnological applications in litter composition, transformation of plant biomass, or the production of aroma compounds (Zorn *et al.*, 2003; Zelena *et al.*, 2009).

1.4.2 *Mycetinis scorodonius* DyP-type peroxidase 1

Mycetinis scorodonius (CBS strain number: 137.83; formerly *Marasmius scorodonius*), the edible garlic mushroom, grows on wood and manure (Ainsworth, 1973) and is used as a spice in human nutrition due to its intense garlic-like flavor. In a screening of 50 filamentous fungi, the cleavage of β-carotene in submerged cultures of *M. scorondonius* was observed (Zelena *et al.*, 2009). Moreover, the volatile flavor compounds β-ionone, dihydroactinidiolide, cyclocitral, and 2-hydroxy-2,6,6-trimethyl-cyclohexanone were formed within mycelium-free culture supernatant, indicating activity of secreted extracellular enzymes (Zelena *et al.*, 2009) later identified as MscDyP1 and 2 (Scheibner *et al.*, 2008). MscDyP1 has been characterized biochemically in previous studies by Zorn and colleagues (Zorn *et al.*, 2003; Scheibner *et al.*, 2008; Puhse *et al.*, 2009; Zelena *et al.*, 2009). MscDyP1 is a striking example of the exceptional substrate versatility of DypPrxs. Besides the aforementioned ability to degrade carotenoids, MscDyP1 also oxidizes phenolic and nonphenolic substrates, including lignin, as shown using the β-*O*-4 lignin model dimer, adlerol, 2,6-dimethoxyphenol, 1,3,5-trimethoxybenzene, the anthraquinone dye Reactive Blue 5, the azo dye Reactive Black 5, and veratryl alcohol, although it oxidizes the two latter ones to a lower extent (Liers *et al.*, 2013). Using a phenol oxidation method, a redox potential of 1.2 ± 0.1 V was estimated for MscDyP1, indicating it belongs to high-redox potential peroxidases (Liers, 2014).
The oxidative degradation of carotenoids by MscDyP1 could have interesting biotechnological applications in the food industry, especially in dairy. In order to maintain a

constant standardized coloring of cheese independent from seasonal variations, e.g. in the production of cheddar, the colorant annatto is added. A part of annatto remains in the whey, which is therefore often bleached for further applications. MscDyP1 was patented for enzymatic whey whitening (MaxiBright®, DSM Food Specialties, Delft, the Netherlands) by Zorn *et al.* (US 2011/0262974 A1), is regarded as generally safe by food and drug administrations and is approved for industrially bleaching of whey (Kang *et al.*, 2010). Enzymatic whey bleaching has advantages over older approved bleaching methods using hydrogen peroxide and benzoyl peroxide since the reaction is more specific than the chemical bleaching and reduces off-flavors (Kang *et al.*, 2010). MaxiBright® also requires the addition of hydrogen peroxide, but as a substrate of MscDyP1 it is consumed, and therefore adding a catalase is not required (Kang *et al.*, 2010). Furthermore, MscDyP1 has promising potential for the biotechnological, cost-effective, large-scale production of carotenoid-derived volatile aroma compounds, including β-ionone and β-cyclocitral, whose extraction from natural sources that contain only trace amounts is expensive and tedious (Zorn *et al.*, 2003).

The crystal structure of this highly interesting DypPrx with broad promising biotechnological potential was recently solved in our group, and it revealed interesting structural features that might contribute to catalysis and redox regulation of MscDyP1. In fact, a single cysteine residue is conserved among MscDyP1, BadDyP, and AauDyP, but had not yet been investigated. The conservation suggests this residue has an important function in DypPrxs. Moreover, this cysteine residue is accessible to small redox-active molecules and might therefore be redox regulated. Furthermore, the structure of MscDyP1 revealed the surface exposition of two methionine residues, Met302 and Met305, which are solely present in MscDyP1, appears to play an important structural role and might contribute to enzymatic activity.

Due to the limited number of available DypPrx structures, the exact catalytic mechanism is still under debate. Therefore, elucidation of the function of these residues via mutational and kinetic studies within the scope of this dissertation might provide additional clues to the mechanism of action of this versatile peroxidase.

2 MATERIALS

2.1 Instruments

Instrument	Company
Autoclave	Webeco, Bad Schwartau
Autoclave VX-95	Systec, Wettenberg
Äkta FPLC system (Pump P-920, monitor UPC-900, injection valve INV-907, mixer M-925, Fraction collector Frac-900, column XK16/60, column material Superdex 200 prep grade)	GE Healthcare, Freiburg
Centrifuge Megafuge 1.0 R	Heraus Instruments, Hanau
Centrifuge MiniSpin	Eppendorf
Centrifuge Salvant SpeedVac SPD111V with Gel Pump GP110	Thermo Life Sciences
Centrifuge Sorvall RC5Plus (rotor S*S*-34 and SLA-3000)	Kendro Laboratory Products, Langenselbold
Centrifuge Sorvall RC 6+ (rotor S*S*-34 and F9*S*-4x1000y)	Thermo Scientific
Centrifuge 5415R	Eppendorf
Cooling coil IKA RV 10 basic	IKA Werke, Staufen
Crystallization robot Honeybee 961	Digilab Marlborough
Crystallization robot mosquito Crystal	TTP Labtech, Melbourne
Electrophoresis Chamber Mini-PROTEAN 3 cell	BioRad
Electrophoresis Chamber B1, B1A, B2	Owl Separation System Inc., Portsmouth, USA
Electrophoresis Power Supply-EPS 200	Pharmacia Biotec, Dübendorf Switzerland
Electroporator GenePulse Xcell	BioRad
GelDoc 2000	BioRad
Heating block neoBlock II	neoLab, Heidelberg
Heating block Thermomixer comfort	Eppendorf, Hamburg
High-purity water system OPTILAB-Plus	MembraPure, Bodenheim
Icemaker F80C	Icematic Deutschland, Meerbusch
Incubation shaker mytron	Thermo Scientific, Dreieich
Incubation shaker KS 500	Junke & Kunkel, IKA-Werke, Staufen
Incubation shaker SM25	Edmund Bühler GmbH, Tübingen
Magnetic stirrer CAT M15	MAGV Laborbedarf, Rabenau-Londorf
Magnetic stirrer color squid	IKA Werke
Magnetic stirrer HI 300N	Hanna Instruments, Kehl am Rhein
Magnetic stirrer RCTbasic	IKA Werke
Microscope Leica KL 1500 LED	Leica Microsystems, Wetzlar
Refrigerated circulator, Minichiller	Huber, Offenburg

Multichannel pipette Discovery 1-10 µL	HTL Lab Solutions, Warsaw
Multichannel pipette Discovery 20-200 µL	HTL Lab Solutions, Warsaw
Multichannel pipette Transferpette 2-20 µL	Brand GmbH, Wertheim
OptimaTM TLX Ultracentrifuge	Beckmann, Munich
PCR cycler Mastercycler	Eppendorf
PCR cycler Mastercycler gradient	Eppendorf
pH meter model Φ 350 pH/Temp/mV Meter	Beckman
Pipette Eppendorf Research	Eppendorf
Pipette Gilson Pipetman P10, P20, P100, P200, P1000	Gilson, Middleton
Pipetting robot Lissy	Zinsser Analytic, Frankfurt
Precision scale ABT 120-5 DM	Kern & Sohn, Balingen
Precision scale AJ100	Mettler-Toledo, Giessen
Precision scale SBC 22	Scaltec Instruments, Göttingen
Scale 474-32	Kern & Sohn
Scale Bosch PE626	Bosch & Sohn, Jungingen
Shaker Heidolph Unimax 2010	MAGV GmbH
Spectrophotometer BioPhotometer	Eppendorf, Hamburg
Spectrophotometer Genesys 10 UV scanning	Thermo Scientific
Spectrophotometer NanoDrop ND-1000	Thermo Scientific
Spectrophotometer U-2001	Hitachi, Schwäbisch Gmünd
Stereomicroscope M165 C	Leica Mikrosysteme, Wetzlar
Stereomicroscope SMZ1000	Nikon GmbH, Düsseldorf
Tecan infinite M 200 multiplate reader	Tecan, Männedorf, Switzerland
Ultrasound device (GM 2070; UW 2070; SH 706; MS 73)	Bandelin Electronic, Berlin
Ultrasound waterbath Sonorex RK100	Bandelin Eletronic
UV/VIS-Spectrophotometer Beckman DU® 650	Thermo Scientific, Dreieich
Vacuum pump Vacubrand CVC 3000	VWR
Vortex mixer MS2 Minishaker	IKA Werke
Water bath IKA HB 10 basic	IKA Werke
Western blot Trans-Blot SD semi-dry transfer cell	BioRad
X-ray cassette IEE 60406	Rego X-Ray GmbH, Augsburg

2.2 Chemicals

Chemical	Company
ABTS (2,2'-Azino-di-(3-ethylbenzthiazoline-6-sulfonic acid)	Sigma
Acetic acid	Roth
Acrylamide/Bisacrylamide (Rotiphorese Gel 30 (37.5:1))	Roth, Karlsruhe
S-Adenosylmethionine chloride	Sigma
Agar-agar	Roth
Agarose (peqGold Universal Agarose)	Roth
5-Amino-2,3,-Dihydro-1,4,-Phthalazinedione (Luminol)	Sigma, Steinheim
6-Aminohexanoic acid	Merck, Hohenbrunn
Δ-Aminolevulinic acid	Sigma
Ammonium molybdate tetrahydrate	Sigma
Ammonium persulfate (APS)	Roth
L-Ascorbic acid	Sigma
ATP (Adenosine triphosphate)	Boehringer, Mannheim
Bradford reagent (BioRad Protein Assay)	BioRad
Bromophenol blue	Sigma
Bovine serum albumin (BSA)	Roth
Calcium chloride	Roth
Carbenicillin	Roth
β-carotene	Sigma
CHAPS (3-[(3-Cholamidopropyl)dimethylammonio]-1-propanesulfonate)	Roth
Citric acid	Sigma
Coomassie Brilliant Blue R250	Sigma
Cumaric acid	Sigma
Cystatin	Sigma
DMSO (Dimethyl sulfoxide)	Roth
DNaseI	Roth
DTNB (5,5'-dithiobis-2-nitrobenzoic acid), Ellman's reagent	Roth
DTT (Dithiotreitol)	Roth
EDTA•2Na•2H2O (Ethylenediaminetetraacetic acid)	Roche, Mannheim
Ethanol	Roth
Ethidium bromide	Roth
Glycerol	Roth
GSH (glutathione)	Sigma
GSSG (glutathione disulfide)	Roche

HCl (fuming, 37%)	Roth
HEPES (2-(4-(2-Hydroxyethyl)- 1-piperazine)-ethanesulfonic acid)	Roth
Hydrogen peroxide	Roth
Iodoacetamine (IAA)	Sigma
Imidazole	Roth
IPTG (Isopropyl-β-D-1-thiogalactopyranoside)	Roth
Isopropanol	Roth
Kanamycin sulfate	Roth
Magnesium chloride	Sigma
2-Mercaptoethanol	Sigma
MES (2-(N-Morpholino)-ethanesulfonic acid)	Roth
Methanol	Roth
L-Methionine	Serva Feinbiochimica, Heidelberg
S-methyl methanethiosulfonate (MMTS)	Sigma
Milk powder	Roth
MPD (2-methyl-2, 4-pentanediol)	Roth
Nicotinamide adenine dinucleotide phosphate, reduced, NADPH	Biomol
Ni-NTA agarose (nickel nitrilotriacetic acid)	Invitrogen, Karlsruhe
PEG (Polyethylene glycol)	Sigma
Pepstatin A	Sigma
PMSF (Phenylmethanesulfonylfluoride)	Roth
Polyethylene glycol 550	Sigma
Ponceau S	Sigma
Potassium chloride	Roth
Potassium dihydrogen phosphate	Roth
Di-potassium hydrogen orthophosphate	Roth
Potassium hydroxide	Roth
Rhamnose	Becton Dickinson, Heidelberg
Rubidium chloride	Roth
Select Agar®	Invitrogen
Sodium acetate	Roth
Sodium chloride, NaCl	Roth
Sodium citrate	Sigma
Sodium dodecyl sulfate (SDS)	Sigma
Sodium hydroxide, NaOH	Roth
TAPS (N-tris(Hydroxymethyl)methyl-3-aminopropanesulfonic acid sodium-potassium salt)	Sigma
TEMED (N, N, N', N'-tetramethylethylenediamine)	Sigma
TRIS (Tris-(hydroxymethyl)-aminomethane)	Roth

Triton X-100	Sigma
Tryptone/Peptone	Roth
TWEEN 20 (Polyethylene glycol sorbitan monolaurate)	Sigma
Yeast extract	Oxoid LTD, Basingstdoke Hampshire
Zinc sulfate heptahydrate	Sigma

2.3 Consumables

Consumables	**Company**
Cannula 0.7 x 50 mm	Unimed, Lausanne
Centriprep YM-30	Millipore, Eschborn
Cover slips, round 21 mm Ø	Menzel, Brunswick
Crystallization plate 24 well, VDX plate	Hampton Research, Aliso Viejo, California, USA
Cuvettes, polystyrol	Sarstedt, Numbrecht
Cuvettes, micro, UV	Brand
Semi-micro cuvettes 10x4x45 mm, polystyrol	Sarstedt
HRP (horseradish peroxidase) anti-mouse antibody	Thermo Scientific
DNA ladder GeneRuler 1 kb	Thermo Scientific
DNA dye NonTox	Applichem GmbH, Darmstadt
Electroporation cuvette Gene Pulser 0.2 cm	Bio-Rad Laboratories, Munich
Falcon™ tube 15 mL, 50 mL	Greiner Bio-One, Frickenhausen
High performance chemiluminescence film Amersham hyperfilmTMECL	GE Healthcare, Freiburg
Glass capillaries 5 µL	Brand GmbH, Wertheim
Membrane filter ME 25, 0.45 µM	Whatman GmbH, Dassel
Micro pipettes	Brand, Wertheim
Microplate 96 well, PP, V-bottom, transparent	Greiner Bio-One
Microplate 96 well, PP, half area, flat bottom, clear	Greiner Bio-One
Microscope lens paper	Glaswarenfabrik Karl Hecht, Sondheim
Mouse anti-His antibody	Dianova, Hamburg
Multiply PCR tube 0.2 Ml	Sarstedt
NAPTM-5 Column Sephadex™ G-25 DNA Grade	GE Healthcare
Parafilm 'M' laboratory film	Pechiney Plastic Packaging, Menasha USA
Pasteur pipette 150 mm	Hirschmann Laborgeräte, Eberstadt
Peleus ball	Deutsch & Neumann, Berlin
Petri dish, 15 cm Ø	Sarstedt, Nümbrecht
Pipette tips and tubes, disposable	Eppendorf
Pipette tips Omnitip FastRack 10 µL, 200 µL	Ulplast, Warsaw

Protein ladder unstained protein MW marker	Fermentas
Protein ladder pre-stained MW marker	Fermentas
PVDF membrane	Roth, Karlsruhe
Serological pipette 5, 10, 25 mL	Greiner Bio-One
Silicone oil 550	Merck, Darmstadt
Sterile filters 0.2 µm FP030	Schleicher & Schull, Kassel
Syringe 1 mL Plastipak	Becton Dickson, Madrid
Syringe 10 mL	B. Braun, Melsungen
24 wells 1,7x1,6 cm MP	Biochemicals Inc., U.S.A
Vivaspin 20, 3,000 MWCO, 10,000 MWCO and 30,000 MWCO	Sartorium Stedim Biotech, Göttigen
Zeba™ Desalt Spin Columns	Thermo scientific, Rockford, USA

2.3.1 Electrophoresis marker

Ladder	Company
GeneRuler 1 kb DNA ladder	Fermentas, St. Leon-Rot
6x Loading dye solution	Fermentas, St. Leon-Rot
PageRuler™ prestained protein ladder	Fermentas, St. Leon-Rot
SpectraTM multicolor broad range protein ladder	Fermentas, St. Leon-Rot
Protein molecular weight marker	Fermentas, St. Leon-Rot

2.3.2 Kits

Kit	Company
Bradford assay kit	Bio-Rad, Munich
QIAprep spin miniprep kit	Qiagen, Hilden
QIAquick PCR purification kit	Qiagen, Hilden
Silver staining kit	Pierce, Rockford

2.4 Buffers and Solutions

2.4.1 Stock solutions

Stock solution	Composition
APS	10% (w/v) in ddH_2O, storage at –20 °C
Carbenicillin	50 mg*mL^{-1} in 50% (v/v) EtOH, storage at –20 °C
Chloramphenicol	35 mg*mL^{-1}, 100% EtOH, storage at -20 °C
Cystatin	40 µM in US buffer, storage at –20 °C
DTT	200 mM in ddH_2O, storage at –20 °C
IPTG	1 M in ddH_2O, sterile filtration 0.2 µm, storage at –20 °C
Kanamycin	25 mg*mL^{-1} in ddH_2O, sterile filtration 0.2 µm, storage at –20 °C
Pepstatin	0.3 mg*mL^{-1} in US buffer, storage at –20 °C
PMSF	100 mM in DMSO, storage at 23 °C

2.4.2 Buffer for molecular biology

Buffer	Composition
DNA sample buffer 6x	0.1% bromophenol blue 60% saccharose 1 mM Tris pH 8.3, HCl adjusted
TBE buffer 5x	89 mM Tris 89 mM boric acid 2 mM EDTA pH 8.3, HCl adjusted
TFB1 buffer for chemocompetence	100 mM rubidium chloride 30 mM manganese chloride 30 mM potassium acetate 10 mM calcium chloride 15% glycerol pH adjusted to 5.8 with HCl, sterile filtered
TFB2 buffer for chemocompetence	10 mM MOPS 10 mM rubidium chloride 75 mM calcium chloride pH 8.0 adjusted with KOH, steril filtered

2.4.3 Buffer for Ni-NTA-affinity chromatography

Buffer	Composition
Elution buffer (*E. coli*) rMscDyP1	50 mM Tris 300 mM NaCl, pH 8.0 with 20 mM 200 mM or 500 mM imidazole
Elution buffer PfalMAT	50 mM Tris 300 mM NaCl, pH 8.0 with 50 mM, 100 mM or 500 mM imidazole
Elution buffer hMAT1a	50 mM Tris 300 mM NaCl, pH 8.0 with 50 mM, 200 mM or 500 mM imidazole
Tris buffer	300 mM NaCl 50 mM Tris, pH 8.0
US buffer	50 mM Na_2HPO_4, pH 8.0 300 mM NaCl

2.4.4 Buffer for electrophoresis

Buffer	Composition
Stacking gel buffer	0.5 M Tris, pH 6.8
Separating gel buffer	1.5 M Tris, pH 8.8
SDS chamber buffer	192 mM glycine
	25 mM Tris-HCl, pH 8.3
	0.1% (w/v) SDS
SDS sample buffer 1x	12.5 mL stacking gel buffer
	25 mL glycerin
	20 mL 10% (w/v) SDS
	2 mL 0.5% (w/v) bromophenol blue
	35 mL H_2O
	storage at room temperature
	before usage 5% (v/v) 2-ME added
SDS sample buffer 4x	3 mL stacking gel buffer
	300 mg DTT
	400 mg SDS
	2 mL glycerin
	tip of a spatula bromphenol blue
Coomassie staining	0.2% (w/v) Coomassie Brilliant Blue R250
	40% (v/v) 2-propanol
	10% (v/v) acetic acid
Coomassie destaining	7% (v/v) acetic acid
	5% (v/v) ethanol

2.4.5 Buffer for semi-dry Western blot

Buffer	Composition
Anode buffer I	300 mM Tris
Anode buffer II	25 mM Tris
Cathode buffer	40 mM 6-Aminohexanoic acid
TBS	10 mM Tris
	55 mM NaCl, pH 7.4, adjusted with HCl (aq)
TBST	10 mM Tris
	155 mM NaCl
	0.05% (v/v) TWEEN 20, pH 7.4
Ponceau S staining	1% (w/v) Ponceau S
	5% (v/v) acetic acid
Ponceau S destaining	1% (v/v) acetic acid
Luminol	1.25 mM luminol
	0.0093% (v/v) H_2O_2
	0.1 M Tris-HCl, pH 8.6

2.4.6 SDS gels

Gel	Composition
15% separating gel (4 gels)	3.6 mL ddH_2O 3.75 mL separating gel buffer 7.5 mL acrylamide/bisacrylamid (30% (v/v)) 0.15 mL SDS (10% (w/v)) 75 µl APS (10%) 7.5 µl TEMED
12% separating gel (4 gels)	5.1 mL ddH_2O 3.75 mL separating gel buffer 6 mL acrylamide/bisacrylamid (30% (v/v)) 0.15 mL SDS (10%) 75 µL APS (10%) 7.5 µL TEMED
4% stacking gel (4 gels)	3.05 mL ddH_2O 1.25 mL stacking gel buffer 0.65 mL acrylamide/bisacrylamid (30% (v/v)) 0.05 mL SDS (10%) 25 µL APS (10%) 5 µL TEMED

2.4.7 Assay buffer and solutions

Assay solution	Composition
Ammonium molybdate assay	
Ascorbic acid solution	12% (w/v) ascorbic acid in 12 N HCl
Ammonium molybdate solution	2% (w/v) ammonium molybdate tetrahydrate in ddH_2O
Stop solution	3% (w/v) sodium citrate tribasic dehydrate, 2% (w/v) sodium acetate in ddH_2O
Assay buffer	100 mM TAPS pH 8.4, 100 mM KCl, 20 mM $MgCl_2$ in ddH_2O
ABTS assay	
Assay buffer	25 mM sodium acetate pH 3.5
ABTS	2 mM in 25 mM sodium acetate pH 3.5
H_2O_2	1 mM in 25 mM sodium acetate
Carotene assay	
Assay buffer	50 mM sodium acetate pH 3.5
β-carotene solution	app. 0.18 mM in ddH_2O
H_2O_2	0.5 mM in ddH_2O

2.4.8 Medium for bacterial cell culture

Medium	Composition
Lysogeny broth (LB)	10 g*L^{-1} NaCl
	10 g*L^{-1} tryptone
	5 g*L^{-1} yeast extract
Terrific Broth (TB)	12 g*L^{-}1 tryptone
	24 g*L^{-1} yeast extract
	4 mL glycerol
	2.2 g*L^{-1} KH_2PO_4
	9.4 g*L^{-1} K_2HPO_4
2xYT	5 g*L^{-1} NaCl
	16 g*L^{-1} tryptone
	10 g*L^{-1} yeast extract

The medium was autoclaved for 30 minutes at 120 °C in 1 L Erlenmeyer flasks for protein expression or in 50 mL Erlenmeyer flasks and 1 mL culture tubes for overnight precultures.

2.5 Enzymes

2.5.1 Restriction enzymes

Enzyme	Company	Restriction site
NcoI	Thermo Scientific	5'...C^CATGG...3'
XhoI	Thermo Scientific	5'...C^TCGAG...3'
NdeI	Thermo Scientific	5'...CA^TATG...3'
DpnI	Thermo Scientific	5'...GA^{-CH3}^TC...3'
EcoRI	Thermo Scientific	5'...G^AATTC...3'
PstI	Thermo Scientific	5'…CTGCA^G...3'
PaeI	Thermo Scientific	5'…GCATG^C...3'

2.5.2 Enzymes for molecular biology

Enzyme	Company
Pfu DNA polymerase	Promega, Mannheim
RedTaq® polymerase	Sigma
T4 ligase	Fermentas, St. Leon-Rot

2.5.3 Recombinant enzymes

Enzyme	Expression system
PfalMAT	pQE30, *E.coli* M15 cells
PfalMAT^{C52S}	pQE30, *E.coli* M15 cells
PfalMAT^{C113S}	pQE30, *E.coli* M15 cells
PfalMAT^{C187S}	pQE30, *E.coli* M15 cells
(*E. coli*) rMscDyP1	pET28 a, *E.coli* BL21 cells
(*E. coli*) rMscDyP1^{C360G}	pET28 a, *E.coli* BL21 cells
(*E. coli*) rMscDyP1 $^{M302K, M305K}$	pET28 a, *E.coli* BL21 cells
(*A. niger*) rMscDyP1	MaxiBright®, source: DSM (Delft, The Netherlands)

2.6 Cloning and expression vectors

Vector	Properties
pEX K	Kanamycin resistance, lac promotor,
pET28 a(+)	Kanamycin resistance, T7 promotor, His-tag coding sequence, T7 tag coding sequence, lac I coding sequence, T7 terminator
pQE30	Carbenicillin resistance, T5 promotor, His-tag coding sequence,lac operator,
pG-Tf2	Chloramphenicol resistance, tetracycline resistance, Pzt1 promotor

2.7 E. coli cells

Strain	Genotype
XL-1 blue	F'::Tn10 proA^{+}B^{+} lacI^{q} Δ(lacZ)M15/recA1 endA1 gyrA96 (NaI^{R}) thi hdgR17 (rK^{-} mK^{+}) glnV44 relA1 lac
BL21 (DE3)	*E. coli* B F^{-} dcm *omp* T *hsd*S(r$_{B}^{-}$ m$_{B}^{-}$) gal λ(DE3)
Single step (KRX) Competent cells	[F', traD36, Δ*omp*P, proA^{+}B^{+}, lacI^{q}, Δ(lacZ)M15] Δ*omp*T, endA1, recA1, gyrA96(Nal(r)), thi^{-}1, *hsd*R17 (r(k)$^{-}$, m(k)$^{+}$), e14^{-} (McrA^{-}), relA1, supE44, Δ(lac- proAB), Δ(rhaBAD)::T7 RNA polymerase
M15	nalS, StrS, rifS, KmR, lac^{-}, ara^{-}, gal^{-}, mtl^{-}, F^{-}, recA^{+}, uvr^{+}

2.8 Protein crystallization screens

Screen	Company
Crystal screen I	Hampton Research, Aliso Viejo, USA
Crystal screen II	Hampton Research, Aliso Viejo, USA

2.9 Oligonucleotides

Oligonucleotide	**Sequence (5'-3')**
Primer for PCR amplification of PfalMAT	
N-terminal	ACGCGCATGCAGTCAGTTGAAAATTAAAAGAGG
C-terminal	ACGCCTGCAGTTAATTTTTTAATGCATTTTTTTCG
Sequencing primer (*E. coli*) rMscDyP1	
OMSPs	TCATGAACACTTTGGCTTTATG
OMSPs1	CAGCGGAACAATAACTTTGAC
OMSPr	TCTCGGCATCAGTAACTTCC
Primer for site-directed mutagenesis	
PfalMAT^{C52S}s	GCAAGGTTGCATGTGAAGTAAGTGCTAAAAAG
PfalMAT^{C52S}as	CTTTTTAGCACTTACTTCACATGCAACCTTGC
PfalMAT^{C113S}s	[Phospho]TGATATAGCTCAAAGTGTACATGAAAATAG
PfalMAT^{C113S}as	[Phospho]CTATTTTCATGTACACTTTGAGCTATATCA
PfalMAT^{C187S}s	[Phospho]GAATAAGGGTAGTAGTGGTGGACATT
PfalMAT^{C187S}as	[Phospho]AATGTCCACCACTACTACCCTTATTC
OMSPCs	GAATCAGACACGCGGCCCTTTTAGTGC
OMSPCas	GCACTAAAAGGGCCGCGTGTCTGATTC
OMSPMs	CCATGCTCTGAACAAGCCGAATAAGACCTCCGAA
OMSPMas	TTCGGAGGTCTTATTCGGCTTCAGAGCATGG

2.10 Software

Software	**Webpage**
GraphPad Prism 6	(http://www.graphpad.com/)
IBM SPSS Statistics 19	
ChemDraw 15.0	(http://www.cambridgesoft.com)
UCSF Chimera 1.10.1	(http://www.cgl.ucsf.edu/chimera/)
MOE 2013	(http://www.chemcomp.com)
Gold 5.2	(http://www.ccdc.cam.ac.uk)
Clustal Ω 1.2.1	(http://www.ebi.ac.uk)
XDS	(xds.mpimf-heidelberg.mpg.de)

3 METHODS

3.1 General methods

3.1.1 Molecular biological methods

2.3.1.1 Plasmid preparation

Plasmid DNA was purified with plasmid miniprep kits (Qiagen, Promega) following the instructions of the manufacturer. Briefly, after alkaline lysis of a bacterial over-night culture of a transformed *E. coli* strain containing the desired plasmid, neutralization, and centrifugation of bacterial chromosomal DNA and proteins, the plasmid DNA in supernatant was purified with a silica membrane column.

2.3.1.2 Determination of DNA concentration

DNA concentration was determined spectrophotometrically at 260 nm using an Eppendorf biophotometer and UV cuvettes or NanoDrop. The purity of DNA was examined using absorbance ratios from 260 nm to 280 nm, which should range between 1.6 and 1.8.

2.3.1.3 Agarose gel electrophoresis

An agarose gel electrophoresis was performed in order to separate and analyze DNA mixtures by size of the DNA fragments. Therefore, a DNA sample, e.g. a PCR product or restriction digested plasmid DNA, was mixed with a 6 x loading buffer and applied onto an 0.7-1.0% agarose gel (prepared in 1 x TBE buffer). DNA was separated electrophoretically in 1 x TBE running buffer for 40 minutes at 100 V. A 1 kb DNA ladder was used to estimate the size of the DNA bands. Gels were incubated with 1 $\mu g*mL^{-1}$ ethidium bromide, which intercalates in the DNA, for 20 minutes, and DNA bands were visualized using UV light (254 nm).

2.3.1.4 Restriction digest

In order to subclone genes into desired expression vectors, plasmid DNA was digested using two or more restriction enzymes to generate ends compatible to the ends of a desired insertion fragment, which was synthesized commercially, with respective restriction enzyme recognition sites. Chapter 2.5.1 summarizes restriction enzymes used within this dissertation.

2.3.1.5 Ligation

After purification, the desired plasmid and the plasmid containing the target gene were digested with the same restriction enzymes and ligated using T4-DNA ligase for one hour at 23 °C.

3.1.2 Microbiological methods

All working steps with *E. coli* were performed in a clean, sterile environment near a flame using autoclaved culture media and autoclaved or ethanol-bathed, flame-sterilized instruments.

2.3.2.1 Preparation of competent *E. coli* cells

Chemo competent *E. coli* cells were prepared as follows: an aliquot of respective cells from a glycerine stock culture stored at –80 °C, was streaked onto an agar plate containing either no antibiotic or an antibiotic if the cell exhibited antibiotic resistance, as in the case of M15 cells resistant to kanamycin, and incubated overnight at 37 °C. A colony was transferred to 10 mL LB medium, either without an antibiotic or with kanamycin in the case of M15 cells and grown overnight at 37 °C. This pre-culture was diluted 1:10 with prewarmed LB medium to a total volume of 100 mL in a 250 mL Erlenmeyer flask and incubated at 37 °C until an optical density at 600 nm (OD_{600}) of 0.7 was reached. The flask was placed on ice for five minutes then the culture was centrifuged for five minutes at 3,000 rpm. The supernatant was discarded, and the cells were resuspended in 30 mL TFB1 buffer containing 100 mM rubidium chloride and 10 mM calcium chloride and incubated on ice for 90 minutes. After centrifugation for five minutes at 2,000 rpm the supernatant was discarded and the cells were resuspended in TFB2 buffer containing 10 mM rubidium chloride and 75 mM calcium chloride. Aliquots of 125 µL were frozen in liquid nitrogen and stored at -80 °C.
Electrocompetent *E. coli* cells were purchased from Invitrogen.

2.3.2.2 Transformation

Chemically competent *E. coli* cells were incubated on ice for 30 minutes with the desired plasmid DNA containing the gene of interest. After heat shock for 30 seconds at 42 °C, cells were allowed to rest for five minutes on ice before incubation at 37 °C in LB medium for one hour and streaking it onto an LB agar plate. The plates were incubated at 37 °C overnight and then stored at 4 °C until inoculation for heterologous gene overexpression.
Electrocompetent *E. coli* cells were transformed with a desired plasmid using 0.2 mm Gene Pulser Cuvettes® (Bio-rad) and Gene Pulser Xcell® Electroporation System (Biorad) using the pre-set protocol for *E. coli* cells, which induces an electrical field for 5 ms at ~3000 V, and ~750 Ω. Immediately after electroporation 1 mL LB medium was added to the cells followed by incubation at 37 °C for one hour before streaking it onto an LB agar plate.

2.3.2.3 Heterologous overexpression in *E. coli*

A single colony of transformed *E. coli* cells was inoculated into 3 mL LB medium containing the respective antibiotic and grown at 37 °C for eight hours in a shaking incubator. 50 mL rich medium containing antibiotics were inoculated with the 3 mL preculture and were allowed to grow overnight at 37 °C. One liter of a rich medium containing the respective antibiotics was inoculated with the 50 mL pre-culture and grown until mid or late log phase, controlled via measurement of OD_{600}, at room temperature (23 °C) or 37 °C depending on the optimal expression conditions, following induction of gene expression with isopropyl-β-D-1-thiogalactopyranoside (IPTG). After induction, cells were grown for four to 48 hours at optimal expression temperature.

2.3.2.4 Cell harvest

E. coli cells were harvested via centrifugation for 15 minutes at 6,800 g and cell pellets were resuspended in buffer (50 mM Tris and 300 mM NaCl at pH 8.0) containing 100 µM PMFS, 150 nM pepstatin and 40 nM cystatin and then stored at -20 °C.

3.1.3 Protein biochemical methods

2.3.3.1 Protein purification

For protein purification, cell pellets were thawed and stirred with 10 µg*mL^{-1} cell culture lysozyme and 2 µg*mL^{-1} DNaseI on ice for 30 minutes for chemical cell lysis. Afterwards, cells were mechanically lysed four times for 20 seconds via ultrasound. Cell debris was centrifuged for 30 minutes at 25,279 g.

Immobilized metal ion affinity chromatography

PfalMAT and its cysteine mutants as well as (*E. coli*) rMscDyP1 and its mutants contained an N-terminal His_6-tag that allowed for the purification of these enzymes from the supernatant via Ni-NTA affinity chromatography. Therefore, the supernatant containing the soluble fractions after cell disruption was applied onto a 1.5 mL Ni-NTA-column, which was previously equilibrated with 50 mM Tris and 300 mM NaCl, pH 8.0. The column was washed with ten column volumes of the same buffer in order to remove nonspecifically bound proteins, and then the His-tagged protein was eluted with increasing concentrations of imidazole (20-500 mM) from the Ni-NTA column.

Preparative and analytical gel filtration chromatography

Gel filtration experiments were conducted using native gel filtration by a HiLoad 16/60 superdex 200 prep grade gel filtration column connected to an ÄKTA/Unicorn FPLC system (GE Healthcare). The column was calibrated using a low and high molecular weight standard kit (GE Healthcare). Before applying samples, the column was equilibrated with buffer (50 mM Tris, 300 mM NaCl, pH 8.0). Eluted fractions of the Ni-NTA affinity chromatography containing the protein, identified via SDS PAGE or Western blot, were pooled and concentrated using a Vivaspin® 20 with 30,000 MWCO (Sartorius) to a final volume of 1 mL and loaded onto the gel filtration column. Proteins were eluted at a flow rate of 1 mL*min^{-1} in a volume of 2 mL and detected spectrophotometrically at 280 nm. Areas under the peak were calculated using Unicorn 4.11 software (GE Healthcare). Pure fractions containing the respective enzyme were pooled and stored at 4 °C.

2.3.3.2 Determination of protein concentration

The protein concentration was determined by measuring the absorbance at 280 nm and using the Bradford assay (Bradford, 1976). The standard curve was prepared using 0-20 µg*mL^{-1} bovine serum albumin.

2.3.3.3 Gel electrophoresis

Denaturing sodium dodecyl sulfate-polyacrylamide gel electrophoresis (SDS-PAGE) was performed in order to separate proteins based on their molecular weights. SDS denatures and coats proteins and gives them a negative charge proportional to their molecular weight; thus proteins migrate in an electric field towards the positively charged electrode and are fractionated by size (Laemmli, 1970). Therefore, 4 x reducing SDS sample buffer containing DTT was added to the protein mixture and samples were boiled for five minutes at 95 °C in order to denature the proteins. Under a constant 200 V, proteins migrated through the gel for 40 minutes. Gels were stained using Coomassie Brilliant Blue R250 in 40% (v/v) 2-propanol and 10% (v/v) acetic acid for ten minutes at room temperature (23 °C) after briefly heating using a microwave. Afterwards, gels were destained using a mixture of 5% (v/v) ethanol and 7% (v/v) acetic acid for ten minutes at 23 °C after heating them in a microwave. If a Western blot analysis was performed, the gels were not stained but were directly used for blotting.

2.3.3.4 Protein immunoblotting

Western blot analysis was used to detect either His-tagged proteins or protein modifications including protein-*S*-glutathionylation or protein-*S*-nitrosylation using specific antibodies. Using semi-dry Western blot, proteins that had been previously separated by size via SD*S*-PAGE were electrophoretically transferred to a polyvinylidene fluoride (PVDF) membrane. In detail, five filter papers were soaked in cathode buffer, three filters paper were soaked in anode buffer I, and two filter papers in anode buffer II for 15 minutes. A PVDF membrane was activated via incubation in 100% methanol for one minute and then soaked in anode buffer II for a few minutes. The graphite plates of the blot device were saturated with ddH_2O. The SDS gel was soaked in cathode buffer for a few minutes before packing the blot. The blot sandwich was packed into the transfer cassette from cathode to anode with five filter papers from cathode buffer, followed by the SDS gel, the PVDF membrane, two filter papers from anode buffer II, and three filter papers from anode buffer I. Proteins were transferred from SDS gel to PVDF membrane at a constant current of 41 mA and 180 V per gel for 55 minutes. After blotting, the PVDF membrane was stained for blotting control with Ponceau S for one minute and destained with 1% (v/v) acetic acid until the protein bands appeared. Afterwards, the PVDF membrane was washed using TBST solution until all bands disappeared. The membrane was blocked with either 5% (w/v) non-fat milk or 5% (w/v) bovine serum albumin, depending on the primary antibody, for one hour at room temperature or overnight at 4 °C. Afterwards, the membrane was washed three times for five minutes with TBST before incubation with the primary antibody, i.e. mouse-anti-His-tag antibody (1:1,000) or mouse-anti-GSH antibody (1:500), for one hour at room temperature or overnight at 4 °C. After incubation with the primary antibody, the membrane was washed three times for five minutes with TBST, and then incubated with the secondary antibody, i.e. anti-mouse IgG HRP-antibody (1:20,000), for one hour at room temperature and then washed three times for five minutes with TBST. Since the secondary antibody is coupled to a horseradish peroxidase (HRP), antibody-labeled proteins can be visualized by incubating them for one minute with a mixture of 10 µL cumaric acid and 1 mL ECL-kit containing luminol, which is oxidized by HRP, thereby leading to chemiluminescence that can be detected with an x-ray film.

3.2 PfalMAT methods

3.2.1 Molecular biological methods

The gene of PfalMAT was previously amplified via PCR from a *P. falciparum* 3D7 gametocyte cDNA library by using primers that contained restriction sites for PaeI and PstI (Chapter 2.5.1). It was then cloned into the pHSG389 vector and subcloned into pQE30 using the respective restriction enzymes. In a master thesis written in parallel to this dissertation the gene of a human counterpart of PfalMAT, hMAT1a, was synthesized commercially and cloned into the pET28a vector for heterologous overexpression in *E. coli* KRX cells (Gehr, 2014).

3.2.2 Site-directed mutagenesis

In a master thesis written prior to this dissertation selected cysteine residues Cys113 and Cys187 of PfalMAT were mutated to serine via site-directed mutagenesis (Eisenkolb, 2008). For this dissertation, site-directed mutagenesis via PCR was used to introduce the C52S mutation into the PfalMAT gene (Table 1) by using Pfu polymerase with pQE30 containing the PfalMAT gene as a template and oligonucleotide primers (0) containing the mutated codon.

Table 1: Mutagenesis PCR for PfalMAT^{C52S}

Reaction mix	
Template DNA	1 µL (176 ng*µL^{-1})
Forward primer	1 µL (100 pmol*µL^{-1})
Reverse primer	1 µL (100 pmol*µL^{-1})
dNTP mix	1 µL (10 mM)
10x Pfu buffer	5 µL
Pfu polymerase	1 µL (3 U*µL^{-1})
Sterile H_2O	40 µL
PCR program	
Denaturation	90 s 94 °C
Cycles	18
Denaturation	30 s 94 °C
Annealing	60 s 60 °C
Elongation	11 min 68 °C
Final elongation	13 min 68 °C

The PCR reaction was validated on an agarose gel and purified using the QIAquick PCR purification kit. The non-mutated, methylated template plasmid was digested with DpnI. Clones containing the correct mutation were confirmed at an in-house sequencing facility.

3.2.3 Heterologous overexpression of PfalMAT

Genes of PfalMAT, PfalMAT^{C52S}, PfalMAT^{C113S}, and PfalMAT^{C187S} were heterologously overexpressed in *E. coli* M15 cells in pQE30, adding an N-terminal His_6-tag to the recombinant proteins. Cells were grown in 2xYT medium containing 50 µg*mL^{-1} kanamycin and 100 µg*mL^{-1} carbenicillin at 37 °C until an optical density (OD_{600}) of 0.5. Temperature was decreased to 23 °C prior to induction of gene expression with 0.2 mM IPTG at an OD_{600} of 0.8 was reached. After induction, cells were grown for 48 hours at 23 °C.

3.2.4 Ammonium molybdate assay

The enzymatic activity of PfalMAT, the cysteine mutants, and the human counterpart hMAT1a were determined using a spectrophotometric colorimetric endpoint assay, which was published to determine glutamine synthetase activity in a microplate format (Gawronski *et al.*, 2004) and adapted for PfalMAT in my master thesis prior to this dissertation (Pretzel, 2011). The basic principle of this assay is the detection of inorganic phosphate with ammonium molybdate. PfalMAT catalyzes the formation of SAM from ATP and L-methionine by forming tripolyphosphate which is subsequently hydrolyzed to pyrophosphate and orthophosphate. The inorganic phosphate reacts with ammonium molybdate and the reducing agent ascorbate to form a colored phosphomolybdate complex, which was measured spectrophotometrically at 655 nm. The assay was performed in 96-well plates and measures in a multiplate reader (Tecan infinite M200). Controls lacking the enzyme were subtracted from the absorbance. The activity of PfalMAT was determined according to the release of inorganic phosphate using the linear function (y = ax + b) of a phosphate standard curve with 0-800 µM K_2HPO_4:

$$P_i\ [\mu M] = \frac{y-b}{a}$$

The volume activity was calculated taking the 10 minutes incubation time and dilution factor (D) into account and then the specific activity corresponding to the enzyme concentration was calculated:

$$\text{Volume activity } [\mu mol*min^{-1}*mL^{-1}] = \left(\frac{\mu mol\ Pi}{1000\ mL*10\ min}\right) * D$$

$$\text{Specific activity } [\mu mol*min^{-1}*mg^{-1}] = \left(\frac{\mu mol}{min*mL}\right) * \left(\frac{mL}{mg}\right)$$

Table 2: Ammonium molybdate assay

Volume	Reagent
25 - x µL	100 mM TAPS, pH 8.4, 100 mM KCl, 20 mM $MgCl_2$
5 µL	10 mM ATP in ddH_2O ad 2 mM
5 µL	5 mM L-methionine in ddH_2O ad 1 mM
x µL	PfalMAT/PfalMAT^{C52S}/PfalMAT^{C113S}/PfalMAT^{C187S}
	10 min, 37 °C
25 µL	1% (w/v) ammonium molybdate in ddH_2O
50 µL	12% (w/v) L-ascorbic acid in 1 N HCl
	5 min, 23 °C
75 µL	2% acetic acid, 2% sodium acetate in ddH_2O
	15 min, 23 °C

3.2.5 Enzyme kinetics

Steady state kinetic parameters K_M and V_{max} were determined by varying one of the substrates, with the second substrate constantly fixed at assay concentration, plotting the reaction velocity against the substrate concentration, and fitting it to the Michaelis-Menten equation by using the software GraphPad Prism. For PfalMAT, the respective cysteine mutants, and hMAT1a, the K_M for ATP was determined in the presence of 10-2,500 µM ATP and 1 mM L-methionine, whereas the K_M for L-methionine was determined by varying the L-methionine concentration from 10-2,500 µM while ATP was fixed at the assay concentration of 2 mM. Importantly, in order to determine ATP kinetic, a control lacking the enzyme was subtracted from the absorption because ATP itself contributes to color formation probably via P_i contamination of the reagent.

3.2.6 Protein-protein interactions

In order to study the role of the selected cysteine residues Cys52, Cys113, and Cys187 in redox regulation of PfalMAT, the interactions of their mutants with the redox-active proteins PfTrx1, PfGrx and PfPlrx were determined by using the ammonium molybdate assay and then compared to PfalMAT. Therefore, 1-20 µM redoxin was incubated with 1-5 µM PfalMAT or a mutant protein.

3.2.7 Protein-*S*-glutathionylation

The effect of protein-*S*-glutathionylation on the enzymatic activity and oligomerization behavior of PfalMAT was studied in detail by using protein immunoblots with an anti-GSH antibody, the ammonium molybdate assay, and gel filtration experiments. Therefore, reduced PfalMAT or the reduced cysteine mutants were incubated with up to 10 mM GSSG for five minutes at 37 °C and desalted prior to measurement in the ammonium molybdate assay in order to remove excess GSSG using Zebaspin Desalting Columns. For deglutathionylation experiments, 12 µM of glutathionylated enzyme was incubated either with the reducing agent DTT (20 mM) or with the reduced redox proteins PfTrx1, PfGrx and PfPlrx (0-70 µM).

3.2.8 Protein-*S*-nitrosylation

In a master thesis concurrent to this dissertation, Marina Gehr studied the protein *S*-nitrosylation of PfalMAT and PfalMAT^{C113S} with protein immunoblots using an anti-biotin antibody after a biotin switch assay and via enzymatic analysis using the ammonium molybdate assay (Gehr, 2014). For this dissertation, the effect of protein-*S*-nitrosylation on PfalMAT^{C52S} and PfalMAT^{C187S} was studied and compared to PfalMAT since the results for PfalMAT^{C113S} indicated that Cys113 is not *S*-nitrosylation's only target in PfalMAT. In detail, PfalMAT and the cysteine mutants were reduced with 5 mM DTT and desalted to remove excess DTT, and the activity in response to adding different concentrations of GSNO (0-800 µM) was determined relative to the enzyme without GSNO as a control using the ammonium molybdate assay.

3.2.9 Oligomerization studies

In order to study the oligomerization behavior of PfalMAT and the cysteine mutants, the enzymes were incubated with either 20 mM DTT or 5 mM GSSG prior to analytical gel filtration chromatography.

3.2.10 Molecular modeling

Dr. Karin Fritz-Wolf modeled the structure of PfalMAT, using the crystal structures of *Homo sapiens* MATA2 (2p02) and *Cryptosporidium hominis* (2odj) MAT as templates in the SWISS-MODEL automated comparative protein modeling server (Schwede *et al.*, 2003). The PfalMAT model was superimposed with other structures using the CCP4 software tool SSM. The insertion loop K184 to H190 was manually modeled with the interactive graphics program Coot (Emsley *et al.*, 2004). Finally, the geometry of the new model was minimized with PHENIX (Adams *et al.*, 2011).

3.2.11 Statistical analyses

Data were statistically analyzed using GraphPad Prism 6 software. The statistical test prerequisites, including balance of experimental design, Gaussian distribution, and homoskedasticity, were tested using automated GraphPad Prism functions and Bartlett's test, respectively. Group means as well as means within groups were compared at 95% confidence level using One-Way ANOVA or Two-Way ANOVA, as indicated at the respective positions in the results. If $p < 0.05$ *post hoc* testing was performed with Dunnett's test for comparing group means to the mean of control after One-Way ANOVA, or Bonferroni's test for comparing every mean to every other mean after One-Way or Two-Way ANOVA.

3.3 MscDyP1 methods

3.3.1 Molecular biological methods

The sequence of MscDyP1 was synthesized commercially (Eurofins MWG Operon) and provided in the pEX-K plasmid with a 5' NcoI and a 3' XhoI restriction site. Codon usage was optimized for *E. coli*. The construct is an N-terminally truncated form, lacking the putative targeting signal predicted by the program SignalP, starting at position 56. The construct was digested with XhoI, NcoI, and NdeI. The plasmid DNA was purified with the PureYield™ Plasmid Miniprep System (Qiagen) by following the manufacturer's instructions. Restriction enzyme digestion was confirmed with a 1% agarose gel. The gene was ligated into a pET28a vector (Novagen) and digested by XhoI and NcoI with T4 DNA ligase using the LigaFast™ Rapid DNA Ligation System (Promega) in accordance to the manufacturer's instructions. The construct was then transformed into *E. coli* BL21 cells. The clones obtained were digested with NcoI and XhoI for analysis. Possible positive clones were sequenced (DNA concentration: 85 $ng*\mu L^{-1}$, 260/280 ratio: 1.83) using sequencing primers obtained from Biolegio. An in-house sequencing facility confirmed the nucleotide sequence of a clone containing the (*E. coli*) rMscDyP1 gene, inserted into the pET28 a vector, by automated sequencing. This clone was selected for gene overexpression and site-directed mutagenesis.

The construct will be referred to as (*E. coli*) rMscDyP1 to distinguish it from the recombinant protein used for protein crystallization, which was produced in *A. niger* (rMscDyP1) and the wildtype expressed in *M. scorodonius* that was not used in this dissertation.

3.3.2 Site-directed mutagenesis

Site-directed mutagenesis of the single cysteine residue Cys306 of (*E. coli*) rMscDyP1 (which corresponds to Cys360 of native MscDyP1) was performed by substituting thymine from the cysteine codon (TGC) with guanine in order to obtain a triplet coding for glycine (GGC). Both methionine residues Met248 and Met251, which contribute to Met302 and Met305 of native MscDyP1, were substituted by replacing the thymine from the methionine codon (ATG) with adenine to obtain the triplet AAG coding for lysine, in a double mutation. PCR based site directed mutagenesis was carried out using Pfu polymerase with pET28a containing the (*E. coli*) rMscDyP1 gene as a template and oligonucleotide primers (0) containing the mutated codon, which were synthesized by Biolegio.

Table 3: Mutagenesis PCR for (*E. coli*) rMscDyP1

Reaction mix	C360G	M302K, M305K
Template DNA	0.5 µL (104 ng*µL^{-1})	1 µL (79.3 ng*µL^{-1})
Forward primer	1 µL (100 pmol*µL^{-1})	1 µL (100 pmol*µL^{-1})
Reverse primer	1 µL (100 pmol*µL^{-1})	1 µL (100 pmol*µL^{-1})
dNTP mix	4 µL (40 mM)	5 µL (40 mM)
10x Pfu buffer	5 µL	5 µL
DMSO	2.5 µL	0.5 µL
Pfu polymerase	1 µL (3 U*µL^{-1})	1 µL (3 U*µL^{-1})
Sterile H_2O	35 µL	35.5 µL
PCR program		
Denaturation	90 s 94 °C	2 min 95 °C
Cycles	20 x	30 x
Denaturation	30 s 94 °C	30 s 95 °C
Annealing	60 s 60 °C	45 s 45 °C
		45 s 50 °C
		45 s 55 °C
Elongation	15 min 68 °C	19 min 68 °C
Final elongation	16 min 68 °C	23 min 68 °C

PCR reactions were validated with an agarose gel and purified using a QIAquick PCR purification kit. The non-mutated, methylated template plasmid was digested with DpnI. An in-house sequencing facility confirmed the clones containing the correct mutation. In order to avoid confusions, the mutated amino acids were named C360G and M302K, M305K according to the numbering of the native MscDyP1 protein.

3.3.3 Heterologous overexpression of (*E. coli*) rMscDyP1 and mutants

Genes of (*E. coli*) rMscDyP1, (*E. coli*) rMscDyP1^{C360G}, and (*E. coli*) rMscDyP1$^{M302K, M305K}$ were overexpressed in the pET28a vector in *E. coli* BL21 cells together with a pG-Tf2 vector for overexpression of the chaperone pair GroE*S*-GroEL-tig according to the protocol of the manufacturer (Takara Bio Inc.). Expression in the pET28a vector added an N-terminal His_6-tag to the recombinant proteins. Cells were grown in Terrific Broth (TB) medium containing 50 µg*mL^{-1} kanamycin, 17.5 µg*mL^{-1} chloramphenicol and 5 ng*mL^{-1} tetracycline, as inductor of the chaperone expression, at 37 °C until an OD_{600} of 0.5 was reached. The heme precursor δ–aminolevulinic acid in a final concentration of 0.5 mM was added to the cell culture prior to inducing protein expression with 0.6 mM IPTG in order to facilitate heme incorporation into the recombinantly produced enzymes. After induction, cells were grown at 23 °C overnight.

3.3.4 Heterologous overexpression of (*A. niger*) rMscDyP1

(*A. niger*) rMscDyP1 gene was heterologously overexpressed in *A. niger*, obtained from DSM (Delft, The Netherlands) and kindly provided by Prof. H. Zorn (Institute of Food Chemistry and Food Biotechnology, Justus Liebig University Giessen).

3.3.5 Determination of heme incorporation and purity of (*E. coli*) rMscDyP1

Purity of eluted fractions containing (*E. coli*) rMscDyP1 or the respective mutants and heme incorporation were determined by measuring absorbance of the Soret band at 405 nm and calculating the Reinheitszahl value ($RZ=A_{405}/A_{280}$).

3.3.6 Assay systems

2.3.6.1 ABTS assay

Peroxidase activity was determined using the ABTS assay according to (Puhse *et al.*, 2009) in half area micro-titer plates. The ABTS assay uses ABTS as an electron donor. The principle of the assay is based on detection of ABTS oxidation by hydrogen peroxide catalyzed by MscDyP1. The increasing absorbance of oxidized ABTS at 420 nm was measured for 10 minutes at 30 °C in a microplate reader (Tecan infinite M200). Controls without the enzyme were subtracted from the absorbance. The mean slope was calculated based on an increase of absorbance at 420 nm, and enzymatic activity was calculated with the Lambert Beer's law using the extinction coefficient of ABTS (ε_{420} = 36.8 mM^{-1}*cm^{-1}) and a path length of 0.5 cm. The path length was calculated according to the well and plate dimensions provided by the manufacturer (Greiner Bio One) for 96-well half-area plates, filled with a total well volume of 80 µL, and the formula for the calculation of cylinder height:

$$h = \frac{4 * \mathrm{V}}{\pi * d^2}$$

Activity of the cysteine mutant and the methionine double mutant was calculated as a percentage of the specific activity of (*E. coli*) rMscDyP1.

Table 4: ABTS assay

Volume	Reagent
8 µL	rMscDyP1 or mutant (in 50 mM Tris, 300 mM NaCl, pH 8.0)
32 µL	25 mM Na-acetate pH 3.5
20 µL	2 mM ABTS (in 25 mM Na-acetate pH 3.5) ad 0.5 mM
20 µL	1 mM H_2O_2 (in 25 mM Na-acetate pH 3.5) ad 0.25 mM

2.3.6.2 β-carotene degradation assay

Degradation of β-carotene by rMscDyP1 and mutants, expressed in *E. coli*, was determined using the β-carotene assay reported in (Puhse *et al.*, 2009). The β-carotene solution was prepared from 5 mg β-carotene and 0.5 g Tween 80 solubilized in dichloromethane. The organic solvent was removed via rotary evaporation (40 °C, 250 rpm, 800 mbar, 20 min). The residue was solubilized in distilled water and remaining solvent was removed (40 °C, 250 rpm, 800 mbar to 200 mbar in 200 mbar steps, each step for 15 min) under N_2. The obtained β-carotene solution was filtered and diluted with demineralized water to a total volume of 50 mL. Stored at 4 °C in the dark, the solution was stable for one week. The assay was performed in half area micro titer plates. The decreasing β-carotene absorbance at 450 nm was measured for 10 minutes at 30 °C in a microplate reader (Tecan infinite M200). Controls without enzyme were subtracted from absorbance and the mean slope calculated from decrease of absorbance at 450 nm.

Table 5: β-carotene degradation assay

Volume	Reagent
8 µL	rMscDyP1 or mutant (in 50 mM Tris, 300 mM NaCl, pH 8.0)
32 µL	50 mM Na-acetate pH 3.5
20 µL	β-carotene (in ddH_2O)
20 µL	0.5 mM H_2O_2 (in ddH_2O) *ad* 0.125 mM

Enzymatic activity of rMscDyP1 and respective mutants was calculated according to Lambert Beer's law using the extinction coefficient of β-carotene (ε=95 $mM^{-1}*cm^{-1}$) and well path length of 0.5 cm. The path length was calculated according to the well and plate dimensions provided by the manufacturer (Greiner Bio-One) for the used 96-well half-area plates, filled with a total well volume of 80 µL as mentioned before. Activity of the cysteine mutant and the methionine double mutant was calculated as a percentage of the specific activity of (*E. coli*) rMscDyP1.

3.3.7 Enzyme kinetics

Steady state kinetic parameters for (*E. coli*) rMscDyP1 were determined in the ABTS assay. Regarding the K_M value for H_2O_2 for (*E. coli*) rMscDyP1, the hydrogen peroxide concentration was varied ranging from 60 µM to 1,500 µM, whereas the concentration of ABTS was fixed to 500 µM. ABTS K_M was determined in the presence of 4-500 µM ABTS and 250 µM H_2O_2.

3.3.8 Statistical analyses

Statistical test prerequisites such as balance of experimental design, Gaussian distribution, and homoskedasticity were tested, and either a parametric or non-parametric test was chosen for statistical analysis. For assessing differences in the specific activity between the mutants (*E. coli*) rMscDyP1^{C306G}, and (*E. coli*) rMscDyP1$^{M248K + M251K}$, and the recombinant wildtype (*E. coli*) rMscDyP1 as well as kinetic analyses, a Kruskal Wallis One-Way ANOVA at 95% confidence level with a Dunn's nonparametric multiple comparison for *post hoc* testing was performed using IBM SPSS Statistics 19 software. A Dunnett's multiple comparison test after One-Way ANOVA at 95% confidence level was performed for the blocking experiment of sulfur-containing amino acids (Figure 40) using GraphPad Prism 6 software.

3.3.9 Protein crystallization

rMscDyP1 produced in *A. niger* was provided by DSM (Delft, The Netherlands) (Scheibner *et al.*, 2008). All crystals (N, D, A, B) were grown at 25 °C using the hanging drop technique. The initial protein concentration in the drop (with a ratio of protein to reservoir of 1:2) was 10 and 8 mg*mL^{-1} for crystals N and D, respectively, and 4 mg*mL^{-1} for crystals A and B. The reservoir solution contained 100 mM $MgCl_2$ in 100 mM Tris, pH 8.5 with 30% PEG 4000 and 1.5% of the additive 1,2,3-heptane triol, which was identified to improve crystallization of MscDyP1 using additive screens (Additive screen HT, Hampton Research; JCSG Core Suite I and II, Qiagen). Crystals A and B were co-crystallized with 84.4 µM annatto or bixin (1:1.5 excess), respectively. Crystal D originates from a batch that is believed to be a dimer (personnel communication Katharina Schmidt, Zorn group, Institute of Food Chemistry and Food Biotechnology, Justus Liebig University Giessen). Crystal D was obtained via microseeding. In detail, previously obtained small crystals of MscDyP1 were destroyed by vortexing them with small beads. Dilutions of the obtained micro-seed solution were used to inoculate a novel protein drop for crystallization via the hanging drop technique. Prior to measurement, crystals were soaked in mother liquor containing a final concentration of 30% glycerol for cryoprotection.

2.3.9.1 Data collection

Dr. Karin Fritz-Wolf collected data and refined the structure at the Max Planck Institute for Medical Research, Heidelberg. Diffraction data of crystals N, A, and B were collected at the X10SA beam line of the Swiss Light Source, Villigen, Switzerland, (rotation/image: 0.25°, λ =1 Å (crystal N), λ =0.97940 Å (crystal A and B), detector: Pilatus, 6M Pixel detector) at 100 °K. Diffraction images of crystal D were recorded at 100 °K by an image plate detector (Mar345 image plate, X-ray-Research, Norderstedt, Germany) using Cu K_α radiation from a rotating anode (Rigaku, MicroMax-007HF, operating at 40 kV and 30 mA) at the Max Planck Institute for Medical Research in Heidelberg. All diffraction datasets were processed with XDS (Kabsch, 2010). Reflection phasing and structure refinements were performed using the PHENIX program suite.

2.3.9.2 Molecular docking studies

MscDyP1 subunit A structure was prepared for docking using MOE 2013 software. All water atoms except H_2O #40, which is located in the active site cleft and is replaced by H_2O_2 upon catalysis, were removed. Furthermore, all ligands except heme were removed; in detail, all PEG, glycerol, and N-acetylglucosamine molecules were removed. Force field Amber 10:EHT was chosen, which is suitable for proteins and ligands, as well as protonation. Charges and hydrogen atoms of the protein and ligand were fixed. Other parameters were set as default. In order to prepare it for docking, the whole structure was protonated using MOE 2013 software. Furthermore, the chemical structure of selected potential substrates, 2,6-dimethoxyphenol and β-carotene, was drawn using MOE 2013, energy minimized, and saved as a .mol2 file. Docking was performed using Gold 5.2 software with 200 GA (genetic algorithm) runs in order to predict a binding pose. All H^+-bond donors and acceptors were forced to be treated as solvent accessible. In the case of 2,6-dimethoxyphenol, ligand flexibility was allowed, whereas for β-carotene these parameters were set as default. Scoring function ChemPLP was selected. Search efficiency was set to highest (200%) for binding mode prediction. Generated docking poses were ranked for PLP-fitness from highest to lowest.

4 RESULTS

4.1 *P. falciparum* methionine adenosyltransferase

One aim of this dissertation was to study the redox regulation of PfalMAT. Therefore, it was necessary to identify possible surface-exposed and solvent accessible cysteines that might be involved in redox regulatory processes affecting PfalMAT. A sequence alignment of PfalMAT with MAT of different species whose crystal structures were available, including *E. coli* MAT (cMAT), *Crytosporidium hominis* MAT (ChMAT), human MAT I/III and human MAT II (hMAT), and rat liver MAT (rlMAT) highlights conserved cysteines and those that are exclusively found in PfalMAT (Figure 8).

```
PfalMAT      -------------MSQLKIKRGNFLFTSESVNEGHPDKICDQISDAILDSCLREDPYSKV    47
ChMAT        MDSSRLSGNKSTYTD-LQTTSEQFLFSSESVCSGHPDKLCDQISDAILDACLEQDPESFV    59
cMAT         --------------------MAKHLFTSESVSEGHPDKIADQISDAVLDAILEQDPKARV    40
rlMAT        -----MNGPVDGLCDHSLSEEGAFMFTSESVGEGHPDKICDQISDAVLDAHLKQDPNAKV    55
hMAT_I/III   -----MNGPVDGLCDHSLS-EGVFMFTSESVGEGHPDKICDQISDAVLDAHLKQDPNAKV    54
hMAT_II      -----MNGQLNGFHE-AFIEEGTFLFTSESVGEGHPDKICDQISDAVLDAHLQQDPDAKV    54
                                  .:*:**** .*****:.******:**: *.:** : *

PfalMAT      ACEVCAKKNYIFIFGEITTKAKVNYDKVTRDVLKHIGYDDESKGLDYKTAEIKVSIDEQS    107
ChMAT        ACETCTKTGFIMVFGEITTKANVNYERVVRETVKEIGYDSEEKGLDYKTMDVIIKLEQQS    119
cMAT         ACETYVKTGMVLVGGEITTSAWVDIEEITRNTVREIGYVHSDMGFDANSCAVLSAIGKQS    100
rlMAT        ACETVCKTGMVLLCGEITSMAMIDYQRVVRDTIKHIGYDDSAKGFDFKTCNVLVALEQQS    115
hMAT_I/III   ACETVCKTGMVLLCGEITSMAMVDYQRVVRDTIKHIGYDDSAKGFDFKTCNVLVALEQQS    114
hMAT_II      ACETVAKTGMILLAGEITSRAAVDYQKVVREAVKHIGYDDSSKGFDYKTCNVLVALEQQS    114
             ***.  *.  ::: ****: * :: :.:.*:.::.***  .  *:* ::  :   : :**

PfalMAT      PDIAQCVHENRSPELIGAGDQGIMFGYATDETENYMPLTHHYATLLGKRLTEVRKLG---    164
ChMAT        NQIAGCVHVDKNVEDIGAGDQGMMFGYATNETKELMPLTHVLATSITRELDYIRMKGVSS    179
cMAT         PDINQGVDRA-DPLEQGAGDQGLMFGYATNETDVLMPAPITYAHRLVQRQAEVRKNG---    156
rlMAT        PDIAQCVHLDRNEEDVGAGDQGLMFGYATDETEECMPLTIVLAHKLNTRMADLRRSG---    172
hMAT_I/III   PDIAQCVHLDRNEEDVGAGDQGLMFGYATDETEECMPLTIILAHKLNARMADLRRSG---    171
hMAT_II      PDIAQGVHLDRNEEDIGAGDQGLMFGYATDETEECMPLTIVLAHKLNAKLAELRRNG---    171
              :*   *.   .    ******:******:**.  **     *  :  .   :*  *

PfalMAT      ILPYLGPDGKTQITIEYKNKGSCGGHLEPLRVHTVLISTQHAEDIKYEQLKTDLMENVIK    224
ChMAT        RVGWLRPDGKAQVTVEYNCK---HGVLIPKRIHTILVSVQHDENIENEEIREFVLENVIK    236
cMAT         TLPWLRPDAKSQVTFQYDDGK-------IVGIDAVVLSTQHSEEIDQKSLQEAVMEEIIK    209
rlMAT        VLPWLRPDSKTQVTVQYVQD---NGAVIPVRVHTIVISVQHNEDITLEAMREALKEQVIK    229
hMAT_I/III   LLPWLRPDSKTQVTVQYMQD---NGAVIPVRIHTIVISVQHNEDITLEEMRRALKEQVIR    228
hMAT_II      TLPWLRPDSKTQVTVQYMQD---RGAVLPIRVHTIVISVQHDEEVCLDEMRDALKEKVIK    228
              : :* **.*:*:*.:*             :.::::*.** *::  . ::  : *::*:

PfalMAT      YVIPEKLLDNETLYYLNPSGKFVLGGPAADAGLTGRKIICDTYGGWGAHGGGAFSGKDAS    284
ChMAT        KVCPSDLMDKETRILINPSGRFTIGGPAADAGLTGRKIIVDTYGGWGAHGGGAFSGKDAT    296
cMAT         PILPAEWLTSATKFFINPTGRFVIGGPMGDCGLTGRKIIVDTYGGMARHGGGAFSGKDPS    269
rlMAT        AVVPAKYLDEDTIYHLQPSGRFVIGGPQGDAGVTGRKIIVDTYGGWGAHGGGAFSGKDYT    289
hMAT_I/III   AVVPAKYLDEDTVYHLQPSGRFVIGGPQGDAGVTGRKIIVDTYGGWGAHGGGAFSGKDYT    288
hMAT_II      AVVPAKYLDEDTIYHLQPSGRFVIGGPQGDAGLTGRKIIVDTYGGWGAHGGGAFSGKDYT    288
              : * . : . *   ::*:*:*.:*** .*.*:****** ***** . ********** :

PfalMAT      KVDRSAAYYLRFIAKSLVANKFCRRVLVQASYSIGIANPISLNVNSYGTVSTGYTDYDLE    344
ChMAT        KVDRSGAYMARLVAKSIVFSGLCSRCLVQVSYGIGIARPLSLYINTFGTAKDGYNDTKLL    356
cMAT         KVDRSAAYAARYVAKNIVAAGLADRCEIQVSYAIGVAEPTSIMVETFGTEKV--PSEQLT    327
rlMAT        KVDRSAAYAARWVAKSLVKAGLCRRVLVQVSYAIGVAEPLSISIFTYGTSKK--TERELL    347
hMAT_I/III   KVDRSAAYAARWVAKSLVKAGLCRRVLVQVSYAIGVAEPLSISIFTYGTSQK--TERELL    346
hMAT_II      KVDRSAAYAARWVAKSLVKGGLCRRVLVQVSYAIGVSHPLSISIFHYGTSQK--SERELL    346
             *****.**  * :**.:*   :. *  :*.**.**::.* *: :  :** .    . .*
```

```
PfalMAT      QIILRNFDLRPGFIIQELKLTEPVFSKTSAYGHFGREGDTFTWEKIKDLSHEKNALKN-     402
ChMAT        EIVNKVFDFRPGILIKQLNLKSPIFKKTSSGGHFGRSEKEFLWEKPIILQ---------     406
cMAT         LLVREFFDLRPYGLIQMLDLLHPIYKETAAYGHFGREH--FPWEKTDKAQLLRDAAGLK     384
rlMAT        EVVNKNFDLRPGVIVRDLDLKKPIYQKTACYGHFGRSE--FPWEVPKKLVF--------     396
hMAT_I/III   DVVHKNFDLRPGVIVRDLDLKKPIYQKTACYGHFGRSE--FPWEVPRKLVF--------     395
hMAT_II      EIVKKNFDLRPGVIVRDLDLKKPIYQRTAAYGHFGRDS--FPWEVPKKLKY--------     395
              :: . **:**  ::: *.*  *::..*:. *****.   * **
```

Figure 8: Sequence alignment of MAT from different species

* Identical residues, **:** Very similar residues, **.** Similar residues. Cysteines are shown in bold and those conserved among PfalMAT and other species are highlighted in gray. Cys52, Cys113 and Cys187 of PfalMAT, which were mutated during this dissertation are colored in red. The conserved substrate binding motif and the phosphate binding P-loop are underlined with a straight line, 1st and 2nd positons, respectively. The loop above the active site is underlined with a wavy line. Active site residues are enclosed in a box. This alignment was prepared using Clustal Omega 1.2.1.

PfalMAT displays a sequence similarity of 40-60% to homologs of other species (ChMAT 57.3%, hMAT 6.7%, rlMAT 57.2% and cMAT 48.8%). PfalMAT contains eight cysteine residues, with four of them conserved among MATs. Interestingly, PfalMAT shares most of its cysteine residues with ChMAT.

4.1.1 Homology model of PfalMAT

Chiang *et al.* published a homology model of PfalMAT in 1999. This model was based on the crystal structure of cMAT (Chiang *et al.*, 1999). The sequence alignment of PfalMAT with cMAT reveals that cMAT lacks most of the cysteines that are present in PfalMAT (Figure 8) but conserved in other MAT species. These include Cys121 of rlMAT, which has been demonstrated to undergo *S*-nitrosylation and therefore likely participates in the redox regulation of rlMAT (Avila *et al.*, 1997) and corresponds to Cys113 of PfalMAT. Furthermore, this cysteine is located at the beginning of the loop above the active site, which has been suggested to regulate substrate access. Therefore, the homology model of PfalMAT based on cMAT published by Chiang *et al.* is not suitable for studying the redox-regulation of PfalMAT, in its entirety. Since the crystal structure of PfalMAT is not yet available, we constructed a homology model based on the crystal structures of MAT from different organisms, the alpha subunit of human MAT isoform 2 (hMAT2A) (PDB ID 2p02) and *C. hominis* MAT (PDB ID 4odj) (Figure 9). According to this model, three cysteine residues are solvent accessible and therefore possible targets of redox-active agents. The formation of intermolecular disulfide bridges in the dimeric assembly of PfalMAT, which might change the oligomeric state of PfalMAT upon redox modification, is possible between Cys52-Cys52' and Cys187-Cys187' since these residues are close enough to each other (~4 Å). Cys187 is located on top of a loop that connects two beta-barrel strands (Figure 9, highlighted in purple). Residues at the other site of these strands, e.g. Lys174, are involved in binding the substrate ATP. In PfalMAT this loop contains an insertion of 3-7 residues including Cys187. Furthermore, the sequence of this loop (KGSCGGH) suggests possible hinges, G185 and G189, that allow for the opening and closing of the intermolecular disulfide between Cys187 and Cys187' of the other subunit. Furthermore, the surface-exposed Cys113 and Cys113' might contribute to a redox regulation of PfalMAT. Cys113 is located at the beginning of the conserved flexible loop above the active site and corresponds to Cys121 of rlMAT, which can be *S*-nitrosylated, indicating Cys113 might also undergo redox-based thiol modifications.

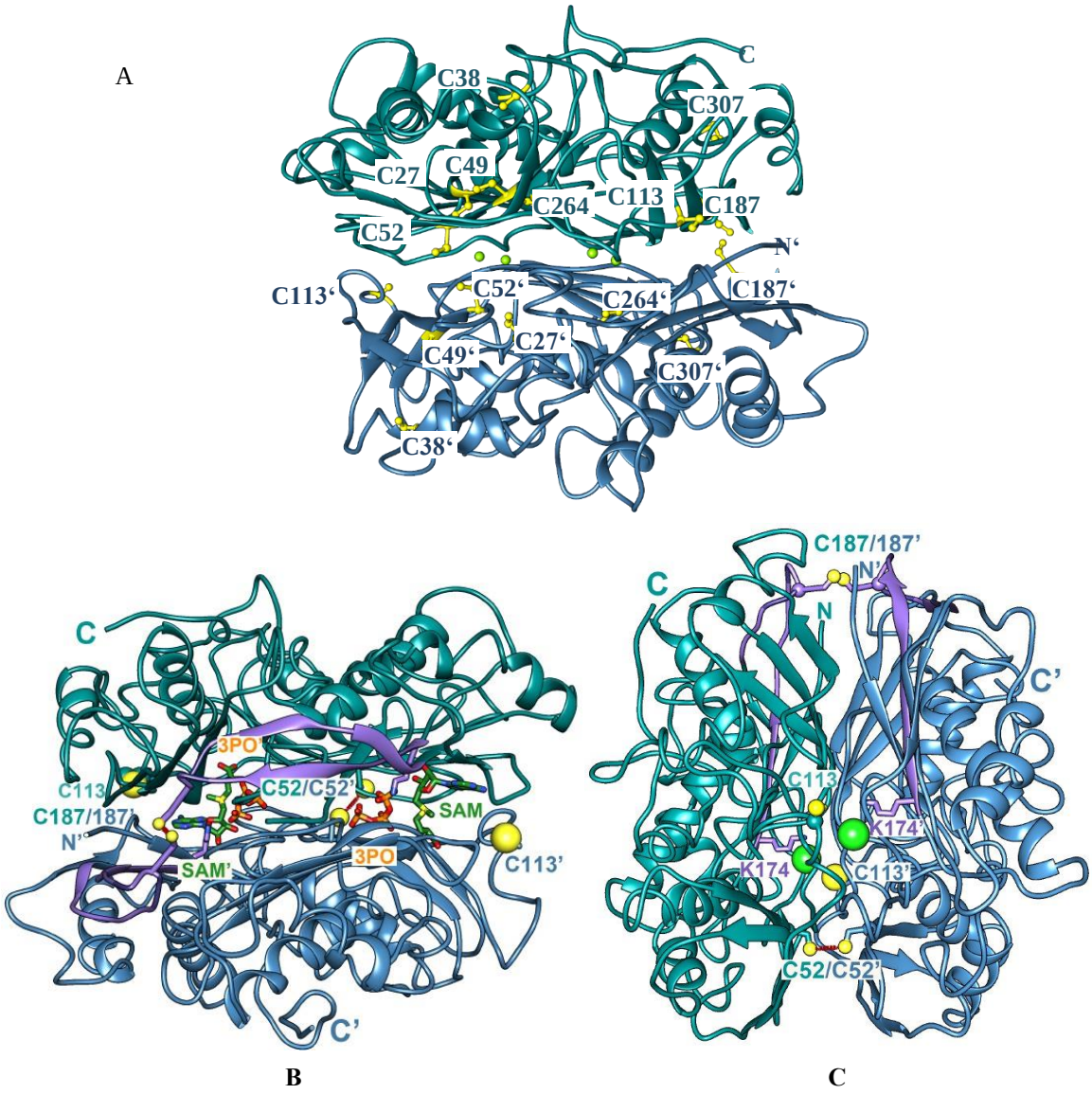

Figure 9: Homology model of PfalMAT

Homology model of PfalMAT based on the crystal structures of ChMAT (PDB ID 4odj) and MATII (PDB ID 2p02). The two subunits of the PfalMAT dimer are shown in petrol and blue, respectively. **A:** Overview of PfalMAT cysteines (shown as yellow balls and sticks). **B:** A triphosphate (orange) and a SAM molecule (light green) are shown in the active sites based on the superposition of different MAT structures. Two beta-strands and an insertion loop are shown in purple. **C:** The active site of each subunit is indicated as a green ball. Possible intermolecular disulfide bonds are indicated with red dashes between cysteine residues (yellow).

4.1.2 Site-directed mutagenesis of PfalMAT

Cysteines that were proposed to be accessible to oxidizing or reducing agents, based on the homology model of PfalMAT were selected for site-directed mutagenesis to serine. Accordingly, Maike Eisenkolb created PfalMAT^{C113S} and PfalMAT^{C187S} mutants for her master thesis (Eisenkolb, 2008). Additionally, a PfalMAT^{C52S} mutant was constructed via site-directed mutagenesis for this dissertation.

4.1.3 Heterologous overexpression and purification of PfalMAT and hMATIII

The heterologous overexpression of PfalMAT gene in pQE30 *E. coli* M15 cells was optimized in Eisenkolb's master thesis (Eisenkolb, 2008). For the production and purification of the

mutants PfalMAT^{C52S}, PfMMAT^{C113S}, and PfalMAT^{C187S} the same protocol as for the wild type enzyme was used. Figure 10 shows respective purifications via immobilized metal ion affinity chromatography for PfalMAT and mutants (44.8 kDa). The proteins were eluted with an imidazole gradient from the Ni-NTA column, and the purest fractions were pooled. A sufficient amount of approximately 15 mg enzyme was obtained per liter of *E. coli* culture. The enzymes were stable and active for approximately one to two weeks at 4 °C.

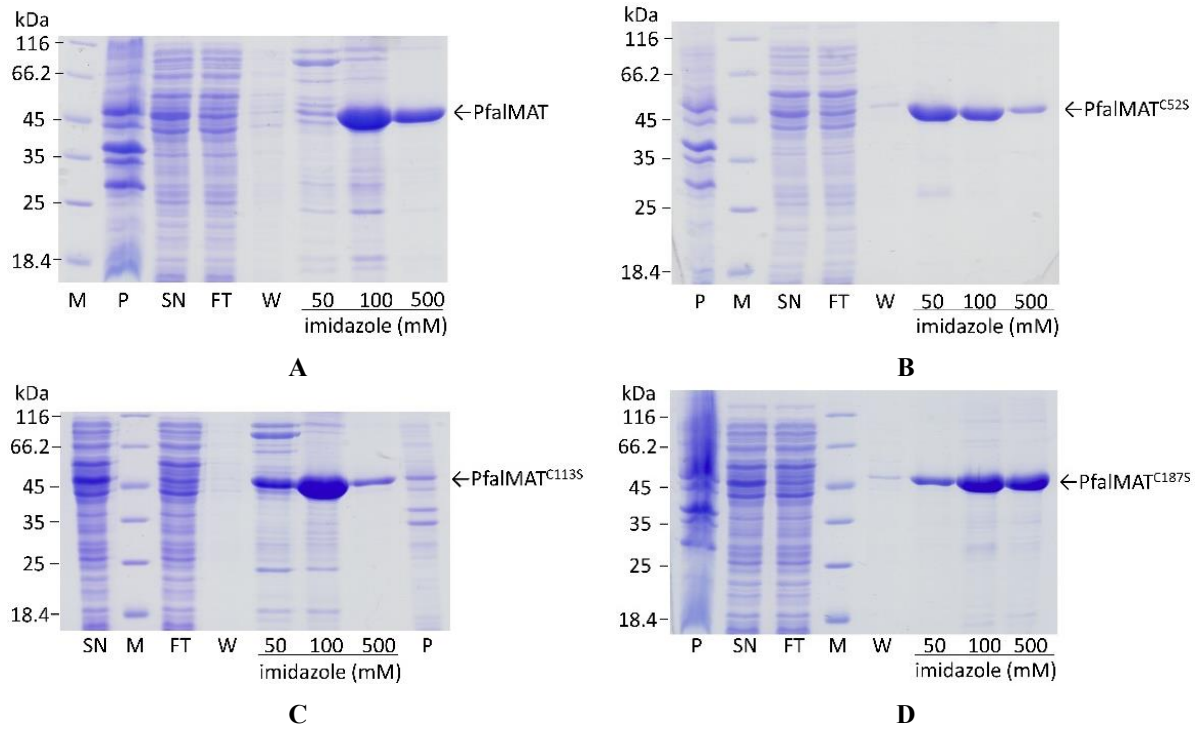

Figure 10: Purification of PfalMAT and mutants via Ni-NTA affinity chromatography

A: PfalMAT, **B**: PfalMAT^{C52S}, **C**: PfalMAT^{C113S}, **D**: PfalMAT^{C187S}; M: marker, P: cell pellet, SN: supernatant, FT: flow through, W: wash, 50-500: fraction eluted with 50-500 mM imidazole.

In order to compare the recombinant PfalMAT with a human counterpart, the hMAT1a gene was heterologously overexpressed in pET28a *E. coli* KRX cells for a master thesis (Gehr, 2014). Figure 11 shows its purification via immobilized metal ion affinity chromatography. The protein was eluted with an imidazole gradient from the Ni-NTA column.

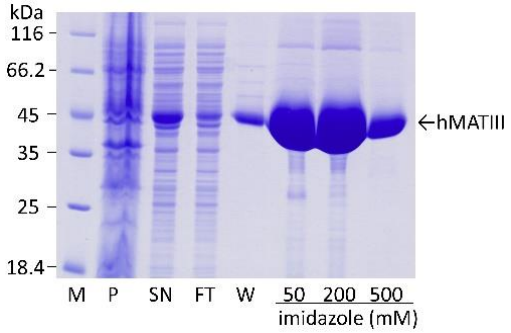

Figure 11: Purification of hMATIII via Ni-NTA affinity chromatography

M: marker, P: cell pellet, SN: supernatant, FT: flow through, W: wash, 50-500: fractions eluted with 50-500 mM imidazole.

The eluted fractions were pooled and stored at 4 °C. Under these conditions the enzyme was relatively unstable. The reduction of hMATIII with 2 mM DTT directly after elution from the Ni-NTA column increased the stability. However, the protein remained stable for only two days. Since the protein yield was relatively high (~100 mg per liter *E. coli* culture), hMATIII was used without further concentration for activity assays after reduction with DTT.

4.1.4 Oligomerization behavior of PfalMAT and mutants

In order to study the effects of oxidation and reduction on the oligomerization state of PfalMAT and the cysteine mutants as well as the contribution of disulfide bridges to the dimeric assembly of PfalMAT preparative gel filtration experiments were carried out (Figure 12). These experiments confirmed that the recombinant PfalMAT was a dimer (molecular size of a monomer: 44.8 kDa). Treatment with the reducing agent DTT didn't show any major effects on the oligomerization state of PfalMAT, suggesting that disulfides were not involved in the dimerization of PfalMAT. PfalMAT^{C113S} showed a similar oligomerization behavior before and after treatment with DTT as PfalMAT. However, the size exclusion experiments with PfalMAT^{C52S} and PfalMAT^{C187S} showed a mixture of monomers and oligomers. Moreover, the reduction of these cysteine mutants with DTT shifted the oligomerization state towards a dimer.

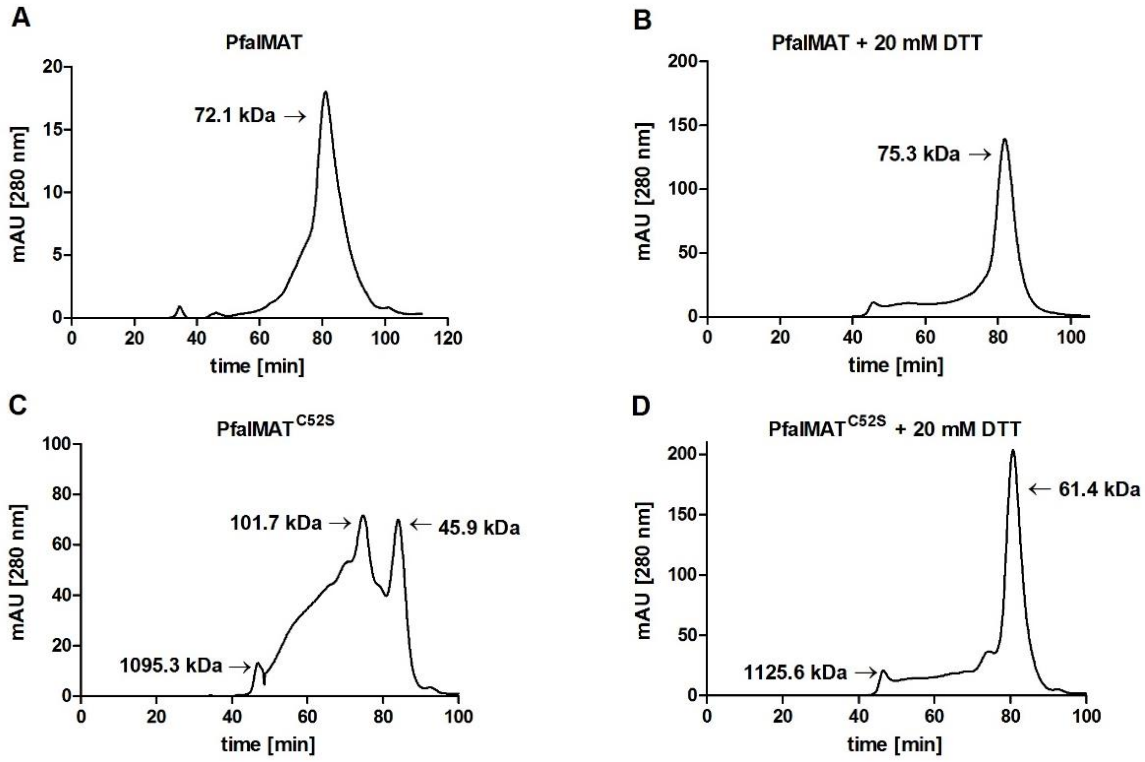

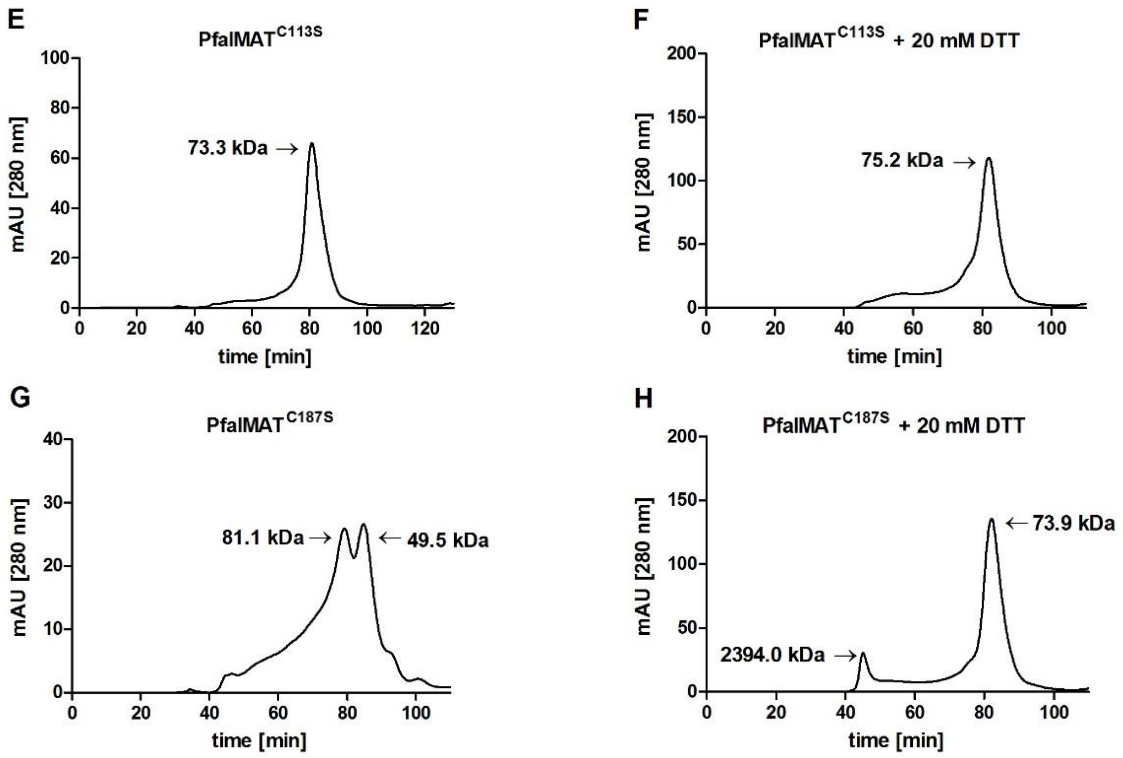

Figure 12: Oligomerization of PfalMAT

A, C, E, G: oligomeric state of PfalMAT, PfalMAT^{C52S}, PfalMAT^{C113S}, and PfalMAT^{C187S}, respectively. B, D, F, H: Oligomerization behavior of PfalMAT, PfalMAT^{C52S}, PfalMAT^{C113S}, and PfalMAT^{C187S}, respectively, after treatment with 20 mM DTT.

The human *mat1a* gene encodes two MAT isoforms: MATI, a homotetramer, and MATIII, a homodimer. In order to examine whether the recombinant hMAT is present in a dimeric or tetrameric form, the oligomerization state of the enzyme was investigated via gel filtration experiments, either with the untreated protein after Ni-NTA affinity chromatography or with the reduced enzyme treated with DTT (Figure 13).

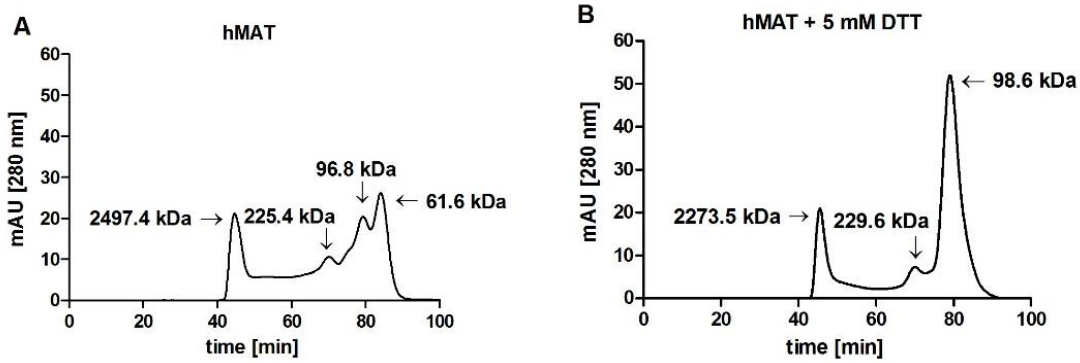

Figure 13: Oligomeric state of hMATIII

Oligomerization behavior of untreated hMATIII (**A**) and after treatment with DTT (**B**).

These gel filtration experiments showed that directly after Ni-NTA affinity chromatography a mixture of monomers (43.6 kDa), dimers and tetramers was present. However, in the reduced state under conditions within the performed experiments, predominantly dimeric hMATIII was present. Therefore, the protein encoded by *hmat1a* used here for comparison with PfalMAT is referred to as hMATIII.

4.1.5 Enzymatic characterization of PfalMAT

In order to assay the activity of PfalMAT, its mutants, and hMATIII, the enzymes were prepared freshly for each experiment, stored at 4 °C, and measured within one to five days after purification. Since reducing PfalMAT with DTT increased the enzymatic activity (Figure 21 A), the enzymes were reduced with 2 mM DTT and desalted to remove excess DTT, prior to the measurements. In order to maintain the reduced state during the experiments, the measurements were performed within three to four hours after reduction. After this period of time, the enzymes were incubated again with DTT and were desalted. Each measurement with hMATIII was performed within 48 hours after purification due to the short period of time in which this enzyme remained stable.
Although PfalMAT had been previously characterized on a molecular level (Chiang *et al.*, 1999), this enzyme had not been characterized kinetically. Initial enzymatic characterization of PfalMAT was attempted in two master theses in this group (Eisenkolb, 2008; Pretzel, 2011). However, the coupled assay previously used (Eisenkolb, 2008) was not suitable for a detailed kinetic analysis. In two master theses (Pretzel, 2011; Gehr, 2014), the ammonium molybdate-based assay system, which is based on the detection of released inorganic phosphate during PfalMAT reaction, was established and optimized for PfalMAT, which paved the way for an in-depth enzymatic characterization of PfalMAT for this dissertation.
A phosphate standard curve, linear up to 800 µM orthophosphate (Figure 14 A), was used to determine the amount of inorganic phosphate released by the PfalMAT reaction, which was proportional to the concentration of PfalMAT in the assay (Figure 14 B).

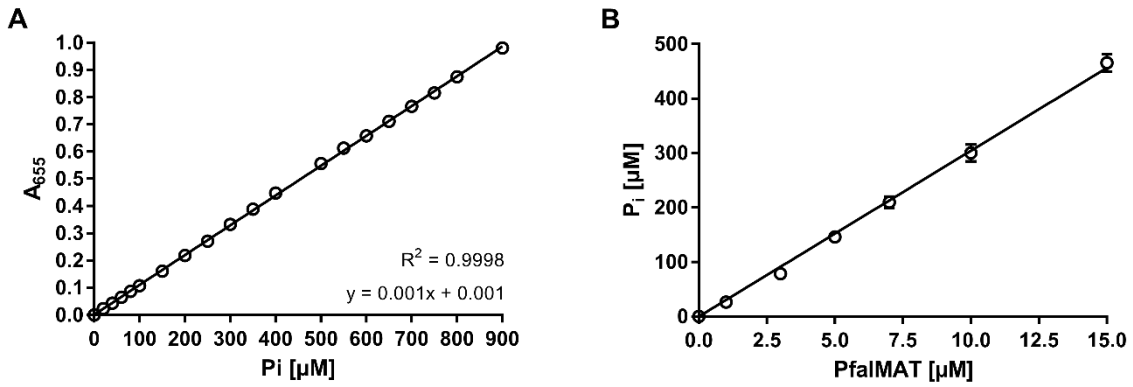

Figure 14: Phosphate standard curve and PfalMAT titration

A: The phosphate standard curve shows high linearity up to 900 µM inorganic phosphate. Data represent means ± SD, whereas SD is smaller than symbol size here. **B**: The amount of orthophosphate detected is directly proportional to the concentration of PfalMAT in the ammonium molybdate assay. Data represent means ± SD.

The PfalMAT reaction showed a broad pH optimum between 7.4 and 9 (Figure 15 A), and mono- and divalent cations were found to be essential for the MAT-catalyzed reaction. Accordingly, PfalMAT showed its maximal activity with $MgCl_2$ at 40 mM which was above the concentration of ATP. Lower concentrations of Mg^{2+} and K^+ as well as higher $MgCl_2$ concentrations inhibited the activity of PfalMAT (Figure 15 B and C).

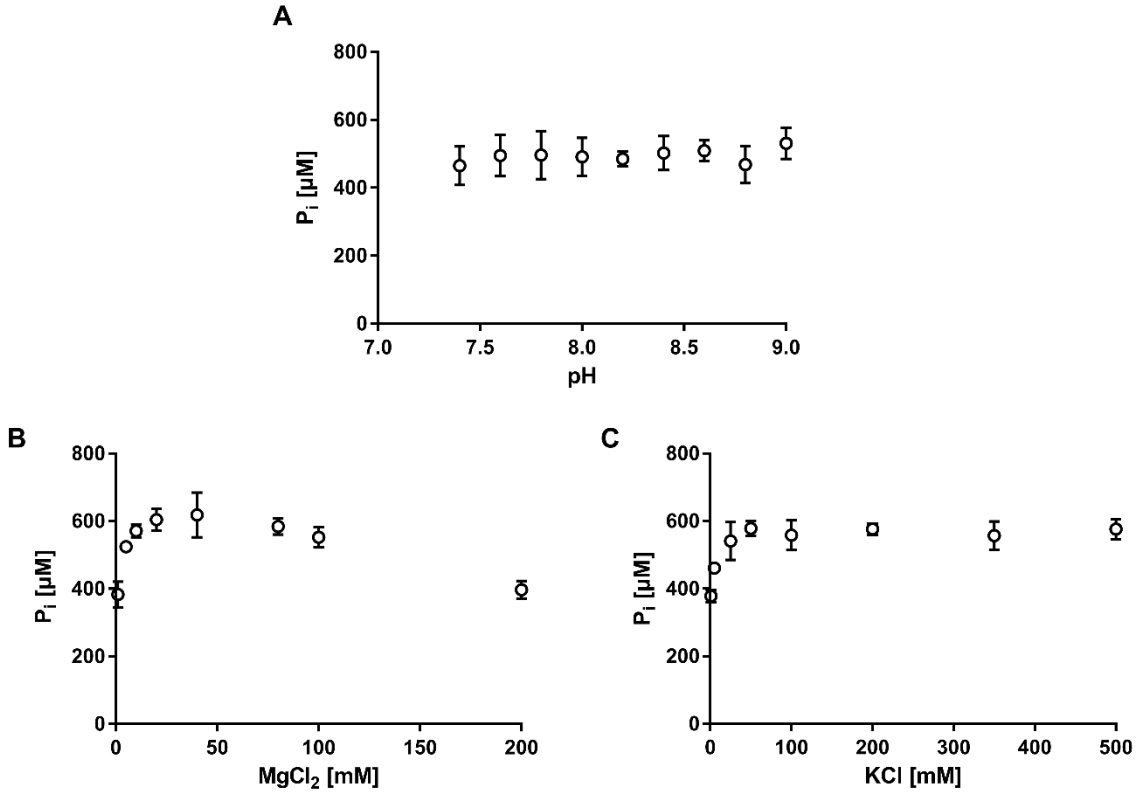

Figure 15: pH and salt profile of PfalMAT

A: pH-dependent PfalMAT activity and salt preference for MgCl2 (**B**) and KCl (**C**) was determined using the ammonium molybdate assay. Data represent means ± SD.

2.3.5.1 Kinetic parameters

The specific activity and steady-state kinetic parameters of PfalMAT, cysteine mutants, and the selected human homolog hMATIII, were determined using the ammonium molybdate assay. Kinetic parameters were determined by varying the concentration of one of the two substrates, ATP or L-methionine, with the other one being fixed, plotting the reaction velocity against the substrate concentration, and fitting it to the Michaelis-Menten equation. Table 6 summarizes the kinetic parameters of PfalMAT, the cysteine mutants, and hMATIII.

Table 6: Kinetic parameters of PfalMAT

	PfalMAT	**PfalMAT^{C52S}**	**PfalMAT^{C113S}**	**PfalMAT^{C187S}**	**hMATIII**
Specific activity [nmol*min^{-1}*mg^{-1}]	379 ± 67	367 ± 63	446 ± 71**	335 ± 54	1,331 ± 204***
K_M [µM] Met	34 ± 6	46 ± 5*	51 ± 4**	43 ± 9	168 ± 23***
K_M [µM] ATP	560 ± 45	680 ± 64***	206 ± 23***	176 ± 12***	330 ± 53***
k_{cat}/K_M (Met) [mM^{-1}*s^{-1}]	31.2 ± 12.3	22.3 ± 9.0**	32.2 ± 9.3	24.5 ± 9.7	14.4 ± 2.2***
k_{cat}/K_M (ATP) [mM^{-1}*s^{-1}]	1.9 ± 0.7	1.5 ± 0.6	7.2 ± 2**	5.9 ± 2.3**	7.3 ± 1.1**

Values are mean values ± SD of at least three independent experiments with at least two measurements each. The given kinetic characteristics were determined using the ammonium molybdate assay. A One-Way ANOVA with a 95% confidence level was performed in order to compare means. $^{*}p < 0.05$, $^{**}p < 0.01$, $^{***}p < 0.001$

The mutants PfalMAT^{C52S} and PfalMAT^{C187S} showed no major differences in the specific activity compared to PfalMAT, whereas PfalMAT^{C113S} had a higher activity. The substitution of Cys52 and Cys113 for serine significantly decreased the affinity to the substrate L-methionine, compared to PfalMAT. This could also be observed for PfalMAT^{C52S} for the second substrate ATP. In contrast, PfalMAT^{C113S} and PfalMAT^{C187S} displayed a higher affinity to ATP compared to PfalMAT. Representative K_M curves for PfalMAT are shown in Figure 16. Furthermore, PfalMAT^{C113S} and PfalMAT^{C187S} showed a higher turnover number than PfalMAT with respect to the substrate ATP, whereas PfalMAT^{C52S} converted more L-methionine molecules per second than PfalMAT.

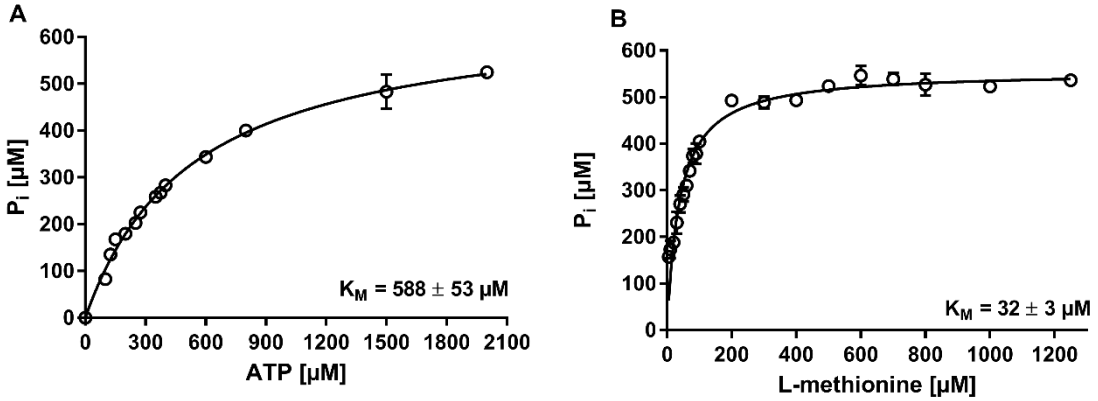

Figure 16: K_M for ATP and L-methionine of PfalMAT

A: K_M determination of PfalMAT in the presence of 2 mM ATP. **B**: K_M determination in the presence of 1 mM L-methionine. Data represent means ± SD.

The specific activity of hMATIII obtained under these assay conditions was more than 3-fold higher than that of PfalMAT. Representative K_M curves for hMATIII are shown in Figure 17.

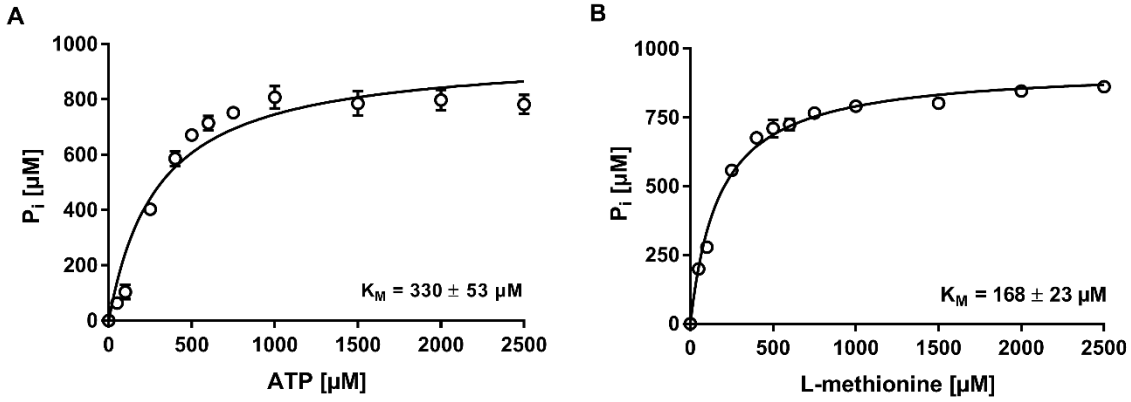

Figure 17: K_M for ATP and L-methionine of hMATIII

A: K_M determination of hMATIII in the presence of 1 mM L-methionine. **B**: K_M determination of hMATIII in the presence of 2 mM ATP. Data represent means ± SD.

2.3.5.2 Allosteric regulation of PfalMAT

The product of the MAT-catalyzed reaction, SAM, is a potent feedback inhibitor of MAT of different species (Markham *et al.*, 1983; Reguera *et al.*, 2002). Accordingly, both PfalMAT (IC_{50} 264 µM) and hMATIII (IC_{50} 1076 µM) are inhibited by their product SAM, albeit weakly (Figure 18).

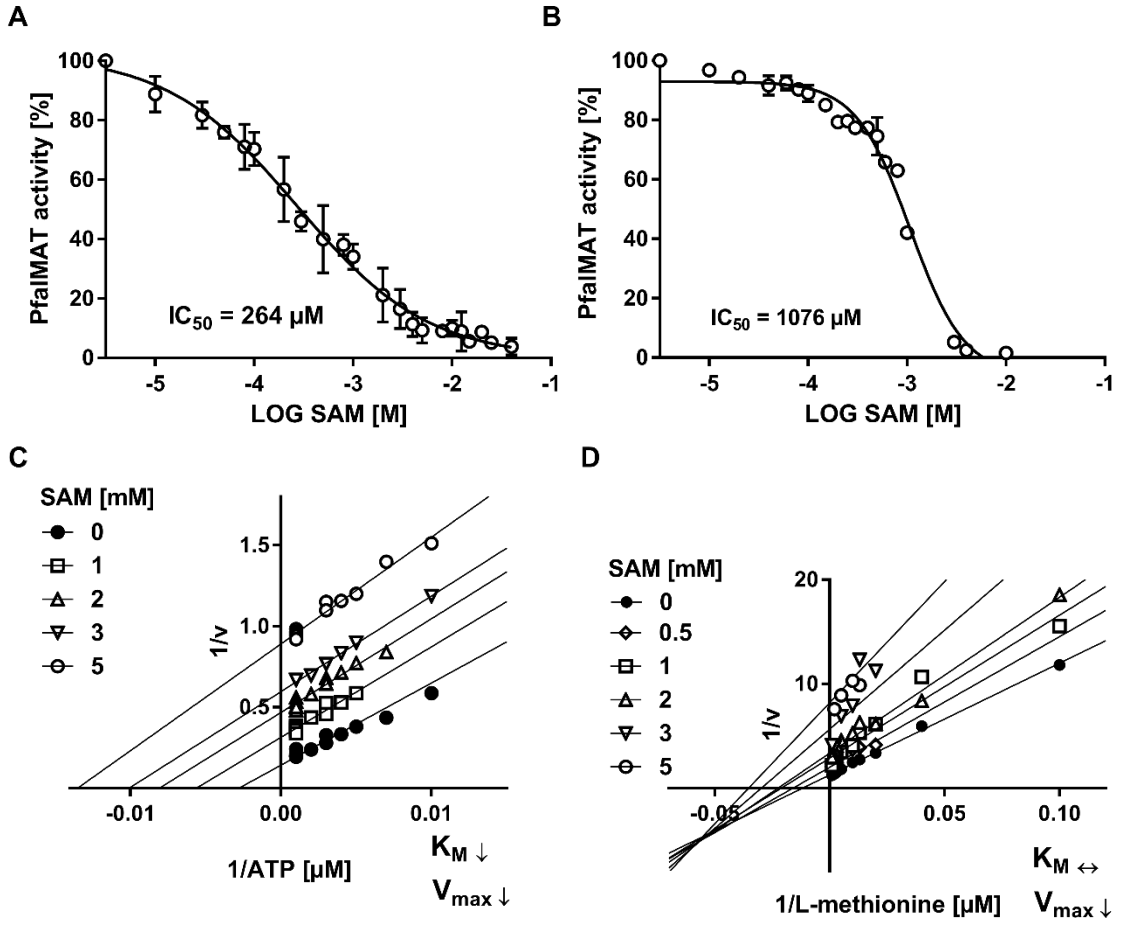

Figure 18: Allosteric regulation of PfalMAT and hMATIII by SAM

IC_{50} of SAM for PfalMAT (**A**) and hMATIII (**B**). Data represent means ± SD. Lineweaver-Burk plots for PfalMAT indicate SAM uncompetitively inhibit PfalMAT with ATP (**C**) and non-competitively with L-methionine (**D**).

A detailed analysis of the inhibition type has been performed in my master thesis, showing a non-competitive inhibition of PfalMAT for L-methionine (0.01-1 mM) with SAM indicated by a decrease of V_{max} and no effect on the K_M for L-methionine (K_i of 0.7 ± 0.2 mM). In contrast, increasing concentrations of SAM decreased both the K_M for ATP and V_{max}, suggesting an uncompetitive inhibition pattern to ATP (K_i 3.6 ± 0.4 mM) (Pretzel, 2011).

4.1.6 Redox regulation of PfalMAT

In order to study the effect of the redox active proteins PfTrx1, PfGrx, and PfPlrx on PfalMAT activity, the enzyme was incubated with different concentrations of these redoxins in a reduced state (Figure 19). Noteworthy, for this experiement PfalMAT was not prereduced with DTT. Both PfTrx1 and PfPlrx increased the activity of PfalMAT, compared to the untreated enzyme, in a concentration-dependent manner. However, in a direct comparison, lower concentrations of PfTrx1 than PfPlrx were necessary to activate PfalMAT. At a molar ratio of 1:1.2 (2.5 µM PfalMAT, 3 µM PfTrx), PfTrx1 was already capable of increasing the activity of PfalMAT to ~130%, whereas a higher molar ratio of PfalMAT (2.9 µM) to PfPlrx (10 µM) (1:3.4) was required for a similar activation (to ~125%) ($p < 0.01$, Two-Way ANOVA). In contrast, PfGrx had no effect on PfalMAT activity.

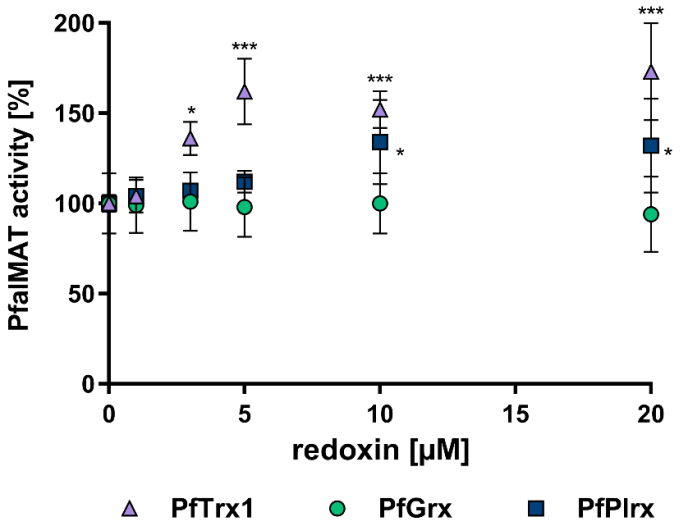

Figure 19: PfalMAT activity depending on redoxin concentration

Relative activity of PfalMAT in the presence of PfTrx1, PfGrx, and PfPlrx. 0 to 20 µM of the reduced redox proteins were added directly to the reaction mixture without prior incubation. Enzymatic activity of PfalMAT without redoxin and without prereduction with DTT was set to 100%. A One-Way ANOVA with a 95% confidence level was performed in order to compare means. *p < 0.05, **p < 0.01, ***p < 0.001

Since PfTrx1 potently activated PfalMAT, their interaction was addressed in more detail. In order to identify the cysteine residue presenting the target of PfTrx1, the activity of the cysteine mutants in the presence of PfTrx1 was compared to PfalMAT (Figure 20).

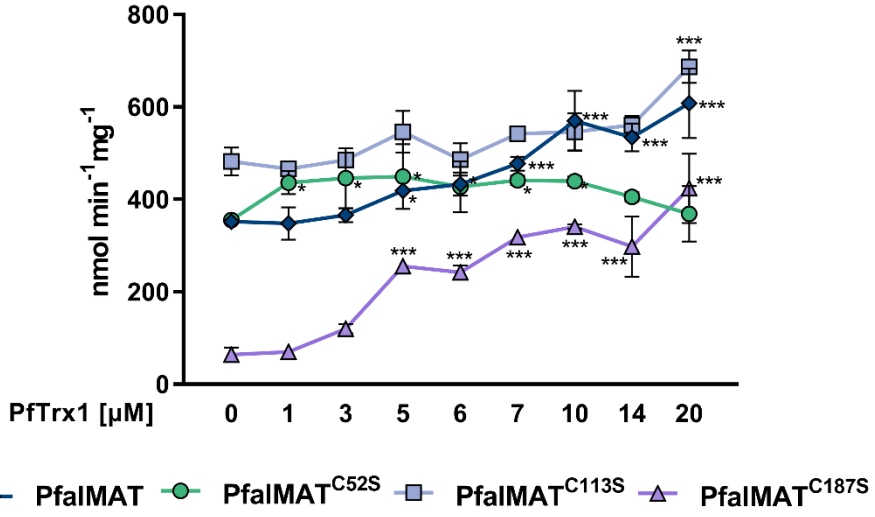

Figure 20: Activation of PfalMAT and mutants by PfTrx1

Activity of not prereduced PfalMAT, PfalMAT^{C52S}, PfalMAT^{C113S}, and PfalMAT^{C187S} in the presence of PfTrx1. 0 to 20 µM of PfTrx1 were added directly to the reaction mixture without prior incubation. Two-Way ANOVA with a 95% confidence level was performed in order to compare means within groups. *p < 0.05, **p < 0.01, ***p < 0.001

PfTrx1 activated PfalMAT^{C52S} and PfalMAT^{C113S} only weakly (PfalMAT^{C52S} by ~20% and PfalMAT^{C113S} by ~40% after adding 20 µM PfTrx1). For activity and kinetic analysis, the enzymes were prereduced with DTT. In order to study the reducing effect of PfTrx1, the enzymes were not prereduced here. In this context, it was observed that while PfalMAT, PfalMAT^{C52S}, and PfalMAT^{C113S} exhibited a similar activity as in the reduced state, PfalMAT^{C187S} had only ~15% residual activity compared to the respective prereduced protein, which was completely restored by 10 µM PfTrx1.

4.1.7 Protein-*S*-glutathionylation of PfalMAT

It had been shown before, that PfalMAT can be S-glutathionylated in the presence of GSSG (Kehr *et al.*, 2011) and that this post-translational modification is in principle reversible (Pretzel, 2011). Indeed, protein-S-glutathionylation of PfalMAT (PfalMAT-SG) resulted in a ~50 % loss of activity (Figure 21 A and B) which could be fully reconstituted by DTT (Figure 21 A). Deglutathionylation of PfalMAT-SG by DTT was proved by the disappearance of the signal upon adding DTT on Western blots using an anti-glutathione antibody (Figure 23). Moreover, PfalMAT-SG activity increased to a similar extent to PfalMAT in response to the addition of DTT, to ~180% of the activity of untreated PfalMAT (Figure 21 A). In contrast to inhibition by GSSG, PfalMAT was activated by incubation with reduced glutathione (three-fold activation in the presence of 10 mM GSH, Figure 21 B), which is most likely due to the reduction of a disulfide bond and does not lead to S-glutathionylation of the enzyme, as indicated by the absence of a signal on Western blots using an anti-GSH antibody (Figure 21 C).

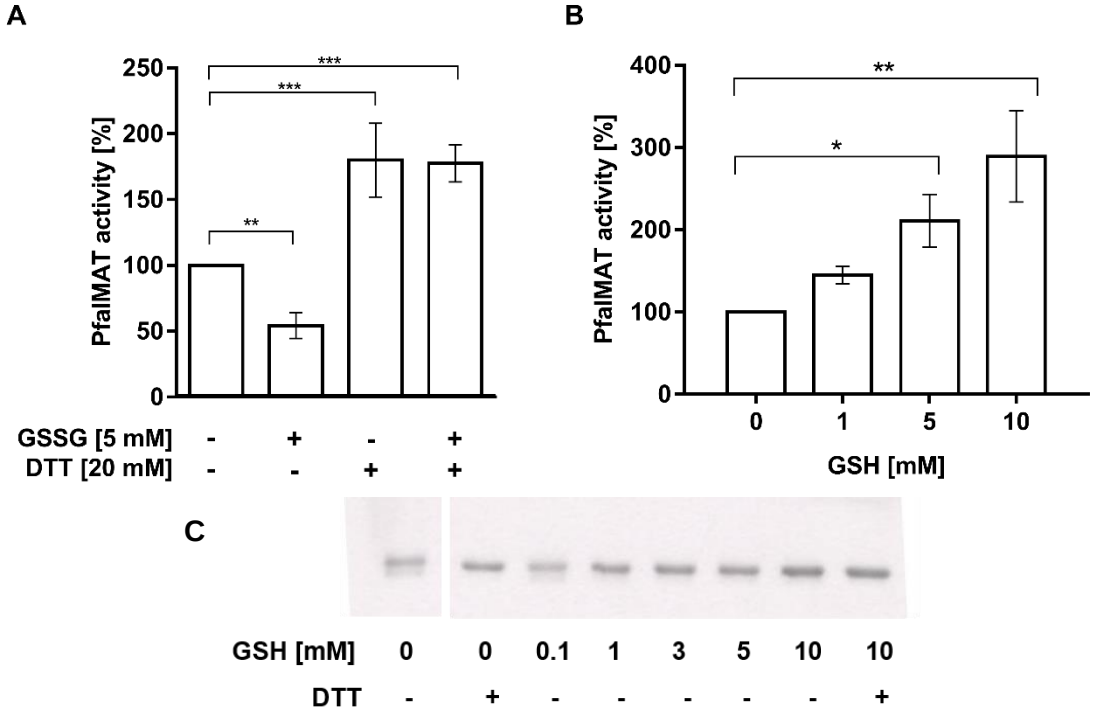

Figure 21: Reversible protein-*S*-glutathionylation of PfalMAT

A: Inhibition of PfalMAT 5 mM GSSG and deglutathionylation mediated by DTT. One-Way ANOVA with a 95% confidence level was performed in order to compare means between groups. **B**: Activity of PfalMAT incubated with different concentrations of reduced glutathione. Kruskal-Wallis One-Way-ANOVA with a 95% confidence interval and Dunn's multiple comparisons test was performed. **C**: Western blot of PfalMAT incubated with different concentrations of GSH using anti-GSH antibody. *p < 0.05, **p < 0.01, ***p < 0.001.

Protein-*S*-glutathionylation of PfalMAT was not only reversible with DTT. The redox-active proteins PfTrx1 and PfPlrx were also able to deglutathionylate PfalMAT-SG, as indicated by restored activity of PfalMAT upon incubation with these redoxins (Figure 22 A) and decreasing signals on Western blots using an anti-glutathione antibody with increasing redoxin concentration (Figure 22 B). In comparison, PfGrx was unable to deglutathionylate PfalMAT-SG up to a molar ratio between PfalMAT and PfGrx of 1:5 (Figure 22 A, B).

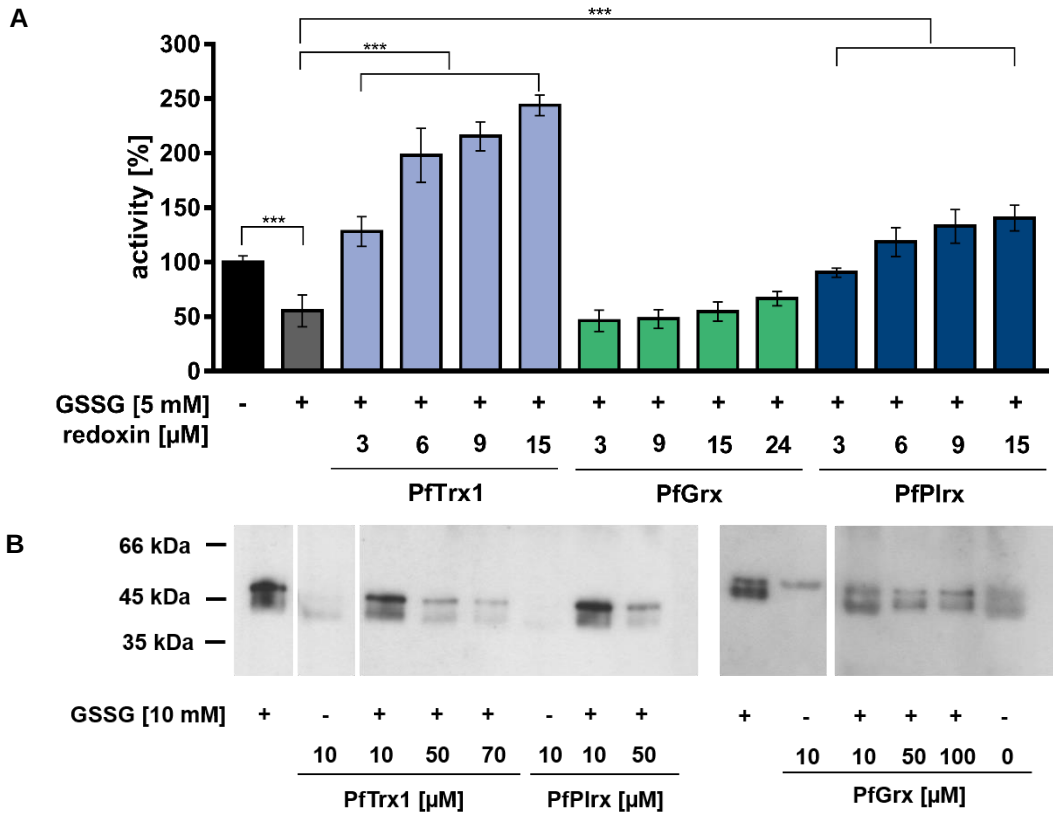

Figure 22: Deglutathionylation of PfalMAT by redoxins.

A: Activity of glutathionylated PfalMAT upon incubation with different concentrations of redoxins. One-Way ANOVA with a 95% confidence level was performed in order to compare means between groups. *p < 0.05, **p < 0.01, ***p < 0.001. **B**: Western blot of glutathionylated PfalMAT incubated with different concentrations of redoxins using anti-GSH antibody.

In order to identify *S*-glutathionylation sites of PfalMAT, the effect on the cysteine deletion in PfalMAT^{C52S}, PfalMAT^{C113S}, and PfalMAT^{C187S} was investigated. Interestingly, each of the cysteine mutants could be *S*-glutathionylated as shown via Western blots using an anti-GSH antibody (Figure 24).

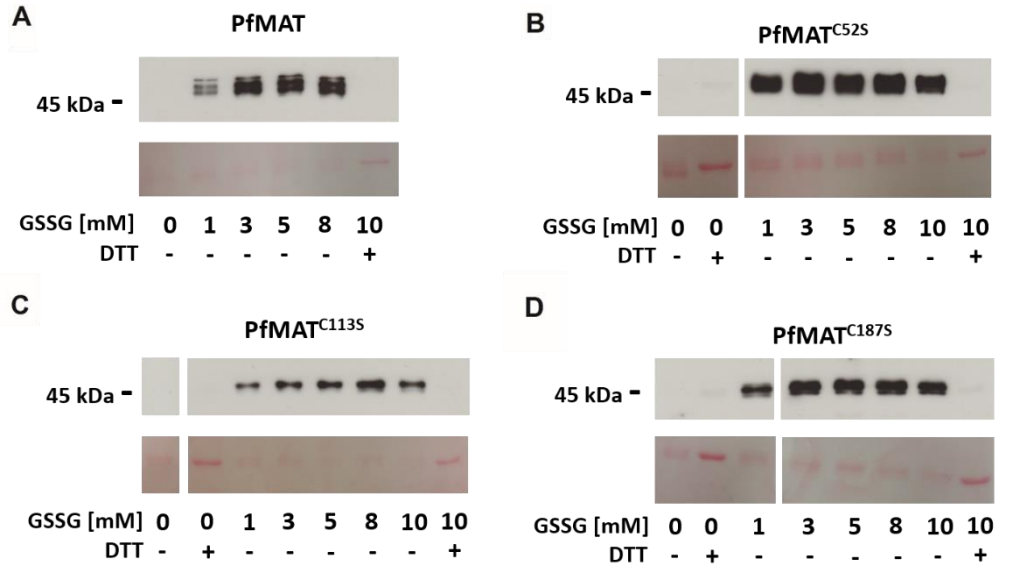

Figure 23: Formation of mixed disulfides between PfalMAT and glutathione

Western blots of PfalMAT (**A**), PfalMAT^{C52S} (**B**), PfalMAT^{C113S} (**C**), and PfalMAT^{C187S} (**D**) incubated with different concentrations of GSSG using anti-GSH antibody.

Even low concentrations of GSSG of 0.1-0.5 mM were sufficient for inhibiting enzymatic activity. PfalMAT^{C52S} showed an inhibition pattern similar to PfalMAT, whereas PfalMAT^{C187S} was more susceptible to inhibition in response to *S*-glutathionylation (by ~ 40%, after adding 3-5 mM GSSG, $p < 0.001$ Two-Way ANOVA) (Figure 24).
The lack of Cys113 resulted in a weaker inhibition (by ~ 20% by 0.5-5 mM GSSG, $p < 0.01$ Two-Way ANOVA) than PfalMAT, which 3-5 mM GSSG inhibited by ~50-60%. Nevertheless, each of the cysteine deletion mutants could still be *S*-glutathionylated.

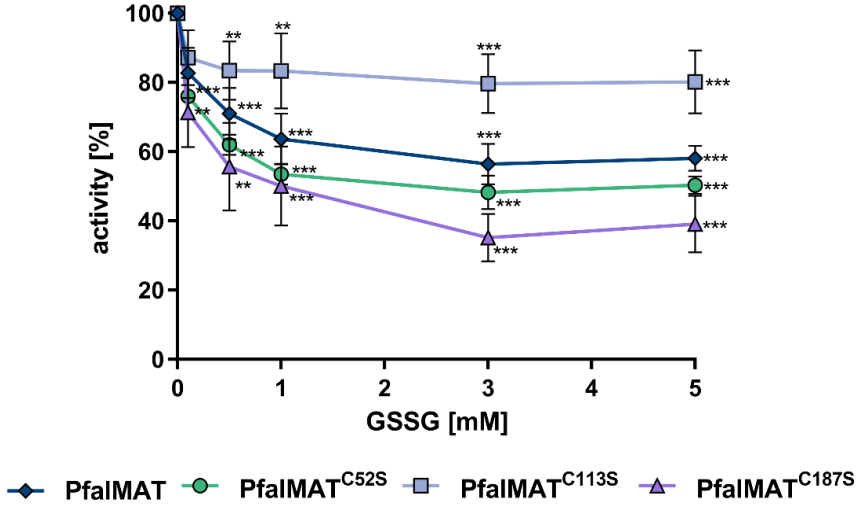

Figure 24: Activity of *S*-glutathionylated PfalMAT and mutants

Activity of reduced PfalMAT, PfalMAT^{C52S}, PfalMAT^{C113S}, and PfalMAT^{C187S} incubated with different concentrations of GSSG. One-Way ANOVA with a 95% confidence level was performed in order to compare means within. *$p < 0.05$, **$p < 0.01$, ***$p < 0.001$

Besides an effect on enzymatic activity, there are hints that the oligomerization states of MATs are possibly regulated via *S*-glutathionylation, as demonstrated for rlMAT, which was monomerized in response to this post-translational modification (Pajares *et al.*, 1992). Based on this, the oligomerization behavior of PfalMAT-SG and glutathionylated mutants was determined via gel filtration (Figure 25). Protein-*S*-glutathionylation indeed affected the oligomerization of PfalMAT. It partly shifted the predominantly dimeric state of the untreated enzyme (Figure 12 A) to high molecular weight oligomers as observed for PfalMAT-SG. This trend was similarly observed for the cysteine deletion mutants. Furthermore, glutathionylation also resulted in a partial monomerization of PfalMAT and the mutants, represented by the shoulders of the peak at ~85 minutes.

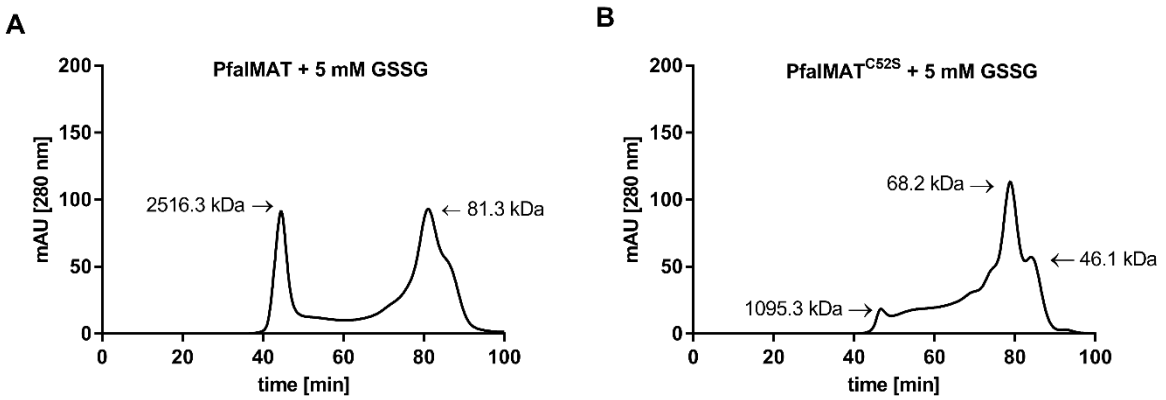

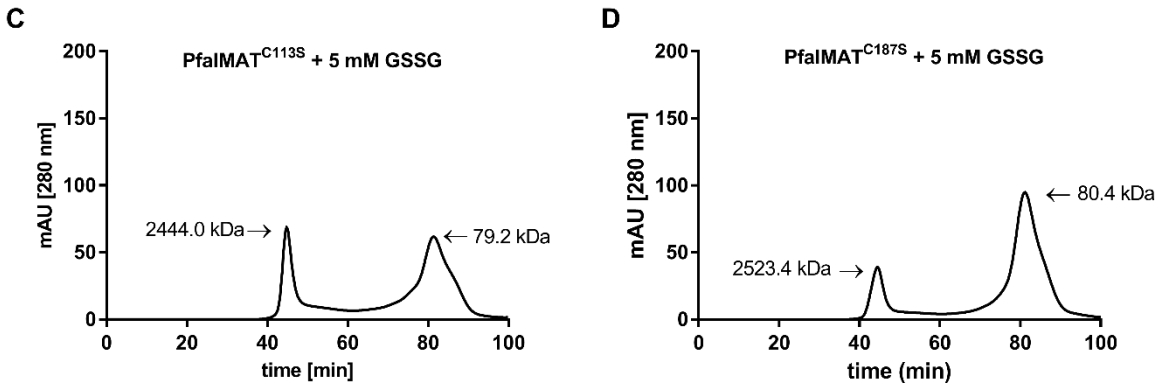

Figure 25: Oligomerization behavior of PfalMAT upon *S*-glutathionylation

Oligomerization behavior of PfalMAT (**A**), PfalMAT^{C52S} (**B**), PfalMAT^{C113S} (**C**), and PfalMAT^{C187S} (**D**) after treatment with 5 mM GSSG.

4.1.8 Protein-*S*-nitrosylation of PfalMAT

In pull-down experiments, PfalMAT hab previously been demonstrated to undergo *S*-nitrosylation (Wang *et al.*, 2014). The interaction of PfalMAT with the physiologically relevant NO donor *S*-nitrosoglutathione (GSNO) was further characterized in a master thesis via Western blots using an anti-biotin antibody after a biotin switch assay and ammonium molybdate assay, showing that PfalMAT is *S*-nitrosylated in a concentration and time-dependent manner (Gehr, 2014). In this dissertation, the effect of *S*-nitrosylation on the selected cysteine mutants as potential *S*-nitrosylation sites for PfalMAT was addressed.

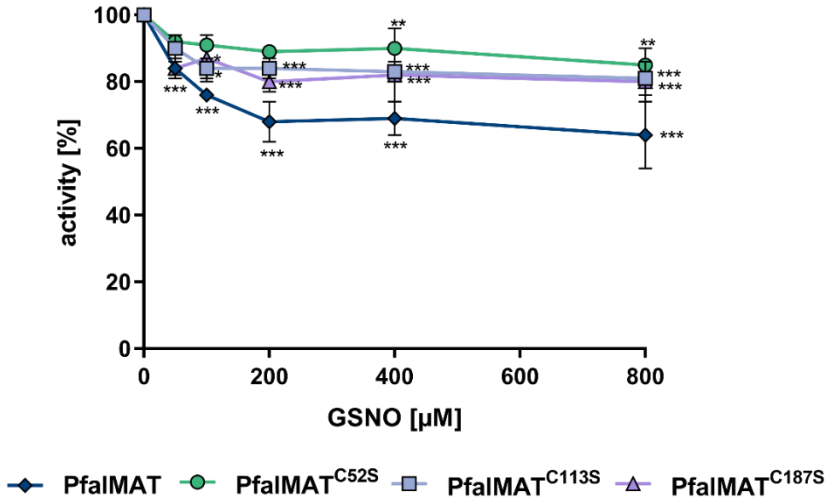

Figure 26: Protein-*S*-nitrosylation of PfalMAT

Inhibition of PfalMAT and mutants after incubation with different concentrations of GSNO. One-Way ANOVA with a 95% confidence level was performed in order to compare means within groups. *p < 0.05, **p < 0.01, ***p < 0.001

PfalMAT as well as the cysteine mutants were only weakly inhibited by GSNO (Figure 26). A Two-Way ANOVA was performed in order to compare the activity of each protein at each GSNO concentration, revealing that there are no significant differences in the extent of inhibition between the three mutants. However, PfalMAT^{C52S}, PfalMAT^{C113S}, and PfalMAT^{C187S} were found to be less susceptible to *S*-nitrosylation than PfalMAT. While PfalMAT was inhibited upon incubation with 200-1000 µM GSNO by ~35%, the mutants PfalMAT^{C52S}, PfalMAT^{C113S}, and PfalMAT^{C187S} were inhibited only by ~15-20% ($p < 0.01$, $p < 0.001$, and $p < 0.01$, respectively).

4.2 *M. scorodonius* DyP-type peroxidase 1

One aim of my dissertation was to provide high quality crystals of MscDyP1 for solving the three-dimensional structure of the protein via X-ray crystallography. Based on the structure of MscDyP1 the yet unknown catalytic structure of MscDyP1 was elicidated via mutational analyses of selected stuctural features.

4.2.1 Crystallization of MscDyP1

During this dissertation the crystallization conditions for MscDyP1 were systematically optimized by screening various conditions including buffer, pH, salt, precipitant and protein concentrations, temperature, crystal additives, and seeding using small crystals which were previously vortexed using beads (Hampton Research) to generate a seed stock, which was then titrated into new drops. Recombinant MscDyP1 produced in *A. niger*, desalted and stored in H_2O, was used for protein crystallization experiments in a ratio 1:2 to reservoir solution using the hanging drop technique. Initially, crystal N (native protein) was obtained under the following conditions (10 mg*mL^{-1} rMscDyP1 in H_2O, 100 mM Tris, pH 8.5 with 100 mM $MgCl_2$, 3 % PEG 4000 and 1.5% 1,2,3-hetane triol) using the additive screen 1 (Hampton Research). Then, crystal D was obtained under the same conditions, but with 8 mg*mL^{-1} rMscDyP1. Crystal D provided better resolution than crystal N and was derived from a highly pure protein fraction that was suggested to be dimeric (personal communication with Katharina Schmidt, Zorn lab, Department of Food Chemistry and Food Biotechnology, Justus Liebig University Giessen). Additionally, rMscDyP1 was either co-crystallized with the pseudo substrates annatto and bixin or previosly obtained native crystals were soaked in mother liquor containing excess amount of the pseudo substrate. Upon soaking with either annatto or bixine, the crystals immediately cracked. However, co-crystallization experiments under the same conditions as crystal N, led to growth of crystal A (4 mg*mL^{-1} rMscDyP1 crystallized in the presence of annatto) and crystal B (4 mg*mL^{-1} rMscDyP1 crystallized in the presence of bixine). All crystals grew within five days at 25°C. All together, four crystals in complex with the heme cofactor with corresponding structures were obtained (Figure 27).

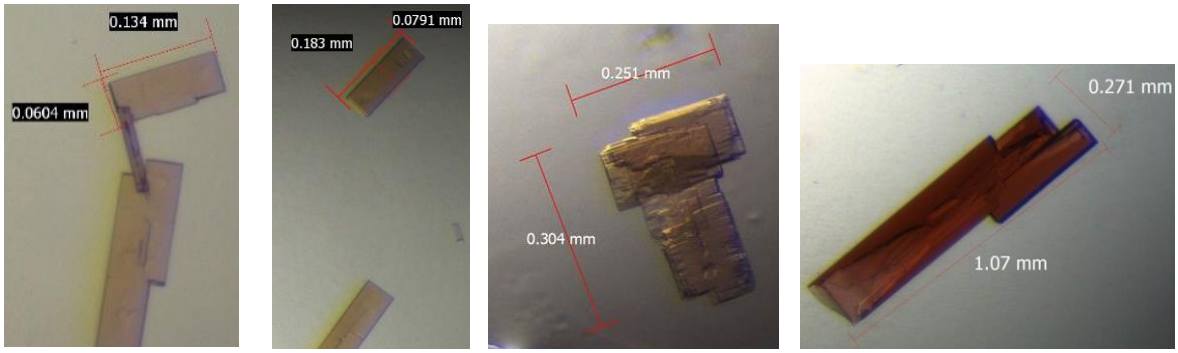

1.6 Å **A** | **1.6 Å** **B** | **2.5 Å** **C** | **2.2 Å** **D**

Figure 27: Protein crystals of MscDyP1

A: crystal A. 4 mg*mL^{-1} (*A. niger*) rMscDyP1 crystallized in the presence of excess amounts of annatto. **B**: crystal B. 4 mg*mL^{-1} (*A. niger*) rMscDyP1 crystallized in the presence of excess amounts of bixin. **C**: crystal N. 10 mg*mL^{-1} (*A. niger*) rMscDyP1 crystallized without substrates. **D**: crystal D. 8 mg*mL^{-1} dimeric (*A. niger*) rMscDyP1. All crystals grew at 25°C in 100 mM Tris, pH 8.5 with 100 mM $MgCl_2$, 3 % PEG 4000 and 1.5% 1,2,3-hetane triol.

Dr. Karin Fritz-Wolf collected the diffraction data and refined the structures. The X-ray diffraction datasets were processed using the XDS software package (Kabsch, 2010). The structures were solved via molecular replacement using BadDyP (PDB ID 3mm1) as a search model. MscDyP1 displays 51.6% and 54.8% sequence identity to BadDyP and AauDyP, respectively (Figure 28). These fungal proteins are secreted and therefore contain a target sequence (residues 1-55 of MscDyP1), which was excluded during structure determination of the processed protein starting at position 56.

```
MscDyP1  ASSSAGLNLTDIQGDILIGMKKNKELFFFFSITDAATFKAKLGSDILGLITS-TNQLLAV 114
BadDyP   -ANDTILPLNNIQGDILVGMKKQKERFVFFQVNDATSFKTALKTYVPERITSAAILISDP  59
AauDyP   ---ATSLNTIDIQGDILVGMHKQKQLFYFFAINDPATFKTHLASDIAPVVAS-VTQLSNV  56
             : *   :******:**:*:*: * ** :.* ::**: * : :   ::* .  :

MscDyP1  ATQPVTAVNVAFSSTGLKALGITDDLKDPVFEAGMLSNAVSDLSDPGTGNWVPGFVGTSV 174
BadDyP   SQQPLAFVNLGFSNTGLQALGITDDLGDAQFPDGQFADAANL--GDDLSQWVAPFTGTTI 117
AauDyP   ATQPLVALNIAFSNTGLLALGVTDNLGDSLFANGQAKDATSF--KESTSSWVPQFAGTGI 114
         : **:. :*:.**.*** ***:**:* *  *  *   :*..       ..**  *.** :

MscDyP1  HGVFLLASDTIDNVNTELANIQTILNGSITEIHRLQGEARPGDQQGHEHFGFMDGISNPA 234
BadDyP   HGVFLIGSDQDDFLDQFTDDISSTFGSSITQVQALSGSARPGDQAGHEHFGFLDGISQPS 177
AauDyP   HGVIILASDTTDLIDQQVASIESTFGSSISKLYSLSASIRPGNEAGHEMFGFLDGIAQPA 174
         ***:::.**  * ::    .*.: : .**:::  *... ***:: *** ***:***::*:

MscDyP1  VDGFTPPAEIRPGQALIPPGIMLLGEANDTFQNDRPPWAKDGSFLVFRQMQQRAPEFNKF 294
BadDyP   VTGWET--TVFPGQAVVPPGIILTGRDGDT--GTRPSWALDGSFMAFRHFQQKVPEFNAY 233
AauDyP   INGFNT---PLPGQNIVDAGVIITGATNDP--ITRPSWAVGGSFLAFRQLEQLVPEFNKY 229
         : *:       *** ::  *::: *   *     ** **  ***:.**:::* .**** :

MscDyP1  LQDHALNM---PNMTSEQGADLLGARIVGRWKSGAPIDLTPLVDDPVLAADNQRNNNFDF 351
BadDyP   TLANAIPANSAGNLTQQEGAEFLGARMFGRWKSGAPIDLAPTADDPALGADPQRNNNFDY 293
AauDyP   LLDNAPA----GSGSLQARADLLGARMVGRWKSGAPIDLTPTADDPALGADAQRNNNFTY 285
            .*       . : :  *::****:.***********:* .***.*.** ****** :

MscDyP1  SDA-----TNQTRCPFSAHIRKANPRGDLGGINKFPN-----QHIIRAGIPYGPEVTDAE 401
BadDyP   SDT----LTDETRCPFGAHVRKTNPRQDLGGPVDT-------FHAMRSSIPYGPETSDAE 342
AauDyP   SHAGFDLGSDQSHCPFSAHIRKTRPRADLGGSLTPPNLSAGANSIMRSGIPYGPEVTSAE 345
         *.:     ::::::***.**:**:.** ****              :*:.******.:.**

MscDyP1  KASNSSSTDPSLERGLAFVAYQSNIQNGFVFLQKNWVDNTNFFRP----GTGVDPLIGTN 457
BadDyP   LASGVT----AQDRGLLFVEYQSIIGNGFRFQQINWANNANFPFSK-PITPGIEPIIGQT 397
AauDyP   SASNTT----TQERGLAFVAYQAQLSQGFHFLQQTWADNANFPPGKTPATVGLDPIIGQN 401
          **  :    : :*** ** **: : :** * * .*.:*:**         *::*:** .

MscDyP1  SRNSGTDAPNTPRVVSGLDPNNATSTIEIGIDFVVSRGGEYFFSPSLSAIRTVLSV     513
BadDyP   ----------TPRTVGGLDPLNQNETFTVP-LFVIPKGGEYFFLPSISALTATIAA     442
AauDyP   N--------GQPRVVNGLLPSNSSASLSIP-QFVVSHGGEYFFSPPISAIGGRLSA     448
                   **.* ** * * . :: :   **: :****** * :**:   ::.
```

Figure 28: Sequence alignment of MscDyP1, BadDyP, and AauDyP

* Identical residues, **:** Very similar residues, **.** Similar residues. The catalytic conserved GXXDG motif is highlighted in gray. Residues involved in the formation of the H_2O_2 binding pocket are enclosed in a box. Cys306, M302 and M305 of MscDyP1, which were mutated during this dissertation, are colored red. The alignment was prepared using Clustal Omega 1.2.1.

4.2.2 Crystal structure of MscDyP1

A PDB file of the unpublished, deprotonated, and minimized structure of crystal D of MscDyP1 was used for preparing the figures in this dissertation. Figures were used to illustrate the underlying hypothesis for mutational studies performed here, to discuss their structural and functional roles for MscDyP1, and to propose and discuss a possible catalytic mechanism.

The three dimensional structure of MscDyP1 indicates all typical structural characteristics of other members of the DypPrx superfamily, including all residues at the heme distal site, Asp228, Arg388, Leu417, and Phe419. Those residues correspond to Asp171, R329, L354 and F356 of BadDyP (Yoshida *et al.*, 2011), are conserved among DypPrx, form the hydrogen peroxide binding pocket, and are necessary for catalytic activity. Furthermore, the structure strongly binds a water molecule at the heme distal site, which will probably be replaced by H_2O_2 upon catalysis.

The superposition of MscDyP1 with BadDyP, the search model used for structure determination and the first and eponymous member of this enzyme family, and superposition with AauDyP indicates highly conserved secondary structure elements (Figure 29). MscDyP1 is highly glycosylated with N-acetyl glucosamine (NAG) and β-D-mannose (BMA). Six sugar molecules were identified in the crystal structure model, whereas the glycosylation pattern differed between the four crystals in the Asn position, depending on whether NAG or BMA was bound. However, BMA and NAG at Asn304 are present in each of the four structures, with NAG likewise being conserved in BadDyP.

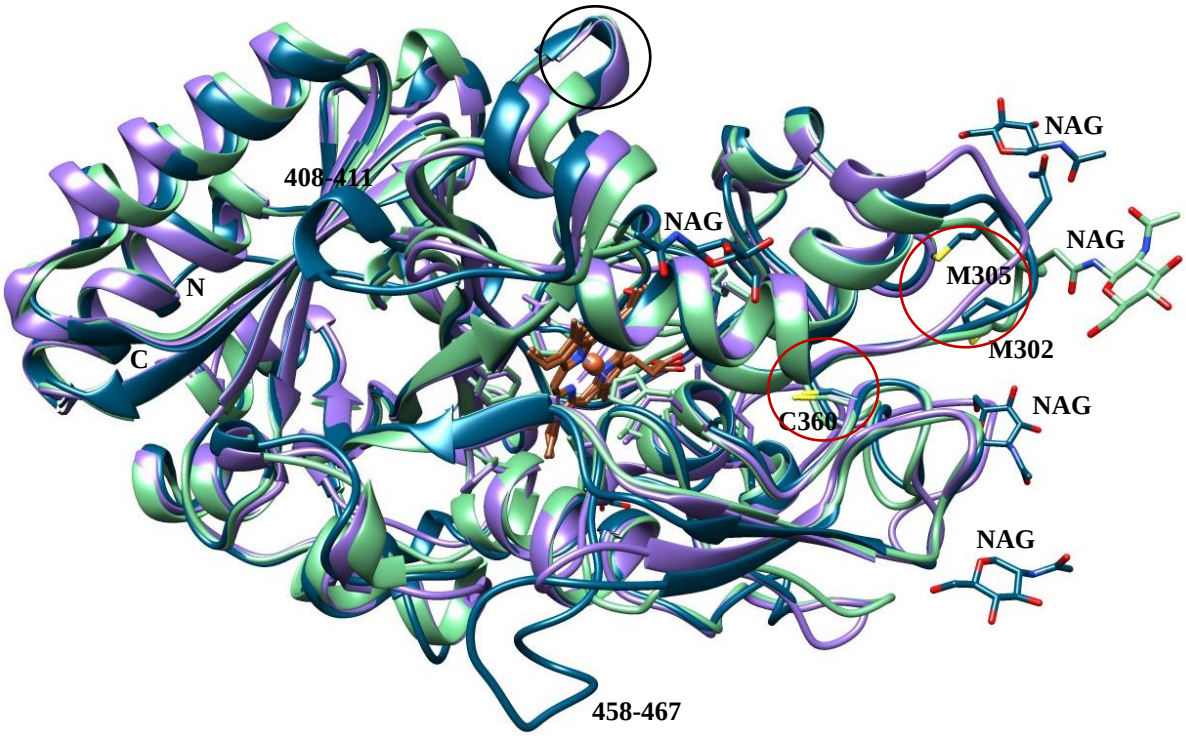

Figure 29: Superposition of MscDyP1, BadDyp, and AauDyP

MscDyP1 subunit A and its respective sugar molecules are colored blue, the BadDyP structure is green, and AauDyP is purple. The heme central atom is indicated in brown. GXXDG motif of MscDyP1 is enclosed in a circle. Conserved sugar molecules, residues of the heme cavity, a single conserved cysteine, and two methionine residues are depicted as sticks and highlighted with a red circle. Superposition was performed using Needleman-Wunsch algorithm and BLOSUM 55 matrix using the program UCSF Chimera.

A single cysteine residue is worthy of note in the superposition, which is conserved among MscDyP1, BadDyP, and AauDyP. In MscDyP1, Cys360 is surrounded by hydrophobic residues; for example I366 which contributes to the formation of the heme-binding pocket. Additionally, two methionine residues, Met302 and Met305, is noteworthy at the surface of MscDyP1. MscDyP1 is suggested to adapt a dimeric assembly (Hayashi *et al.*, 2012) and both methionine residues are located at the possible dimer interface. Furthermore, Met302 and Met305 are located in a hydrophobic pocket and at the top of a helix, which is involved in the formation of the heme-binding pocket.
Although they are suggested to form a biochemically active dimer, interestingly, only weak intersubunit interactions are present in MscDyP1, whereas the main contact is mediated via conserved sugar molecules (BMA and NAG) located in the subunit interface as shown in Figure 30. In detail, intersubunit interactions are mediated via NAG, which is covalently bound between both subunits via hydrogen bonds to Asp138' of subunit B and mediated via a water molecule to Thr306 and the backbone of Asn304 of subunit A. Furthermore, Asp138' accepts a hydrogen bond from BMA. Direct monomer-monomoer interaction is facilitated by Asn304, that covalently binds to the nitrogen backbone of Trp272', and by van der Waals forces between Pro303 of subunit A and Thr509' and Val510' of subunit B, as well as between the flexible Met305 of subunit A and Pro271' of subunit B (Figure 30).

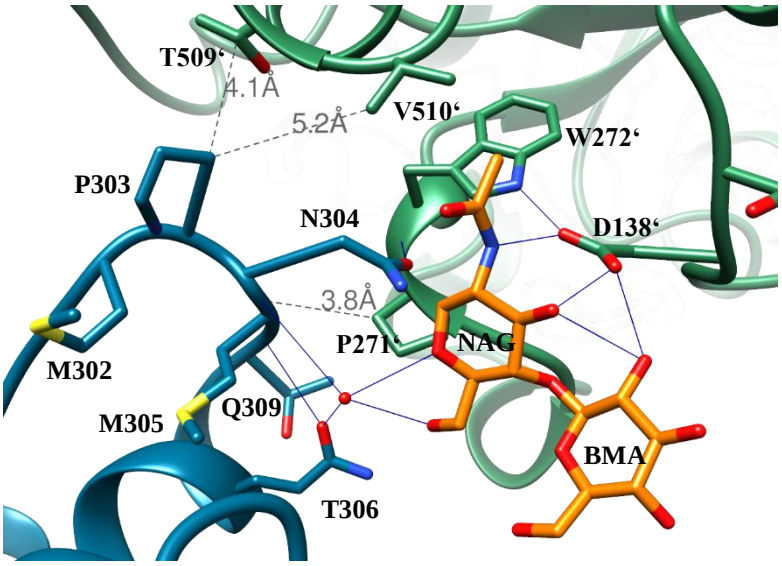

Figure 30: Dimer interface of MscDyP1

Dimer interface of MscDyP1 crystal D. Subunit A is indicated in blue, subunit B in green, and the sugar molecule mediating dimerization is orange. Possible intersubunit interactions mediated via hydrogen bonds are indicated with light blue lines, and via van der Waals forces in light gray. Residues of subunit B are indicated by a single quotation mark to distinguish them from residues of subunit A. This figure was created using UCSF Chimera.

Two solvent-accessible cavities are observable in the structure of MscDyP1 (Figure 31), including the accession channel through Lys76, Asn78, Gln219, and Gly229 toward the heme plane for H_2O_2 entry (Figure 31 A).

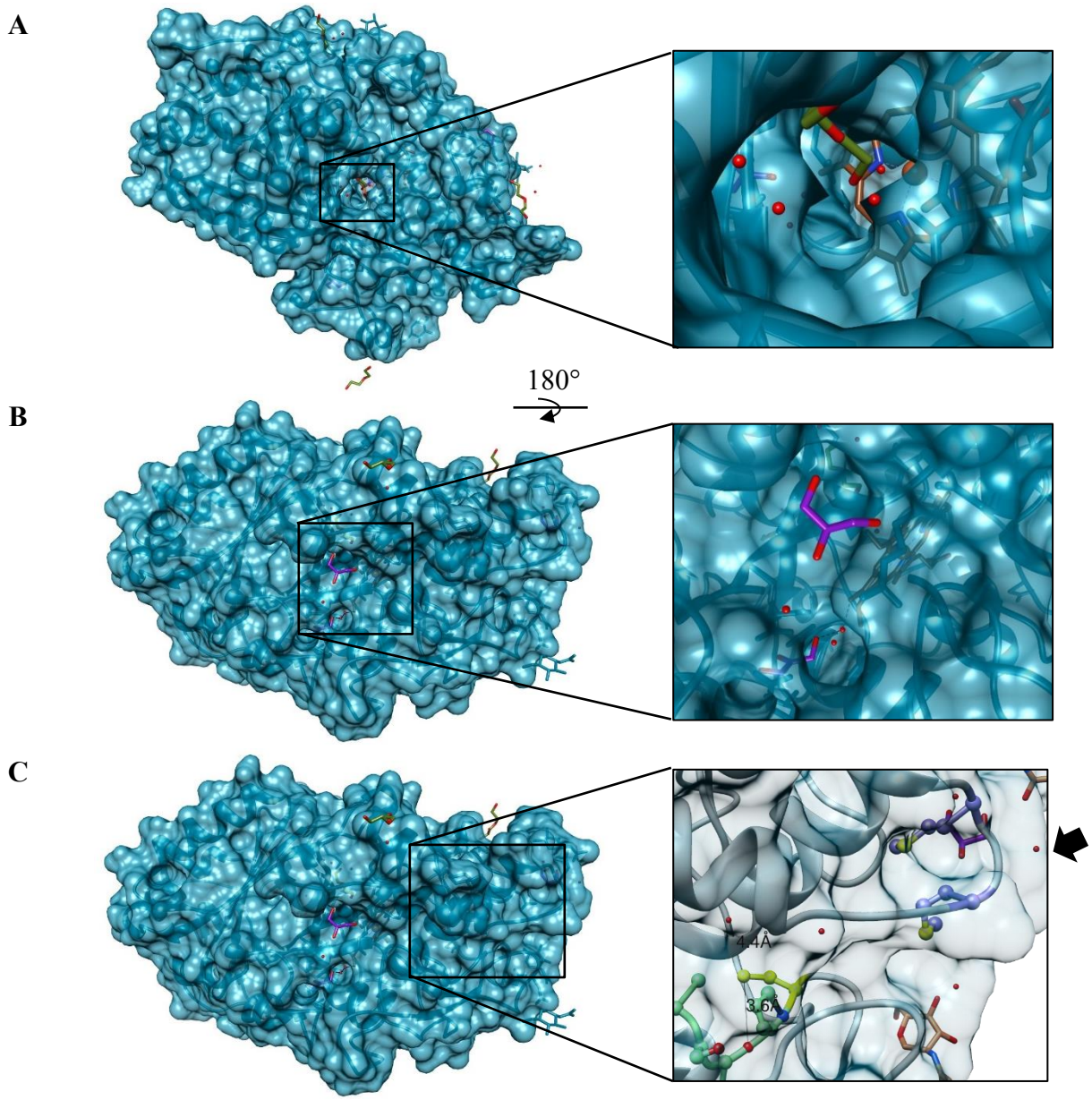

Figure 31: Solvent accessible cavities of MscDyP1

A: Channel toward heme (brown) plane of MscDyP1 with a bound PEG molecule (green) and conserved water atoms (red balls). **B:** Second solvent-accessible cavity with a bound glycerol molecule (purple) and conserved water molecules [heme to water 265 (3.1 Å) and from water to glycerol (2.2 Å)]. **C:** Cysteine cavity. Two possible entrances to Cys (yellow) are connected via water molecules to the protein surface. The position of the first entrance is indicated by the protecting NAG molecule (orange) and the second entrance is located at the two Met residues (purple), indicated by the black arrow. Here, the solvent is indicated by the violet GOL molecule. The main chain backbone is colored light green. This figure was created using UCSF Chimera and subunit A of crystal D.

Interestingly, in each of the crystal structures of MscDyP1, a PEG molecule is present in the heme cavity, except in crystal A, where it is missing. A further cavity is approximately located on the opposite side enclosed by the residues Asn164, Arg287, Pro466, Asn467, and Val492 (Figure 31 B). Although this second cavity is too narrow for substrate binding it at least allows small molecular weight compounds to enter, as represented by a glycerol observable in the crystal structure. A third cavity could be identified containing the conserved cysteine residue (Figure 31 C). This cysteine cavity is accessible to small molecules, e.g. H_2O or H_2O_2.

H_2O is suggested to form a hydrogen bond to the sulfur atom of Cys360 (distance of 4.2 Å between SG of Cys360 and conserved H_2O). The cysteine cavity is formed by conserved hydrophobic residues, e.g. Ile366 in MscDyP1, which contribute to the formation of the heme-binding pocket. The cysteine cavity has two possible entrances: one is protected by a NAG molecule, the other entrance is not solvent exposed but rather connected via a network of water molecules to the methionine residues in the dimer interface.

4.2.3 Molecular docking of substrates into MscDyP1 structure

Co-crystallization attempts of MscDyP1 using the carotenoid pseudo-substrates bixin and annato were not successful. As a result, crystals A and B did not contain the expected ligands. Therefore, molecular docking of the substrates β-carotene and 2,6-dimethoxyphenol into the crystal structure of MscDyP1 without constraints was performed using the provided pdb file of crystal D with the program Gold 5.2. The docking poses were ranked according to PLP-fitness from highest to lowest. Selected docking poses are shown in Figure 32.

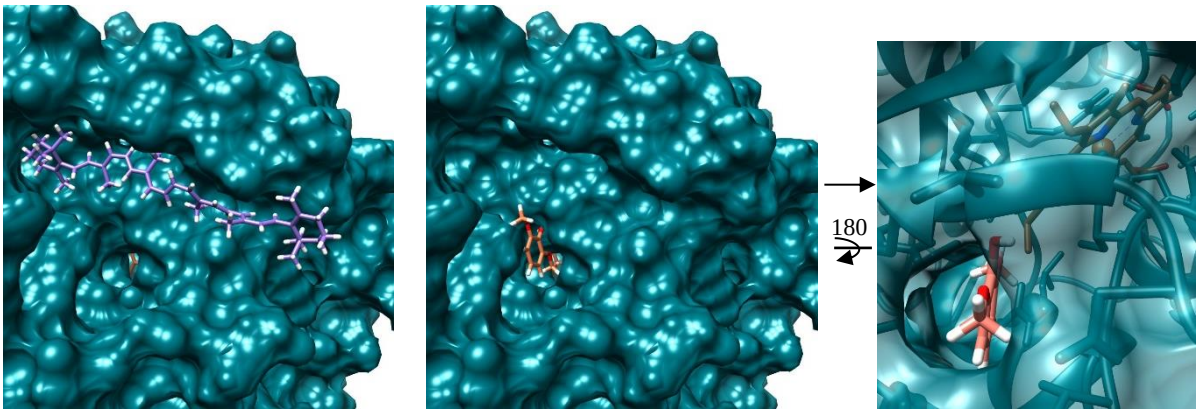

Figure 32: Docking poses of β-carotene and 2,6-dimethoxyphenol

A: Best-scored docking pose of β-carotene (BCR, purple) #167. **B**: Best-scored docking pose of 2,6-dimethoxyphenol (3MD, orange) #72. **C**: Docking pose #56 of 3MD with scoring rank 25. Subunit A is colored petrol, and the heme cofactor is depicted in brown. This figure was created using UCSF Chimera.

The first 196 docking poses of β-carotene showed a similar pose in the cleft at the entrance to the heme accession channel as seen in the best scored energetically favorable position #167. Docking 2,6-dimethoxyphenol into the MscDyP1 structure revealed three different clusters of docking poses. In the best-ranked poses, the substrate was docked into the entrance of the heme accession channel in a manner similar to the PEG molecule bound in crystals N, B, and D. The predominant part of the residual docking poses displayed 3MD near and around the heme accession cavity. One remarkable docking position was #56, which was ranked at scoring position 25 and showed 3MD docked into the second solvent-accessible cavity of MscDyP1, similarly to the solvent component glycerol present in the crystal structure.

4.2.4 Site-directed mutagenesis of structural features of MscDyP1

One aim of this dissertation was to study in detail the role of the sulfur-containing residues Met302, Met305, and Cys360 of MscDyP1. In order to mutate these three residues, the MscDyp1 gene was synthesized commercially, with codon usage optimized for *E. coli* and

cloned into a pET28a vector in order to heterologously overexpress it in *E. coli* BL21 cells. A mutant lacking the sole and conserved cysteine residue was created by substituting Cys360 with glycine via site-directed mutagenesis. Furthermore, a double mutant was created by substituting Met302 and Met305 with lysine.
In order to distinguish the recombinant protein produced in *E. coli* from the one produced in *A. niger*, which was used for crystallization, the respective enzymes will be called (*E. coli*) rMscDyP1 and (*A. niger*) rMscDyP1.

4.2.5 Heterologous overexpression and purification of rMscDyP1 variants

First attempts to heterologously overexpress the (*E. coli*) rMscDyP1 gene were performed in pET28a in KRX cells with the addition of the heme precursor δ-aminolevulinic acid to the expression medium. Using this approach the main fraction remained insoluble (Figure 33).

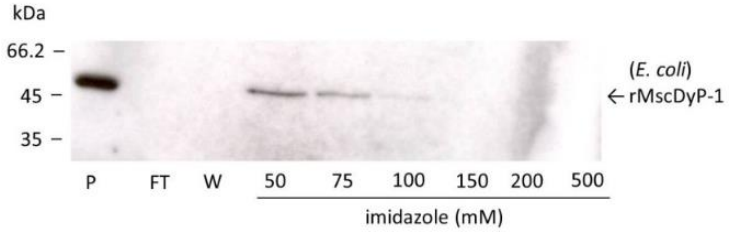

Figure 33: Heterologous overexpression of (*E. coli*) rMscDyP1 in pET28a in KRK cells

Western blot after IMAC using anti-His antibody. P: cell pellet, FT: flow through, W: wash, 50-500: fractions eluted with 50-500 mM imidazole.

Several efforts were made to increase protein solubility: decreasing expression temperature or IPTG concentration to induce gene expression, increasing time for cell lysis with lysozyme and DNaseI from one hour to overnight, increasing buffer volume during lysis to a volume ten-times larger than the cell pellet, using different buffers, adding detergents such as Triton X100, and adding 1-10% glycerol or urea ranging from 0.5 M up to 8 M. However, none of these efforts could increase solubility of (*E. coli*) rMscDyP1. Therefore, several chaperones were tested to assist correct folding and thereby probably increase solubility (Figure 34).

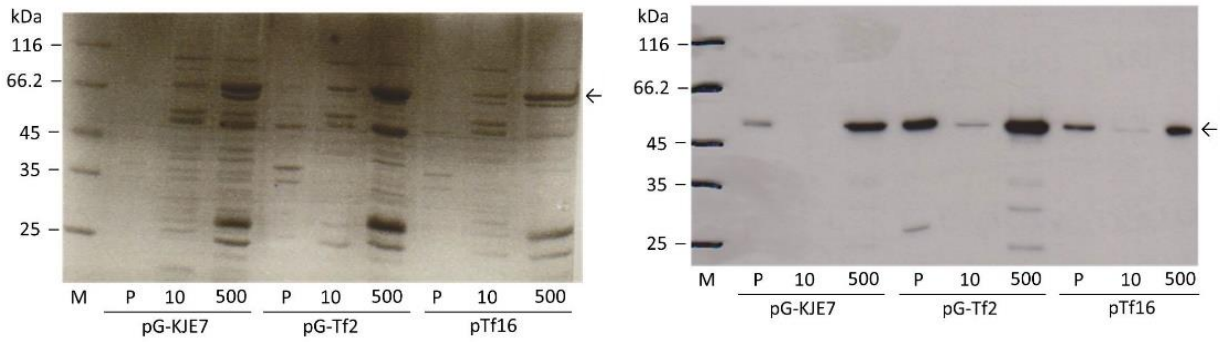

Figure 34: Co-expression of (*E. coli*) rMscDyP1 with chaperones

M: protein ladder, P: cell pellet, 10: 10 mM imidazole for column washing, 500: elution with 500 mM imidazole. SDS PAGE after IMAC (**A**) and Western blots using anti-His-antibody (**B**) for coexpression of (*E. coli*) rMscDyP1 with chaperones dnaK, dnaJ, and grpE (plasmid pG-KJE7); with chaperones groEL, groES, and tig (plasmid pG-Tf2); and with chaperone tig (plasmid pTf16).

The GoEL/GroES chaperone pair was selected for coexpression with (*E.coli*) rMscDyP1 in pET28a in KRX cells with δ-aminolevulinic acid. This approach increased the soluble protein fraction (Figure 35). The purest fraction eluted with 500 mM imidazole was used for biochemical evaluation of the mutants.

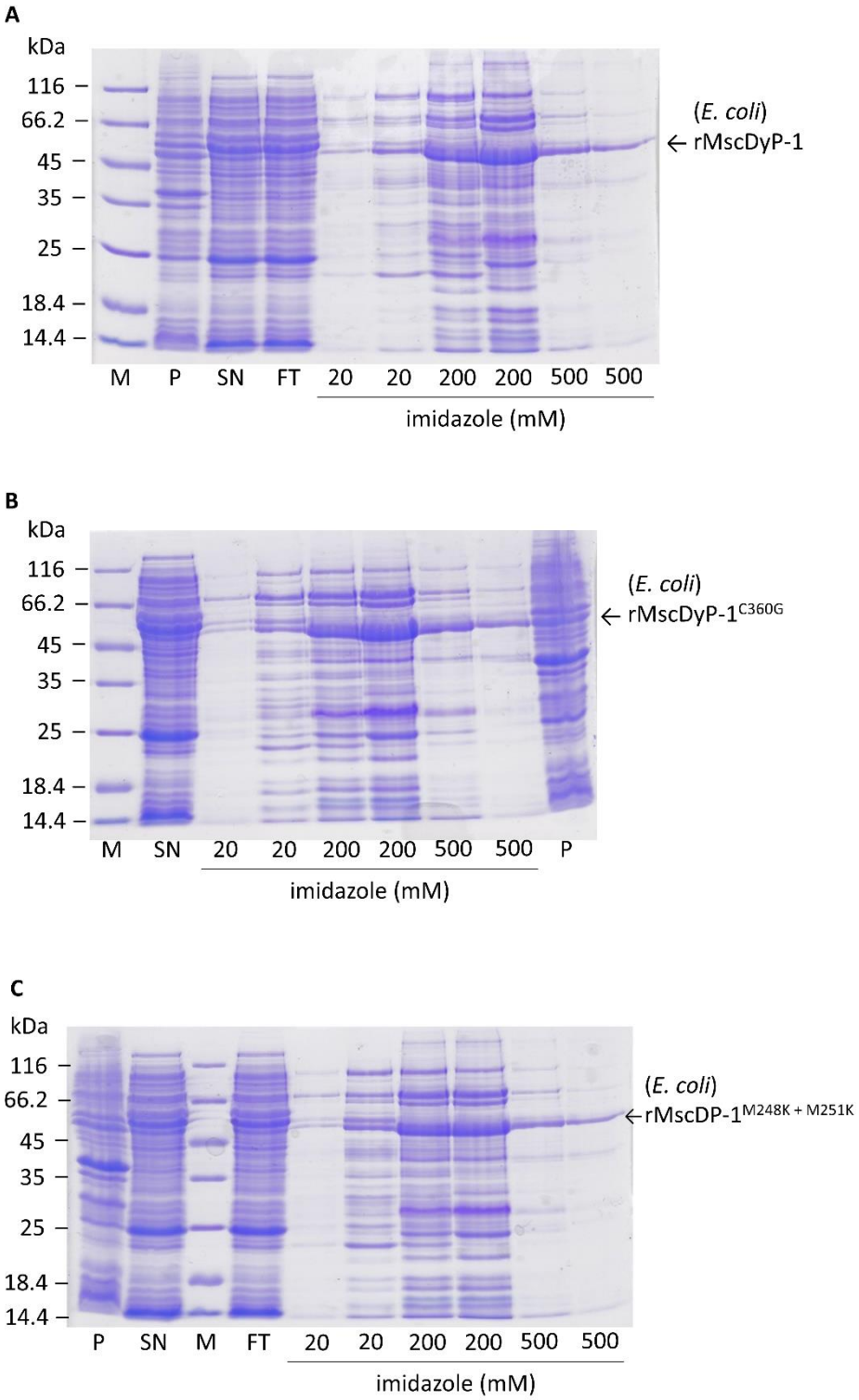

Figure 35: Purification of (*E. coli*) rMscDyP1 via Ni-NTA affinity chromatography

Purification of (*E. coli*) rMscDyP1 (**A**), ($^{E. coli}$) rMscDyP1^{C360G} (**B**), and (*E. coli*) rMscDyP1$^{M302K + M305K}$ (**C**). M: protein ladder, P: cell pellet, SN: supernatant, FT: flow through, 20-500: fractions eluted with 20-500 mM imidazole. The proteins were coexpressed with groEL, groES, and tig.

4.2.6 Kinetic characterization of rMscDyP1 mutants

The peroxidase activity of the recombinantly produced (*E. coli*) rMscDyP1 and the mutants lacking either the single conserved cysteine (Cys360) or the two selected methionine residues (Met302 and Met305) was assessed using the ABTS assay. Table 7 summarizes the respective specific activities. The specific activity of both mutants differs significantly from the specific activity of (*E. coli*) rMscDyP1 within the ABTS assay, indicating that both mutants display a lower peroxidase activity. As shown before, MscDyP1 degrades β-carotene (Zelena *et al.*, 2009). Therefore, ABTS was replaced with β-carotene as a substrate in order to follow β-carotene degradation by (*E. coli*) rMscDyP1 and by both mutants in comparison. Similar results were obtained revealing that both mutants displayed a lower β-carotene degradation activity than (*E. coli*) rMscDyP1. Conspicuously, the relative residual activity following mutation was higher than that obtained within the ABTS assay (Table 7). Additionally, the apparent K_M values of the substrates H_2O_2 and ABTS (Figure 36) were determined (summarized in Table 8).

Table 7: Specific activity of (*E. coli*) rMscDyP1 and mutants

	Specific activity [nmol*min^{-1}*mg^{-1}][a]	
	ABTS assay	β-carotene assay
(*E. coli*) rMscDyP1	1,460 ± 1,340 (100)	9.2 ± 5.0 (100)
(*E. coli*) rMscDyP1^{C360G}	39.1 ± 21.1 (2.7)***	1.2 ± 0.9 (13.0)***
(*E. coli*) rMscDyP1$^{M302K + M305K}$	37.3 ± 20.7 (2.6)***	1.2 ± 0.7 (12.6)***

[a] Values in parentheses are relative activity (%) with the value for (*E. coli*) rMscDyP1 set at 100%. Values are mean values ± SD of at least 5 independent experiments with at least 3 measurements each. *** $p < 0.001$ Dunn's nonparametric multiple comparison for post-hoc testing after Kruskal-Wallis One-Way-ANOVA.

Table 8: Apparent K_M values of (*E. coli*) rMscDyP1 and mutants

	$K_{M, app}$ [μM][a]	
	ABTS	H_2O_2
(*E. coli*) rMscDyP1	51.5 ± 16.7	235 ± 57.1
(*E. coli*) rMscDyP1^{C360G}	60.4 ± 12.7	372 ± 103***
(*E. coli*) rMscDyP1$^{M302K + M305K}$	78.6 ± 8.6**	293 ± 86.8

[a] Apparent K_M of H_2O_2 in the presence of 0.5 mM ABTS and apparent K_M of ABTS in the presence of 0.25 mM H_2O_2 determined using the ABTS assay. The values represent mean values ± SD of at least three independent experiments with at least three reproductions. ** $p < 0.05$, *** $p < 0.001$ Dunn's nonparametric multiple comparison for *post hoc* testing after Kruskal-Wallis One-Way-ANOVA using (*E. coli*) rMscDyP1 as a control.

Cys360 appears to contribute to H_2O_2 reduction by (*E. coli*) rMscDyP1, but does not contribute to the affinity to the substrate ABTS. The lack of the methionine residues has no effect on enzyme affinity to the substrate H_2O_2. In contrast, these data suggest that at least one of the mutated methionine residues affects ABTS binding.

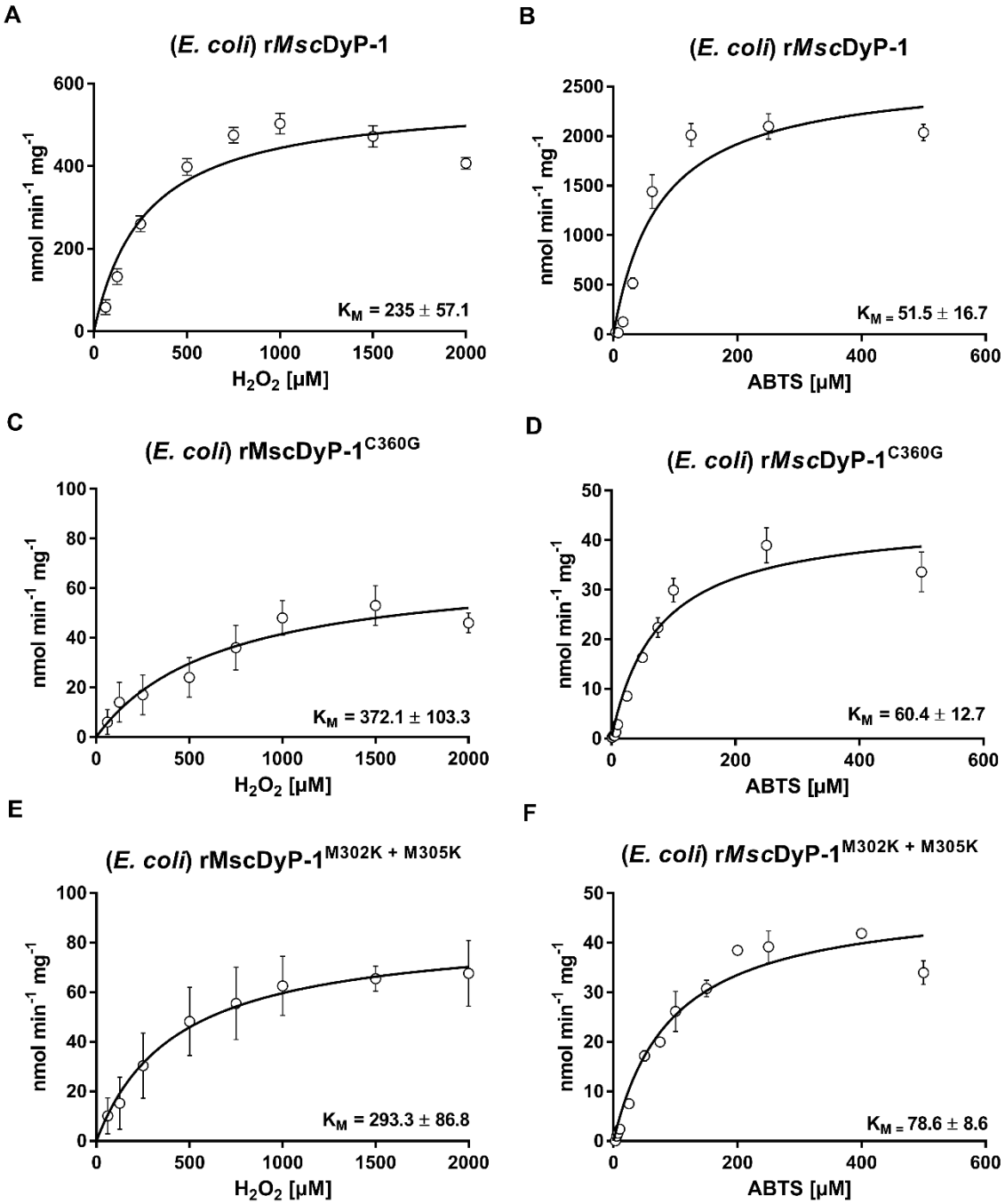

Figure 36: K_M curves for H_2O_2 and ABTS for (*E. coli*) rMscDyP1 and mutants

The graphic shows representative graphs of apparent K_M curves for H_2O_2 (left) in the presence of 0.5 mM ABTS and for ABTS (right) in the presence of 0.25 mM H_2O_2 obtained in the ABTS assay for (*E. coli*) rMscDyP1 (**A, B**), (*E. coli*) rMscDyP1^{C360G} (**C, D**), and (*E. coli*) rMscDyP1$^{M302 + M305}$ (**E, F**), respectively.

Furthermore, both mutants appear to possess a higher H_2O_2 resistance than (*E. coli*) rMscDyP1 (Figure 37). While (*E. coli*) rMscDyP1 is strongly inhibited by H_2O_2 concentrations above 1 mM to approximately 65% activity, both mutants retain about 80% residual activity.

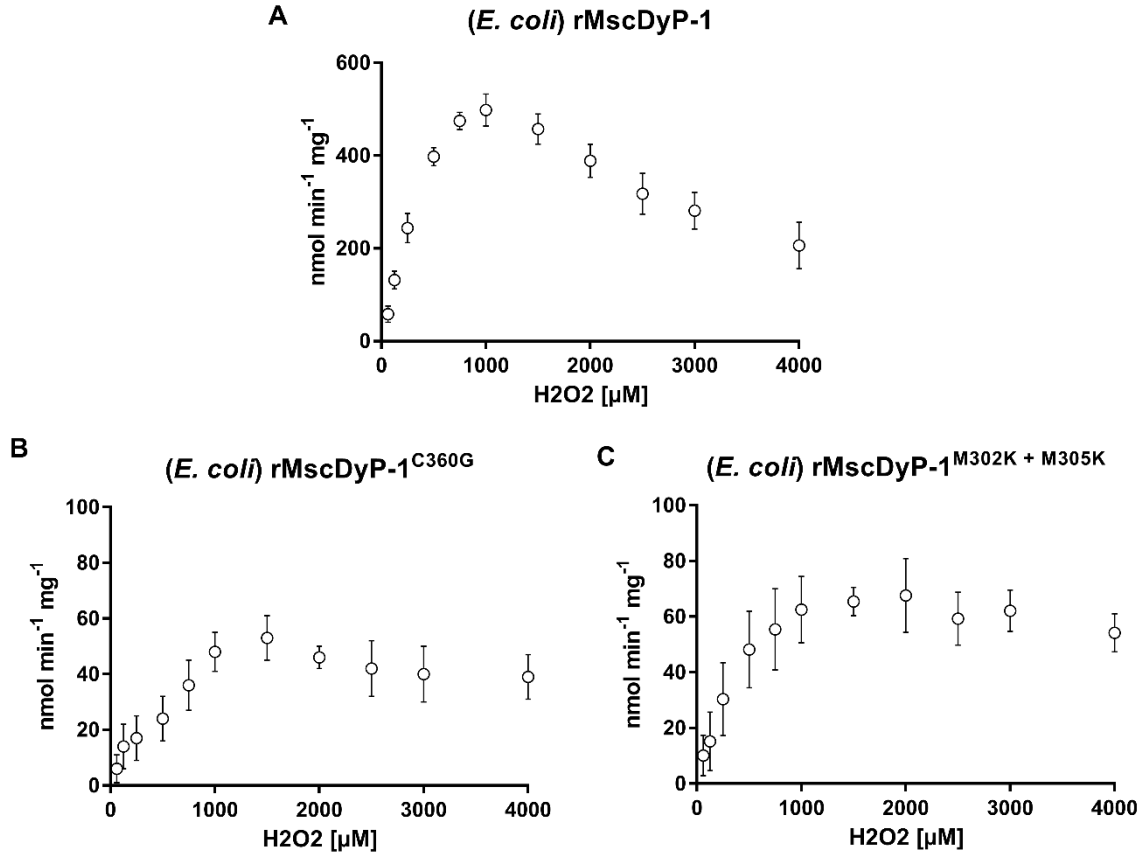

Figure 37: Inhibition of (*E. coli*) rMscDyP1 by excess H_2O_2

The graphic shows representative graphs of activity of (*E. coli*) rMscDyP1 (**A**), (*E. coli*) rMscDyP1^{C360G} (**B**), and (*E. coli*) rMscDyP1$^{M302 + M305}$ (**C**) depending on different H_2O_2 concentrations in the presence of 0.5 mM ABTS obtained in the ABTS assay.

In order to study the contribution of Met305 to the dimerization of (*E. coli*) rMscDyP1, the protein was loaded onto a Superdex 200 prep grade gel filtration column (Figure 38).
The spectrum observed at 280 nm during gel filtration chromatography indicated that the IMAC protein fractions contained a mixture of a ~50 kDa protein, a ~160 kDa protein, and high molecular weight oligomers (~500-2200 kDa). Western blots, using anti-His antibodies to detect His-tagged (*E. coli*) rMscDyP1, indicated that the ~50 kDa protein was a different protein than (*E. coli*) rMscDyP1 (Figure 39) and contributed to the band at around 25 kDa that was co-purified with (*E. coli*) rMscDyP1 via IMAC. It is not the band for the chaperones, since this band was also present in the previous expression approaches without chaperones. Furthermore, an anti-His Western blot assigned all remaining peaks to (*E. coli*) rMscDyP1 and confirmed the presence of these different oligomerization states in (*E. coli*) rMscDyP1. Both mutants exhibited similar oligomerization states to (*E. coli*) rMscDyP1, suggesting that neither Cys360, Met302 nor Met305 contributed to the oligomeric assembly of (*E. coli*) rMscDyP1.

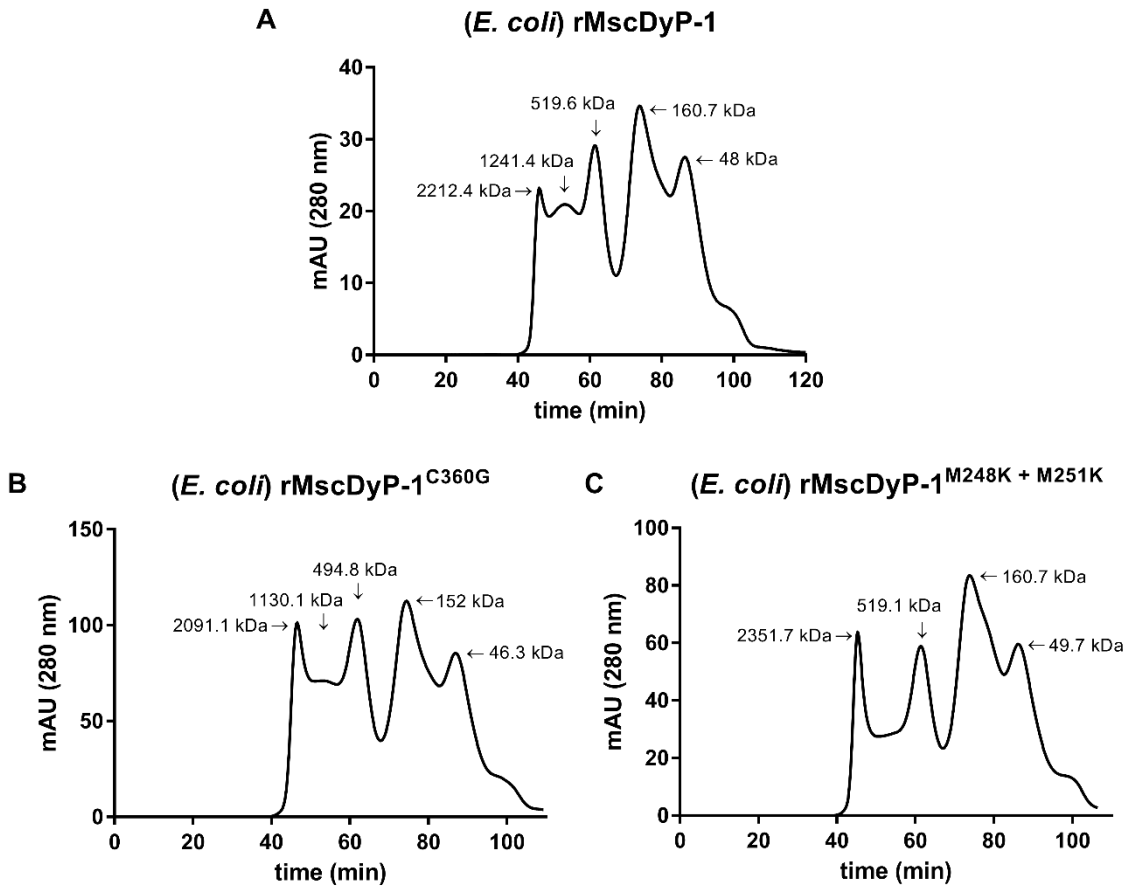

Figure 38: Size exclusion chromatography of (*E. coli*) rMscDyP1 and mutants

Oligomerization behavior of (*E. coli*) rMscDyp1 (**A**), (*E. coli*) rMscDyp1^{C360G} (**B**), and (*E. coli*) rMscDyp1$^{M302 + M305}$ (**C**).

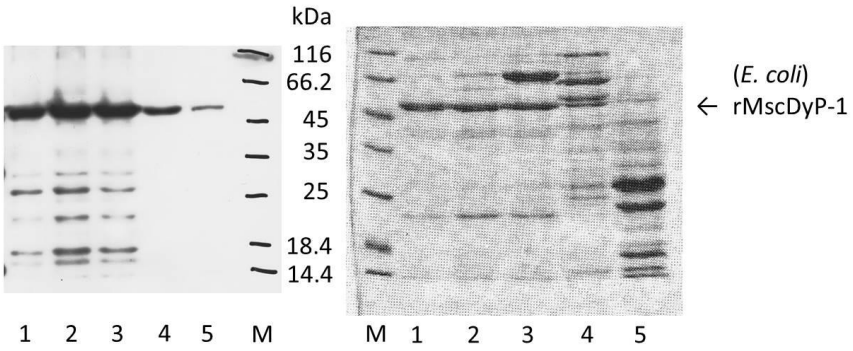

Figure 39: Western blot of (*E. coli*) rMscDyP1 after gel filtration chromatography

Western blot (left) using anti-His antibody and SDS-PAGE of the 1st to 5th eluted peaks detected at 280 nm via gel filtration chromatography. M: protein ladder.

Attempts to partly unfold the high molecular weight aggregates of (*E. coli*) rMscDyP1 by increasing or decreasing the buffer salt concentration (0-500 mM NaCl), reducing the enzyme with 10-20 mM DTT, or partly denaturation with 0.5 M urea had no effect on the oligomerization state.

In order to confirm the role of sulfur-containing amino acids in the enzymatic activities of MscDyP1 and (*E. coli*) rMscDyP1, the recombinant (*A. niger*) rMscDyP1 was treated with the thiol-blocking agents methylmethanethiosulfonate (MMTS) and iodoacetamide (IAA). MMTS blocks the sulfhydryl group of cysteine via sulfenylation, whereas excess iodoacetamide was reported to alkylate cysteine, methionine, lysine, and histidine residues (Fruchter *et al.*, 1967; Kruger *et al.*, 2005). Blocking Cys360 with MMTS or blocking cysteine and methionine residues with excess iodoacetamide from (*A. niger*) rMscDyP1 had no effect on the enzyme activity, whereas (*E. coli*) rMscDyP1 was inhibited by 40% following treatment with MMTS or IAA (Figure 40).

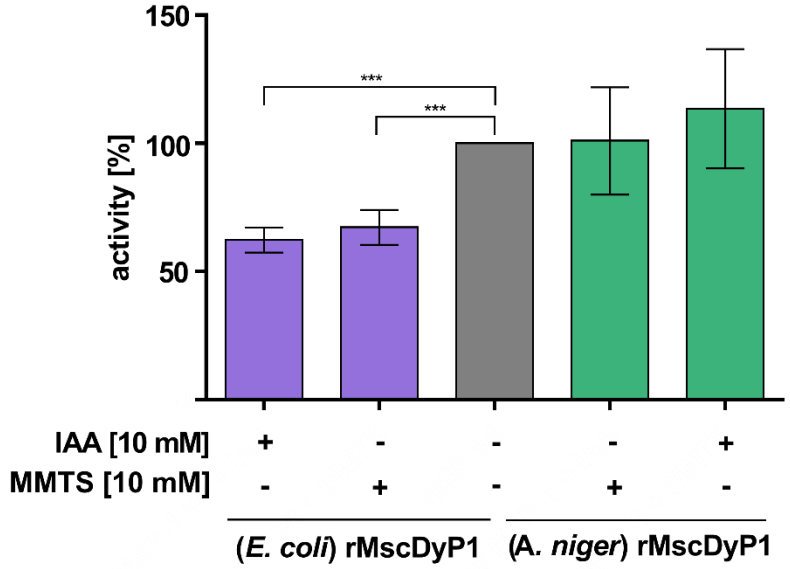

Figure 40: Blocking the sulfur-containing amino acids of MscDyP1

Mean values ± SD of at least three independent experiments with at least three reproductions. ***p < 0.001 Dunnet's multiple comparisons test after One-Way ANOVA. IAA: iodoacetamide, MMTS: methyl methanethiosulfonate.

5 DISCUSSION

5.1 PfalMAT

Previous mass spectrometric analyses of the *S*-glutathionylome and *S*-nitrosylome of *P. falciparum* identified PfalMAT as a potential target of these post-translational modifications in the parasite cell lysate. This suggested a potential role for these redox modifications in regulating of the PfalMAT activity. Furthermore, similar approaches indicated an interaction of PfalMAT with the plasmodial thiol disulfide reductases PfTrx1, PfGrx, and PfPlrx. The aim of this dissertation was to characterize the interaction of PfalMAT with these redox partners in detail and to identify the target sites of the thiol modifications *S*-glutathionylation and *S*-nitrosylation as well as their conformational and catalytic consequences for PfalMAT.

5.1.1 Homology model of PfalMAT

Chemical modifications of MAT cysteine thiols and site-directed mutagenesis studies pointed to a role of cysteines in the activity and oligomerization of MATs (Pajares *et al.*, 1991; Mingorance *et al.*, 1996). Therefore, their contribution to the oligomerization and activity of PfalMAT had been investigated here. PfalMAT contains eight cysteines. However, the homology model using ChMAT and hMATII as templates indicated that only two intermolecular disulfide bridges capable of mediating monomer-monomer interactions are possible, namely between Cys52 and Cys52' and between Cys187 and Cys187' (Figure 9). Furthermore, these residues, as well as Cys113, are solvent accessible and hence potential targets of redox-based modifications. They were therefore selected for further investigation.
Cys52 and Cys187 are not conserved in rlMAT, cMAT, or human homologs, but Cys52 is present in ChMAT. Cys187 is located on top of a loop connecting two beta-barrel strands. This loop is a typical structure among MATs; however, in PfalMAT this loop contains an insertion along with Cys187. Furthermore, the loop contains possible hinges, Gly185 and Gly189, which allow the intermolecular disulfide between Cys187 and Cys187' to open and to close. Cys113 is located at the beginning of the conserved flexible loop above the active site and corresponds to Cys121 of rlMAT, which has been shown to be *S*-nitrosylated (Avila *et al.*, 1997). This loop is involved in binding the adenine ring of the substrate ATP and can adapt two conformations (Taylor *et al.*, 2002). Structures of homologous MAT with bound substrates, e.g. SAM, ATP analogs, or L-methionine (1p7I, 1rg9, 4odj), show an ordered helical conformation of this loop (Taylor *et al.*, 2002; Taylor *et al.*, 2003). In MAT structures without substrates the loop that opens the entrance to the active site is disordered (Komoto *et al.*, 2004).

5.1.2 Oligomerization of PfalMAT

As it had been shown here via gel filtration analysis, recombinant PfalMAT is a homodimer, as previously suggested by a homology model using cMAT as a template (Chiang *et al.*, 1999). In contrast, it was later reported that PfalMAT might be a monomer, however, without published experimental evidence (Muller *et al.*, 2008). The two active sites are located at the dimer interface and consist of residues of both subunits, as shown for cMAT (Takusagawa *et*

al., 1996) and also indicated by our homology model. Therefore, an active monomer is rather unlikely. Most MAT isoenzymes appear as homotetramers (e.g. cMAT, rlMAT, human MATα2) (Markham *et al.*, 2009) composed of two subunits that forms a tight dimer, and a pair of these dimers form a tetrameric enzyme (Takusagawa *et al.*, 1996).
Since it was reported that the MAT oligomerization depends on disulfide bridges (Corrales *et al.*, 1990; Markham *et al.*, 2009), here the influence of selected cysteine residues on the oligomerization behavior of PfalMAT was investigated in detail. These cysteines were conservatively mutated to isosteric serine in order to minimize any effects on protein function and integrity via mutation itself as well as to study the role of these cysteine residues.
The reduction of disulfide bridges with the reducing agent DTT did not affect the oligomerization of PfalMAT. This result alone indicated that PfalMAT dimerization is not mediated exclusively via disulfide bridges. Nevertheless, the PfalMAT variants lacking Cys52 or Cys187 showed a mixture of monomers and dimers in gel filtration experiments. These seemingly contrary results can be explained by numerous additional intersubunit interactions observable in the homology model of PfalMAT. Monomer-monomer contacts are mainly mediated via ionic interactions such as salt bridges. Therefore, reducing and thereby cleaving the two disulfide bridges might not affect dimerization, but a lack of Cys52 or Cys187 might lead to insufficient dimerization. Interestingly, reducing these mutants shifted the monomer/dimer mixture exclusively towards dimers, which might be due to a reduction of false/non-native disulfides in these protein variants, which were solved with DTT to enable a correct folding and conformation. A cysteine corresponding to Cys52 or Cys187 in PfalMAT is present in neither mammalian MAT nor cMAT. However, altered oligomerization behavior after cysteine mutation was likewise reported for cMAT, where a mutation of Cys90 (Ala97 in PfalMAT) shifted the oligomerization state from a tetramer to a mixture of dimers and tetramers (Reczkowski *et al.*, 1995). Furthermore, mutations of Cys69 (Phe61 in PfalMAT), Cys312 (Cys307 in PfalMAT), and Cys377 (Ala374 in PfalMAT) in rlMAT led to a dimerization of the tetramer/dimer mixture in the wildtype (Mingorance *et al.*, 1996). Additionally, folding studies with *L. donovani* MAT showed a proper folding pattern only under reducing conditions. Here, Cys22 (Cys27 in PfalMAT), Cys44 (Cys49 in PfalMAT), and Cys305 (Val310 in PfalMAT) participated in the oligomerization process (Perez-Pertejo *et al.*, 2003).

5.1.3 Enzymatic characterization of PfalMAT

In this dissertation, a sensitive colorimetric endpoint assay detecting the formed amount of orthophosphate by ammonium molybdate was used to monitor PfalMAT activity. This assay was previously developed for glutamine synthetase (Gawronski *et al.*, 2004). It is non-radioactive, therefore safer and more time and cost effective, than the methods using radioactive labelling. A similar assay had been used to monitor hMATI/III and rlMATI/III (Gonzalez *et al.*, 2000; Sanchez del Pino *et al.*, 2002). A number of different assay systems had been employed for monitoring MAT activity; the use of radioactive labels following SAM formation is the most widespread method (Markham *et al.*, 1980; Chiang *et al.*, 1999).
The pH profile of PfalMAT revealed a broad pH optimum between 7.5 and 9.0, which was in the range of reported pH optima (pH 6-10) of MATs from other organisms (Pajares *et al.*, 2011). However, the TAPS assay buffer limited the testable pH range, it might actually be

even broader. PfalMAT activity depended on the presence of the monovalent cation K^+ and the divalent cation Mg^{2+}, as shown for other MATs (Takusagawa *et al.*, 1996; Mato *et al.*, 1997). Crystal structures of MAT from different species indicate the presence of two magnesium ions and one potassium ion within the active site (Takusagawa *et al.*, 1996). These cations are essential for catalysis and contribute to stability and substrate binding (Takusagawa *et al.*, 1996; Mato *et al.*, 1997). Mg^{2+} directly interacts with the tripolyphosphate chain of ATP, which might explain the decreasing activity of PfalMAT with decreasing magnesium concentration in the assay. Interestingly, high magnesium concentrations also inhibited PfalMAT. This might be due to a greater ionic strength (Geller *et al.*, 1986). Furthermore, low potassium concentrations inhibited PfalMAT. One potassium ion is located in the intersubunit interface (Takusagawa *et al.*, 1996). It probably does not directly contribute to catalysis, since neither crystallographic, spectroscopic nor mutagenesis data indicated a direct binding to the substrates (McQueney *et al.*, 1995; Pajares *et al.*, 2011), but has been suggested to help assemble the subunits and thus maintain the geometry of the active site, which is located in the intersubunit interface (Takusagawa *et al.*, 1996; Komoto *et al.*, 2004).
The specific activity of recombinant PfalMAT is in a similar order of magnitude as the activity of recombinant *L. infantum* MAT (Reguera *et al.*, 2002) and *Bacillus subtilis* MAT (Kamarthapu *et al.*, 2008). However, the corresponding enzyme in other human pathogenic organisms such as *E. coli*, *T. brucei* and *M. smegmatis*; and in the archea *P. furiosus, Methanocaldococcus jannaschii,* or *Thermococcus kodakarensis,* and the human counterpart hMATIII exhibit a higher activity than PfalMAT (Table 9).

Table 9: Specific activity of MAT from different species

Species	Specific activity [nmol*min^{-1} *mg^{-1}]	K_M ATP [µM]	K_M Met [µM]	Reference
P. falciparum	379	588	32	this work
L. infantum	200	5,000 (native), 370 (recombinant)	35 n. d.	(Reguera *et al.*, 1999; Reguera *et al.*, 2002)
B. subtilis	362	110	80	(Kamarthapu *et al.*, 2008)
E. coli	2,200	920	260	(Markham *et al.*, 1980)
T. brucei	2,800	1750	150	(Yarlett *et al.*, 1993)
M. smegmatis	1,300	n. d.	96	(Berger *et al.*, 2003)
P. furiosus	4,300	115	31	(Porcelli *et al.*, 2015)
M. janaschii	3,000	350	140	(Graham *et al.*, 2000)
T. kodakarensis	1,950	6,540	310	(Schlesier *et al.*, 2013)
H. sapiens (hMATIII)	1,331	330	168	this work
H. sapiens (erythrocytic)	n.d.	n.d.	2.2	(Oden *et al.*, 1983)
H. sapiens (lymphocytic)	n.d.	31	3.3	(Kotb *et al.*, 1985)

n.d.: not determined

Although the same assay reagents were used in order to determine MAT activity of different organisms, the assay systems varied in terms of the detection method used, ranging from spectrophotometric measurements and HPLC based methods to scintillation detection (Markham *et al.,* 1980; Chamberlin *et al.,* 2000; Berger *et al.,* 2003). Therefore, the published specific activity of MAT of different organisms is difficult to compare, and inter-species differences in MAT activity would require a comparison within one assay system. However, PfalMAT and hMATIII activity were determined using the ammonium molybdate-based assay within this dissertation, thereby allowing a direct comparison.

The specific activity of hMATIII obtained under assay conditions in this dissertation was by a factor of 30-100 higher than the specific activity reported in the literature (12.02 to 39.84 $nmol*min^{-1}*mg^{-1}$, (Chamberlin *et al.*, 1997; Chamberlin *et al.*, 2000). This might be explained by the different assay systems that were used. Chamberlin *et al.* measured the activity using radioactive labelled L-methionine in order to determine SAM synthesis (Chamberlin *et al.*, 2000), whereas the tripolyphosphatase activity of hMATIII was monitored here using the ammonium molybdate assay. Therefore, the results are hardly comparable. However, the K_M for L-methionine of hMATIII that was determined here (168±23 µM) was in a similar range of the one previously reported (220 µM) (Chamberlin *et al.*, 2000).

As shown for most other organisms (Table 9) PfalMAT exhibited a higher affinity towards L-methionine than towards ATP. The physiological concentration of L-methionine is 430 ± 290 µM; the intracellular ATP concentration is in a low millimolar range (1-3 mM) as reported for saponin-isolated *P. falciparum* parasites (van Schalkwyk *et al.*, 2008; Teng *et al.*, 2009). Therefore, the K_M values determined for both substrates of PfalMAT, which were lower than the reported cellular concentrations, suggest substrate saturation of PfalMAT under physiological conditions.

Interestingly, deleting Cys113 increased the activity of PfalMAT and its affinity to the substrate ATP. The homology model of PfalMAT indicated that Cys113 is located on the "gate" loop above the active site. The lack of Cys113 might result in conformational changes to this loop, favoring ATP binding since this loop is important for ATP binding (Deigner *et al.*, 1995). Deleting Cys187 had no effect on enzymatic activity, whereas the affinity and turnover of ATP was increased. This matches the homology model well, showing that Cys187 is structurally connected to residues participating in ATP binding, i.e. via a possible shift in the affiliated β-strand, which is connected to the active site residue Lys174. Likewise, Cys52 mutation decreased substrate affinity, which might be due to conformational changes affecting substrate binding, since it is located in the intersubunit interface between both active sites. In the future it might be worth testing the effect on the substrate binding for these PfalMAT variants in comparison to the wildtype with additional methods, e.g. surface plasmon resonance (SPR), with PfalMAT immobilized on a sensor chip and ATP or L-methionine used as an analyte.

5.1.4 Inhibition of PfalMAT

Even if only weakly, PfalMAT had been shown to be allosterically regulated by SAM in a non-competitive manner with L-methionine (Ki 0.7 ± 0.2 mM with L-methionine) and uncompetitively with ATP (Ki of 3.6 ± 0.4 mM). This indicated that SAM does not bind directly to the ATP binding site of PfalMAT, but can only bind to the enzyme-ATP complex.

Thus, according to the kinetic data, SAM can bind both to the enzyme without methionine and to the enzyme-methionine complex, but not to the enzyme without ATP. This suggests that ATP leads to a conformational change that allows SAM binding, while SAM binds independently from L-methionine. The same feedback inhibition pattern were observed for MAT from human lymphocytes (Kotb *et al.*, 1985), whereas for human erythrocytic MAT, an uncompetitive inhibition by SAM with respect to L-methionine was observed (Oden *et al.*, 1983). SAM competively inhibits *L. infantum* MAT to ATP and non-competitively towards L-methionine (Perez-Pertejo *et al.*, 2003), which was also observed for cMAT (Markham *et al.*, 1983). SAM uncompetively inhibits MAT from *Saccharomyces cerevisiae* towards both substrates ATP and L-methionine (Greene, 1969). Therefore, there appear to be different binding modes and different regulatory mechanisms for feedback inhibition by SAM. The fine tuning of this regulation is not yet fully understood.

Likewise, other parasitic MATs, e.g. from *T. brucei* (K_i 0.24 mM, (Yarlett *et al.*, 1993)) and *L. infantum* (K_i 1.5 mM, (Perez-Pertejo *et al.*, 2003)) , are weakly inhibited by SAM in contrast to other organisms showing K_i values in the micromolar range (Oden *et al.*, 1983; Geller *et al.*, 1986). The weak inhibition of PfalMAT suggests that SAM synthesis might be regulated *in vivo* on a transcriptional level rather than protein level via enzymatic activity. This is reasonable because SAM synthesis efforts a high amount of energy (ATP). Since SAM is especially needed as a polyamine precursor for rapidly reproducing, fast-growing cells, necessiating a high amount of energy, a tight regulation of SAM synthesis according to the temporal demands of the cell is necessary.

Chiang *et al.* tested the classic MAT inhibitor cycloleucine, an amino acid analog, against PfalMAT, and it also showed weak inhibition (K_i 17 mM) (Chiang *et al.*, 1999). However, cycloleucin generally inhibits MATs in a millimolar range (0.2-17 mM) (Lombardini *et al.*, 1983; Yarlett *et al.*, 1993). Nevertheless, the promiscuous metabolic roles of SAM encouraged the search for potent MAT inhibitors. The most potent reported isozyme-selective MAT inhibitors include intermediate analogs, e.g. diimidotriphosphate (K_i 2 nM, (Reczkowski *et al.*, 1999)) and substrate analogs, such as the methionine analog inhibitor L-2-amino-4-methyl-cis-but-3-enoic acid (K_i 5.7-21 µM, (Sufrin *et al.*, 1993)). The later one inhibits *T. brucei* MAT *in vivo* (Goldberg *et al.*, 1998). However, these compounds are synthezised via complex synthetic routes that limit their therapeutic potential. Therefore, further selective bioavailable MAT inhibitors are required.

For this purpose, PfalMAT was screened against the Open Access Malaria Box in a master thesis (Gehr, 2014). This inhibitor library contains 200 drug-like and 200 probe-like, diverse antimalarial compounds active against blood stage *Plasmodium* parasites (Spangenberg *et al.*, 2013). PfalMAT (62 µM) was screened in the ammonium molybdate assay with ATP and L-methionine at K_M concentrations against the Malaria Box at a final concentration of 1 mM. None of the 400 tested compounds inhibited PfalMAT at pharmacological concentrations. Therefore, none of the compounds was investigated further. However, the ammonium molybdate assay monitors tripolyphosphatase activity of PfalMAT; therefore, the screen only provided a limited view of PfalMAT inhibition by compounds from the Malaria Box. For example, active site mutants of rlMAT (D180G, K182G, F251G, and F251D) nearly incapable of SAM synthesis still retained tripolyphosphatase activity, suggesting that both reactions occur at different areas of the active site (Gonzalez *et al.*, 2000). Thus, inhibitors binding to

the catalytic site of SAM synthesis might not have been detected using the ammonium molybdate assay used here. A secondary assay with a divergent detection method that determines the SAM synthesis activity of PfalMAT, e.g. via radioactively labelled L-methionine or via an HPLC-based assay, might identify potential inhibitors of PfalMAT that were not detected with the ammonium molybdate based assay.

5.1.5 Redox regulatory processes affecting PfalMAT

It was previously shown that PfalMAT interacts with the plasmodial thiol disulfide reductases PfTrx1, PfGrx, and PfPlrx (Sturm *et al.*, 2009). However, it has been shown here that the effect size of these oxidoreductases on PfalMAT activity differs. While PfGrx had no major effects, PfTrx1 and Plrx potently increased PfalMAT activity, even at low molecular ratios at subcellular concentrations. PfTrx1 is present at a concentration of 10 µM and mainly in its reduced form due to the cytosolic reducing milieu. This indicates that PfTrx1 and PfPlrx likely regulate PfalMAT under physiological concentrations *in vivo*. Since the strongest activation was observed upon addition of PfTrx1, the interaction of PfalMAT with this redoxin was studied in more detail. PfTrx1 could increase the activity of each of the three cysteine deletion mutants. However, the extent of this activation was weaker for PfalMAT^{C52S} and PfalMAT^{C113S} than for PfalMAT, indicating that both residues contribute to the interaction of PfalMAT with PfTrx1. During these experiments it was observed that partly oxidized PfalMAT^{C187S} was barely active. Interestingly, PfTrx1 completely restored its activity. This suggests that Cys187 is somehow involved in the activity, probably by contributing to the necessary conformation. This is consistent with the results of the oligomerization studies, where a mixture of dimers and oligomers was observed for PfalMAT^{C187S}, when it was not pre-reduced, which was shifted to a dimeric state upon reduction with DTT. The presence of dimers within this mixture might explain the residual activity of ~20% of PfalMAT^{C187S} before reduction with PfTrx1. This suggests the presence of wrong, non-native disulfides in PfalMAT^{C187S} that negatively affected the activity, which could be cleaved upon reduction.
Furthermore, another plasmodial enzyme, ornithine aminotransferase (PfOAT), has been shown to be regulated by PfTrx1, PfGrx, and PfPlrx (Jortzik *et al.*, 2010). Similar to PfalMAT, PfOAT was activated by PfTrx1 and even though to a lesser extent by PfPlrx, whereas PfGrx did not affect the enzymatic activity. It has been experimentally validated that the interaction between PfOAT and PfTrx1 is mediated covalently via a disulfide bond between both proteins, whereas PfGrx bound unspecifically to PfOAT (Jortzik *et al.*, 2010). Therefore, it might be worth testing the interaction of PfalMAT and the cysteine mutants with PfTrx1 using surface plasmone resonance (SPR) or co-crystallization experiments to validate the binding mode. OAT converts ornithine, which presents another precursor for the polyamine synthesis beside dcSAM, to glutamate-5-semialdehyde and glutamate. Therefore, increasing activity of PfOAT by PfTrx1 might impair polyamine synthesis, whereas activation of PfalMAT by PfTrx1 likely promotes polyamine synthesis by providing the precursor dcSAM. This strengthen the hypothesis of a redox regulation of enzymes involved in polymamine synthesis by PfTrx1 in *Plasmodium*. An upregulation of the polyamine synthesis may favor proliferation and growth of the parasite and might be advantageous for *Plasmodium*. Nevertheless, this hypothetical differential regulation of the pathway by PfTrx1 raises the question of the *in vivo* relevance, since both result were obtained *in vitro* with

purified enzymes. Increasing OAT mRNA and protein levels decrease cellular polyamine levels in Caco-2 intestinal cells (Dekaney *et al.*, 2008). *Mat2A* silenced colon cancer cells exhibit reduced levels of the polyamine putrescine (Tomasi *et al.*, 2013). However, the regulatory role of PfTrx1 *in vivo* should be addressed in the future.

MAT from different organisms are redox regulated (Pajares *et al.*, 1992; Martinez-Chantar *et al.*, 1996; Avila *et al.*, 1997), even though, evidence for a direct involvement of cysteines in catalysis is missing. Purified rlMATI/III was inactivated dose-dependently by H_2O_2 and his inactivation was reversible in the presence of GSH (Sanchez-Gongora *et al.*, 1997). Hydrogen peroxide treatment of hamster ovary CHO cells overexpressing rlMATI/III induced enhanced cell death compared to wildtype CHO cells. Moreover, the rlMATI/III overexpressing CHO cells did not show altered MAT protein levels compared to the wildtype but a reduced MAT activity (Sanchez-Gongora *et al.*, 1996). *In vivo* studies with rats showed that drug-induced changes in GSH levels dcreased MATI/III activity (Corrales *et al.*, 1991). These effects were neither mediated by a change in mRNA nor protein levels, but by regulation of the enzymatic activity.

2.3.5.1 Protein-*S*-glutathionylation of PfalMAT

Protein-*S*-glutathionylation was shown to regulate activity by activating or inhibiting numerous enzymes via *S*-glutathionylation of structurally or functionally critical cysteines. Phosphofructokinase (Yoshitake *et al.*, 1994), protein tyrosine phosphatase-1B (Barrett *et al.*, 1999), carbonic anhydrase III (Cabiscol *et al.*, 1996), and NF-κB (Pineda-Molina *et al.*, 2001) are reversibly inactivated by protein-*S*-glutathionylation, whereas other enzymes, e.g. microsomal glutathione-*S*-transferase (Dafre *et al.*, 1996), and matrix metalloproteinase (Okamoto *et al.*, 2001), are activated upon glutathionylation.

Likewise, PfalMAT was previously identified as a member of *P. falciparum S*-glutathionylationylome (Kehr *et al.*, 2011). Indeed, protein-*S*-glutathionylation of PfalMAT resulted in a 50% loss of activity. Even low concentrations of GSSG (e.g. 100 µM) inhibited enzymatic activity, suggesting that protein-*S*-glutathionylation likely occurs *in vivo*.

The inhibition of PfalMAT after adding GSSG was based on formation of mixed disulfides with GSH and the formation of intrasubunit disulfides as shown for rlMAT (Pajares *et al.*, 1992), or wrong intersubunit interactions leading to the formation of higher molecular weight oligomers. Protein-*S*-glutahionylation via formation of mixed-disulfides is suggested to be restricted to GSH, whether reaction with GSSG rather leads to a thiol-disulfide exchange (Priora *et al.*, 2010). Western blots, using an anti-glutathione antibody clearly demonstrated the formation of mixed disulfides between PfalMAT and glutathione in the presence of GSSG. Nevertheless, formation of mixed disulfides between PfalMAT and GSSG is unlikely based on the redox potential of cysteines and the slow reaction rate. Furthermore, this reaction would lead to formation of GSH which, taken the high cellular GSH concentration of 1-10 mM into account, would be kinetically as well as thermodynamically unfavourable (Priora *et al.*, 2010). Therefore, treatment of PfalMAT with GSSG rather led to formation of mixed disulfides between PfalMAT and GSH, which might have been present in small portions in the reagent. However, the presence of GSSG in this reaction appeared to be necessary since anti-GSH Western blots using PfalMAT treated with different concentrations of reduced glutathione showed signal intensities equal to the untreated control even with high GSH

concentrations. Furthermore, the plasmodial cytosol represents a highly reducing environment with an estimated glutathione redox potential of -314 (Kasozi *et al.*, 2013). Therefore, the reduced form GSH is predominantly present in the parasitic cytosol and *S*-glutahionylation of PfalMAT is likely to occur under conditions of oxidative stress, where the GSH/GSSG ratio (10,000:1 (Ostergaard *et al.*, 2004)) is shifted towards GSSG, rather than under physiological conditions.

The reduced activity of *S*-glutathionylated PfalMAT was fully restored by PfTrx1 and PfPlrx, whereas PfGrx was not able to deglutathionylate PfalMAT up to a molar ratio between PfalMAT and PfGrx of 1:5. This was consistent with the results for redox regulation of PfalMAT by these redoxins, where PfGrx was less able to activate PfalMAT than PfTrx1 and PfPlrx. This suggests that PfTrx1 and PfPlrx rather than PfGrx regulate PfalMAT activity *in vivo*. All three redoxins are located in the cytosol of the parasite (Kehr *et al.*, 2010). PfalMAT wass likewise suggested to be cytosolic, because it lacks a sequence for nuclear localization, as observed for rat MATI in extrahepatic tissues (Lys340, Lys341, Arg344, Lys393) (Reytor *et al.*, 2009). Likewise to PfalMAT, addition of Trx (0.5 mM) to rlMAT previously incubated with GSSG (0-30 mM) increased the K_i value from 4 mM (rlMAT + GSSG) to 18 mM (rlMAT + GSSG + Trx) (Martinez-Chantar *et al.*, 1996).

Comparing the activity of the cysteine deletion mutants upon *S*-glutathionylation with PfalMAT revealed that Cys113 contributed to the inhibition of PfalMAT with GSSG, since GSSG inhibited the respective mutant less than PfalMAT. While the effect of GSSG on PfalMAT^{C52S} showed no major differences to those on PfalMAT, PfalMAT^{C187S} was more strongly inhibited upon *S*-glutathionylation than PfalMAT. An intresting fact since PfalMAT^{C187S} was also more susceptible to reduction by PfTrx1, as mentioned before. The lack of Cys187 might result in conformational changes, increasing the accessibility and susceptibility of other cysteines e.g. Cys113 to GSSG.

Taken together, these results indicate that neither Cys52 nor Cys187S formed mixed disulfides with GSH in the presence of GSSG, whereas Cys113 contributed at least partially to the *S*-glutathionylation of PfalMAT. However, since even the Cys113 deletion mutant was still inhibited, albeit to a lesser extent than PfalMAT, these results further suggest that at least one more cysteine of PfalMAT can be *S*-glutathionylated. This could be confirmed with Western blot results using an anti-GSH antibody that shows the formation of mixed disulfides between GSH and a cysteine for each of the PfalMAT variants in the presence of GSSG.

Similar to PfalMAT, PfOAT was inhibited upon *S*-glutathionylation (Jortzik *et al.*, 2010). Moreover, the bifunctional *S*-adenosylmethionine decarboxylase/ornithine decarboxylase was identified as a target of protein-*S*-glutathionylation in *Plasmodium* (Kehr *et al.*, 2011), supporting the suggestion that structually or functionally important cysteines are likely protected via *S*-glutathionylation of critical enzymes of the polyamine synthesis pathway under oxidative stress *in vivo* in *P. falciparum*. An inhibition upon *S*-glutathionylation was also observed for rlMAT (Pajares *et al.*, 1992). Here, the effect was suggested to be based on monomerization of rlMAT, but not on the formation of mixed disulfides between rlMAT and GSh in the presence of GSSG (Pajares *et al.*, 1992; Martinez-Chantar *et al.*, 1996). Likewise, *S*-glutathionylation of PfalMAT probably resulted at least partly in monomerization. However, the main effect of *S*-glutathionylation observed with respect to the oligomerization behavior of PfalMAT was the formation of higher molecular weight oligomers. This was probably

based on disulfide bridges being formed. The restored activity and deglutathionylation with DTT or the disulfide reductases PfTrx1 and PfPlrx might be explained by cleavage of these disulfide bonds upon reduction, thereby enabling a correct conformation.

2.3.5.2 Protein-*S*-nitrosylation of PfalMAT

Our group's previous studies have demonstrated that PfalMAT is a target of *S*-nitrosylation by using the physiologically relevant NO donor GSNO (Gehr, 2014; Wang *et al.*, 2014). Interestingly, as with *S*-glutathionylation of PfalMAT, *S*-nitrosylation did not completely abolish PfalMAT activity. Likewise, *S*-nitrosylation only partly inhibited rlMAT, however to a higher extent (~80% inhibition by GSNO) than PfalMAT (~35% inhibition by GSNO) (Ruiz *et al.*, 1998). MAT from *Arabidopsis thaliana* was also inhibited upon *S*-nitrosylation of Cys114 of the SAM1 isoenzyme; however, it is not conserved in PfalMAT. In rlMAT Cys121 was shown to be the target of *S*-nitrosylation, which corresponds to Cys113 in PfalMAT and is located on the flexible loop above the active site (Takusagawa *et al.*, 1996; Sanchez-Gongora *et al.*, 1997; Perez-Mato *et al.*, 1999). Site-directed mutagenesis studies of rat liver MATI/III indicated that the acidic Asp355 and the basic Arg357 and Arg363 in the vicinity of Cys121 are important for deprotonating the cysteine sulfur group and subsequently facilitate *S*-nitrosylation of Cys121 (Perez-Mato *et al.*, 1999). These acidic and basic amino acids localized next to Cys113 are conserved in PfalMAT (Asp352, Arg354, and Gln360, a conservative substitution, respectively). It was suggested that this "gate loop" to the active site adapts a closed conformation to prevent access to the active site upon *S*-nitrosylation of Cys121 (Takusagawa *et al.*, 1996). Moreover, *S*-nitrosylation of rlMAT corresponded to decreased SAM levels *in vivo* (Ruiz *et al.*, 1998). Accordingly, GSNO inhibited the respective mutant, PfalMAT^{C113S}, to a lesser extent than PfalMAT, indicating that this residue indeed mediated *S*-nitrosylation of PfalMAT. However, here it was shown that each of the cysteine deletion mutants was inhibited to a lesser extent than PfalMAT, indicating that Cys52, Cys113, and Cys187 contributed to the *S*-nitrosylation of PfalMAT. Nevertheless, each of these mutants could still be *S*-nitrosylated suggesting that they were not the only targets of *S*-nitrosylation in PfalMAT. Therefore, unlike rlMAT, several cysteines likely regulate PfalMAT activity, including Cys52, Cys113 and Cys187, in response to NO stress.

S-nitrosylation was studied in this dissertation by using the ammonium molybdate assay. Although ascorbate, the reducing agent used within the ammonium molybdate assay, can reverse *S*-nitrosylation (Foster *et al.*, 2009; Huang *et al.*, 2010), this assay was still suitable for studying the effect of nitrosylation on PfalMAT activity, since the PfalMAT reaction was finished before ascorbate was added to the reaction mixture.

Induction of the endogenous NO-production in rats via intraperitoneal injection of bacterial lipopolysaccharides lead to rlMATI/III inhibition, whereas the mRNA and protein levels remained constant (Avila *et al.*, 1997). An NO synthase has not yet been identified in *P. falciparum* (Pajares *et al.*, 1992); however, endogenous NO production was observed in intraerythrocytic *P. falciparum* parasites and in isolated food vacuoles of *P. falciparum* (Pajares *et al.*, 1991). To gain more hints for the *in vivo* relevance it might be worth treating *P. falciparum* parasites with drugs inducing NO stress and subsequently measure the PfalMAT activity in cell lysates e.g by HPLC-based detection of SAM.

5.1.6 Conclusion and outlook

Figure 41 provides an overview of the redox processes affecting PfalMAT activity or structure that were studied during this dissertation and possible affected downstream pathways.

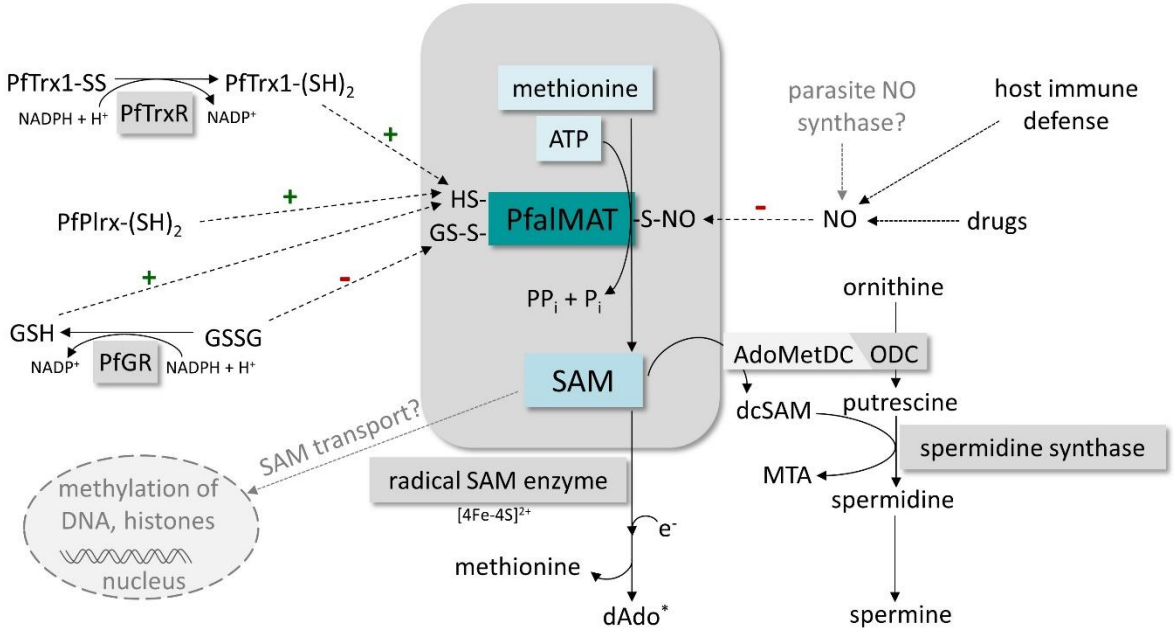

Figure 41: Regulation of SAM metabolism via the redox state of PfalMAT

SAM is a precursor for polyamine synthesis and the generation of radical SAM. It is also the most important methyl group donor involved in the trans-methylation of DNA and proteins and may be transported into the nucleus of *P. falciparum*, although this has not yet been proved (gray dotted arrow). Dashed arrows indicate a regulatory effect by activating (+) or reducing (-) the enzyme activity via cysteine reduction, protein *S*-glutathionylation, or protein *S*-nitrosylation. The origins of NO production are indicated with black dotted arrows. An NO synthase has not yet been identified in *P. falciparum* (Pajares *et al.*, 2013); however, endogenous NO production was observed in intraerythrocytic *P. falciparum* and in isolated food vacuoles (Pajares *et al.*, 1991). Abbreviations: AdoMetDC/ODC bifunctional *S*-adenosylmethionine decarboxylase/ornithine decarboxylase, dAdo* 5'-deoxyadenosyl radical, dcSAM decarboxylated *S*-adenosylmethionine, GR glutathione reductase, GSH reduced glutathione, GSSG glutathione disulfide, MTA 5′-methylthioadenosine, NO nitric oxide, PfalMAT methionine adenosyltransferase of *P. falciparum*, Plrx plasmoredoxin, SAM *S*-adenosylmethionine, Trx1 thioredoxin 1, TrxR thioredoxin reductase.

A regulation of PfalMAT activity and thus SAM synthesis in response to the GSH/GSSG ratio as well as alterations to the redox state of the cell are reasonable with respect to the central position of SAM in multiple vital downstream pathways of *P. falciparum*. An activation of PfalMAT with PfTrx1 and PfPlrx preserves polyamine biosynthesis, which is crucial for this rapidly growing and multiplying parasite, especially under the harsh conditions it has to cope with within its host organisms. Protecting critical cysteine residues of PfalMAT under oxidative and nitrosative stress via *S*-glutathionylation and *S*-nitrosylation and restoring the activity via deglutathionylation with PfTrx1 and PfPlrx maintains the functionality of this important enzyme. It also regulates and protects downstream pathways. Inhibiting PfalMAT under oxidative stress might cause DNA/histone hypomethylation resulting in increased gene expression (Lu *et al.*, 2001; Jani *et al.*, 2009) which might be necessary to counteract increased ROS or RNS levels. However, whether PfalMAT itself is translocated or its product SAM is transported into the nucleus has yet to be verified. Therefore, it would be of great interest to study the subcellular localization of PfalMAT in the parasite, e.g. with confocal

microscopy. Furthermore, it might be interesting to measure the intracellular SAM level after challenging the parasite with redox-active compounds to prove the *in vivo* relevance of PfalMAT redox regulation, *S*-glutathionylation, and *S*-nitrosylation e.g. by HPLC detection of SAM in *P. falciparum* cell lysate after drug treatment.

The results pointed towards an additional cysteine that participates in redox regulation of PfalMAT. Cys52, Cys113, and Cys187 were selected as potential candidates because all of them are located in the dimer interface and are clearly surface exposed (Figure 9 A). However, Cys38 and Cys307 might also be accessible, since they are located on the surface of PfalMAT. Nevertheless, both residues project into the protein core, and thus appeared incapable of interacting with redox-active small molecules and forming an intermolecular disulfide bridge. The other three cysteine residues Cys264, Cys27, and Cys49, are integrated into the protein backbone and buried inside the protein core. They are therefore unable to interact with oxidizing or reducing agents, and none of them has a cysteine in their direct structural neighborhood that could act as an interaction partner for disulfide bond formation. According to the homology model of PfalMAT, Cys187 might be capable of forming an intramolecular disulfide with Cys307. This corresponds to Cys312 of rlMAT, which probably contributes to oligomerization since a site-directed mutagenesis shifted the tetramer/dimer mixture towards a dimeric state of rlMAT (Mingorance *et al.*, 1996). Taking all results into account, it would be interesting to study the contribution of Cys38 and Cys307 to *S*-glutathionylation and *S*-nitrosylation of PfalMAT in order to draw a complete picture of the redox-regulatory modifications affecting PfalMAT. Furthermore, crystallographic data of PfalMAT and the cysteine deletion variants may provide more insights into the contribution of these residues to the regulation of PfalMAT activity and oligomerization.

Although PfalMAT is a promising drug target, the homology model revealed a high structural similarity to its human counterparts that hampers development of selective inhibitors of the plasmodial enzyme. Nevertheless, Cys52 and Cys187 are only present in PfalMAT and therefore might be worth focussing on with respect to rational design of covalent inhibitors selectively targeting PfalMAT. Computational approaches such as virtual screening of compound databases e.g. PubChem, ChEMBL, eMolecules, or ZINC using the homology model of PfalMAT and docking studies, may provide promising molecular scaffolds as starting points for a rational drug design.

5.2 MscDyP1

5.2.1 Crystal structure of MscDyP1

The crystal structure indicated that MscDyP1 is highly glycosylated, which is typical for secreted heme peroxidases (Sugano *et al.*, 2000; Sugano, 2009; Hofrichter *et al.*, 2010). Glycosylation stabilizes the secreted, extracellular proteins within hostile environments (Nie *et al.*, 1999). Furthermore, it was proposed that carbohydrate side chains are not required for activity but rather increase thermostability (Nie *et al.*, 1999) and protect from proteolytic degradation (Hayashi *et al.*, 2012). Likewise, glycosylation of MscDyP1 appeared to play an important role. BMA and NAG at Asn304 were present in each of the four crystal structures, located between the subunits and therefore strongly bound. As a result, the structure strongly implied that dimerization requires glycosylation. NAG is also conserved in BadDyP at this position. However, BadDyP is a monomer (Yoshida *et al.*, 2011). This indicates that further residues contribute to dimerization of MscDyP1. Since only weak intersubunit interactions were present in MscDyP1, the crystal structures also indicated that it is a monomer rather than a dimer, but they allowed for possible dimerization. Moreover, the enzyme biochemically appeared as an active dimer (Zelena *et al.*, 2009). Therefore, MscDyP1 was treated as a dimer based on the intersubunit contacts observed.

The sequence and tertiary structure are highly conserved within DypPrxs. However, the structure of MscDyP1 revealed interesting structural features, including two methionine residues, Met302 and Met305, at the surface of MscDyP1. Hydrophobic residues such as methionine are normally buried inside the protein core. Hydrophobic residues are likewise present in BadDyP in these positions (Leu247 and Ala244, respectively). Met302 and Met305 are located at the possible dimer interface. In fact, Met305 participates in intersubunit interactions and thus facilitates dimerization. Furthermore, both residues were located in a hydrophobic pocket and on top of a helix involved in the formation of the heme-binding pocket, suggesting modification of these amino acids via redox-active agents, for example, and they might affect enzymatic activity.

Remarkably, a single cysteine residue is conserved within MscDyP1, BadDyP, and AauDyP, but has not been previously investigated. The conservation suggests an important function of this residue for either catalytic activity or structural integrity. This cysteine residue is located in a small cavity accessible to small molecules such as H_2O or H_2O_2. H_2O is suggested to form a hydrogen bond to the sulfur atom of Cys360 (distance of 4.2 Å between SG of Cys360 and conserved H_2O). Residues forming this cavity are conserved among these three DypPrx. The thiol group of Cys360 is connected via hydrogen bonds to the oxygen atom of Pro361 backbone (3.7 Å distance of SG of Cys360 to oxygen of P361, Figure 42). Therefore, modifying Cys360 might induce a shift in the main chain at the heme proximal site, including His365, one of the coordination partners of the central heme atom, thereby affecting the geometry of the heme cavity that might inhibit enzyme activity. The cysteine cavity has two possible entrances. In comparison to BadDyP and AauDyP where both entrances are accessible without hindrance, in MscDyP1 one of them is protected by a NAG molecule. The other entrance is exposed to solvent in BadDyP and AauDyP but in MscDyP1 the cysteine cavity is connected via a network of water molecules to the methionine residues in the dimer

interface. This suggests that the second entrance to the Cys cavity is blocked in the dimeric assembly of MscDyP1. However, the weak intersubunit interactions of the MscDyP1 dimer allow a restricted movement of both subunits, which might allow entrance to the Cys cavity. However, further experimental validation would be necessary to prove this movement, e.g. molecular dynamic simulation.

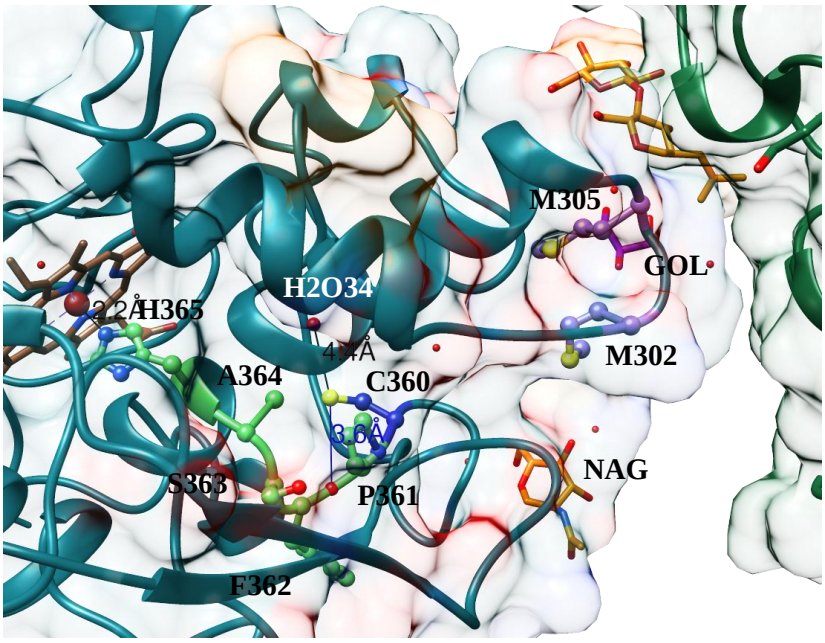

Figure 42: Cys cavity and second H_2O binding site of MscDyP1

The conserved H_2O34, which is probably replaced by H_2O_2 is connected with a distance line to the SG of Cys360 (dark blue). SG is also connected via a hydrogen bond to the oxygen atom of Pro361, which is connected to the main chain (light green) leading to His365. His365 represents the proximal fifth ligand of heme. Thus oxidation of Cys360, which solves the H-bond, might induce a shift in the main chain affecting the activity. Two possible entrances to the Cys cavity could be identified, which are connected via conserved water molecules to the surface. The position of the first entrance is indicated by the protecting NAG molecule; the second entrance is located at the two Met residues (purple). Here, the violet GOL molecule indicates the solvent. The heme molecule is depicted as a brown stick model. Sugar molecules are colored in orange, and residues of the main chain leading to the proximal heme side are highlighted in light green. The second subunit is indicated in green. This figure was prepared using UCSF Chimera.

The role of the three sulfur-containing amino acids Cys360, Met302, and Met305 was studied in greater detail during this dissertation.

5.2.2 Characterization of MscDyP1 variants

The specific activity varied between several enzyme batches, represented by a high standard deviation. This was likely due to impurity of the enzyme and the resulting divergence between the measured protein concentration and the real concentration of (*E. coli*) rMscDyP1 due to contaminations with *E. coli* proteins. Accordingly, the Reinheitszahl value for the enzymes produced in *E. coli* was rather low (~0.4), it should be around three for pure heme proteins (Theorell, 1950). Nevertheless, the activity of both mutants was significantly reduced compared to the unmodified rMscDyP1 produced in *E. coli*, indicating that inhibition is based on the mutation. The impurity of the enzymes necessitated verification of these results in a more specific assay system using β-carotene as a substrate since according to current knowledge MscDyP1 is the only DypPrx capable of degrading β-carotene, and to the current

knowledge *E. coli* lacks β-carotene-degrading enzymes (e.g. carotenoid dehydrogenase, oxidase or desaturase gene has not been deposited in the National Center for Biotechnology Information, (NCBI)). The relative residual activity following mutation was higher than obtained within the ABTS assay. This might be explained by the higher specificity of the β-carotene degradation assay compared to the ABTS assay or a divergent catalysis of both substrates. Since substrate saturation of MscDyP1 with β-carotene could not be accomplished within a measureable absorption range, it was impossible to determine a K_M for β-carotene. The specific activity of (*E. coli*) rMscDyP1 was 100 times lower than that of the respective recombinant enzyme produced in *A. niger* (~110 µmol*min^{-1}*mg^{-1}, personal communication with Katharina Schmidt, Zorn lab, Department of Food Chemistry and Food Biotechnology, Justus Liebig University Giessen), which was used for protein crystallization. Additionally, the K_M value for H_2O_2 of (*E.coli*) rMscDyP1 was 47 times higher than the one reported for the respective enzyme produced in *A. niger* (5 µM) (Liers *et al.*, 2013). Furthermore, a lower pH stability of the enzymes produced in *E. coli* was observed. This might be explained by the lacking glycosylation of (*E. coli*) rMscDyP1 since it was produced in a bacterial expression system. Therefore, overexpression of the mutants in a eukaryotic expression system and comparison with the data obtained for the enzmyes produced in *E. coli* would be of high interest for future studies.

Although MscDyP1 was suggested to be a dimer, no experimental data are available on the recombinant enzyme produced in *A. niger*, that claim that the dimer is the only active form. The enzyme produced in *E. coli* contained a mixture of dimers and higher molecular weight oligomers because gel filtration chromatography was not suitable for clearly separating these fractions. Further purification methods, e.g. based on charge, would therefore be necessary in order to distinguish between dimer activity and higher molecular weight fractions.

A lack of Cys360 decreased enzymatic activity. Since residues that form the Cys cavity also contribute to form the heme-binding pocket, deleting Cys360 likely induced a conformational change in the heme-binding pocket that affected activity. Furthermore, the cysteine deletion mutants showed less affinity to the substrate H_2O_2. This might be explained by the size of the Cys cavity, which is accessible to H_2O_2 but too narrow to allow ABTS access. Nevertheless, it might also be explained by a shift in the mainchain due to the mutation that affects geometry of the heme cavity and thus H_2O_2 binding in the heme distal site. Therefore, deleting the cysteine might affect H_2O_2 binding in the distal or proximal heme site.

In contrast, the methionine double mutant showed decreased activity and affinity to the rate-limiting electron donor ABTS. Both residues are not conserved within DypPrx. Mutating the methionine residues may have induced structural changes that affected activity, e.g. shifting a closely neighboring helix involved in the formation of the heme-binding pocket. They might also present substrate binding sites for bulky substrates, e.g. anthraquinone dyes, since the weak intersubunit interactions of the MscDyP1 dimer allow restricted movement of both subunits, which might allow access to the Cys cavity. However, this requires further investigation. The main function of these surface-exposed hydrophobic residues remains unclear. The observed partial loss of activity of both mutants, compared to (*E. coli*) MscDyP1, might not only be due to a possible functional role of these residues in enzyme activity but might also be a result of the mutation itself. Polar cysteine was mutated into non-polar glycine, which might have affected the structural integrity of the enzyme affecting the

activity, probably by shifting the loop on which Cys360 is located, which projects into the direct heme environment. Furthermore, the non-polar methionine residue was replaced by the basic, electrostatically charged, lysine, which might similarly have induced structural changes affecting enzymatic activity. Additional mutants containing the polar and structurally similar serine instead of Cys360 and the non-polar residues alanine or leucine instead of Met302 and Met305, might provide more hints. However, chemically modifying the sulfur-containing amino acids with excess IAA and MMTS confirmed that these residues contribute to the activity of (*E. coli*) rMscDyP1 since the activity was decreased, albeit to a lesser extent than upon mutation. However, the enzyme produced in *A. niger*, which was glycosylated, was not inhibited. A possible explanation is that glycosylation protects these residues. The first entrance to the cysteine cavity is blocked by NAG, as observed in the crystal structure, and glycosylation contributes to dimerization. Dimerization blocks access for bigger molecules to Cys360 via the second entrance to the cysteine cavity from the methionine side. This might explain why the recombinant enzyme produced in *A. niger* was not inhibited upon adding IAA or MMTS. The loop containing Met302, Met305, and Asn304, which mediates intersubunit contact, is flexible in the *E. coli*-derived recombinant MscDyP1 due to a lack of NAG and BMA, which probably affects dimerization and opens the entrance to the cysteine cavity. This enables MMTS and IAA to access Cys360 in (*E. coli*) rMscDyP1. Treatment with deglycosylases, e.g. N-acetlyglucosaminidase, in order to remove N-linked sugar molecules from (*A. niger*) MscDyP1 would be necessary to prove this hypothesis.

5.2.3 Substrate inhibition of MscDyP1

The mutant variants of MscDyP1 appeared to possess a greater H_2O_2 stability. Hydrogen peroxide-mediated oxidation of Cys360 might induce a shift in the main chain, including His365, one of the coordination partners of the central heme atom, thereby affecting the geometry of the heme cavity and inhibiting enzyme activity. In the bacterial DypPrx AnaPX methionine mutation has been shown to increase H_2O_2 stability compared to the wildtype (Ogola *et al.*, 2010). However, these residues are not conserved in MscDyP1. Non enzymatic methionine oxidation with ROS forming methionine sulfoxide can induce conformational changes (von Eckardstein *et al.*, 1991) and alterations in hydrophobicity (Chao *et al.*, 1997) and can lead to a loss of activity (Brot *et al.*, 1983; Stadtman *et al.*, 2003). Generally, methionine sulfoxide reductases (Msr A and B) can reduce methionine sulfoxides in a thioredoxin-dependent manner (Bigelow *et al.*, 2011). However, Msr is yet to be found in *M. scorodinius*. A comparison to (*A. niger*) rMscDyP1 would be interesting, as would spectral analysis in order to determine possible compound III formation and heme bleaching. H_2O_2 is required for activity, but at a certain threshold concentration, in the submillimolar range, it has an inhibitory effect on MscDyP1 under acidic conditions. The mechanism-based H_2O_2 inhibition of heme peroxidases, the so-called suicide inactivation, has been observed in numerous cases (Valderrama *et al.*, 2002), e.g. HRP (Hiner *et al.*, 2001), lignine peroxidase (Wariishi *et al.*, 1990), manganese peroxidase (Wariishi *et al.*, 1988) and cytochrome c peroxidase (Villegas *et al.*, 2000). If a substrate is absent or if high concentrations of H_2O_2 are present, hydrogen peroxide mediates conversion of compound II of the heme molecule to compound III, a highly reactive peroxy-iron(III)porphyrin free radical (Valderrama *et al.*, 2002).

5.2.4 Proposed catalytic mechanism of MscDyP1

The MscDyP1 structure indicated the presence of two heme accession channels. The first one represents the classic channel towards the active site composed of conserved residues. The second channel towards the heme cavity was proposed based on the MscDyP1 structure. A second, similar channel towards the heme plane is present in BadDyP (Yoshida *et al.*, 2011) and AauDyP (Strittmatter *et al.*, 2015) but has not yet been discussed.
Attempts to co-crystallize MscDyP1 with the substrates bixin or annatto failed. Remarkably, except for crystal additives or solvent components (Strittmatter *et al.*, 2015), none of the published DypPrx crystal structures contained a substrate in the heme cavity of the active site. Therefore, β-carotene and 2,6-dimethoxyphenol were docked here, revealing poses in or near the active site cleft. These poses appeared to present possible binding modes since a water network connected the entrance of this heme accession channel with the heme molecule enabling electron transfer from the substrates to the central heme molecule. β-carotene was chosen for docking studies because MscDyP1 is the only DypPrx known to be capable of degrading β-carotene. 2,6-dimethoxyphenol was selected for molecular docking in order to compare it to the binding mode indicated by the structure of BadDyP, which was solved upon co-crystallization with 2,6-dimethoxyphenol (Yoshida *et al.*, 2012). In this structure 2,6-dimethoxyphenol was exclusively bound to residues on the surface, but not within the classic heme accession channel. However, the presence of a PEG molecule at this position in the crystal structure of MscDyP1 indicated the heme accession channel is wide enough to allow entrance of selected small molecules despite H_2O_2 to reach the direct heme environment. This is supported by docking studies performed for AauDyP with imidazole, which showed a similar pose at the distal heme side (Strittmatter *et al.*, 2015). Interestingly, one of the best-ranked docking poses of 3MD indicated localization within the second heme cavity. The presence of the solvent component glycerol in the crystal structure indicated that small molecules can access this cavity. It contained a conserved water molecule that allows electron transfer to the heme cofactor.
Recently, is was suggested that substrate oxidation in DypPrx occurs at redox-active sites on the protein surface, probably catalyzed by surface radicals (Strittmatter *et al.*, 2013; Linde *et al.*, 2015) as indicated for ascorbic acid (PDB ID 3vxi) and 2,6-dimethoxyphenol (PDB ID 3vxj) (Yoshida *et al.*, 2012). This is reasonable taking the broad substrate specificity of DypPrx into account, which includes large molecules such as lignin, which are unlikely to fit into the heme cavity. Weak substrate binding and oxidation on the surface of MscDyP1 might explain the unsuccessful co-crystallization with the pseudo substrates annatto and bixin.
Substrate oxidation on the surface requires electron transfer from the protein surface to the heme molecule. Accordingly, several long-range electron transfer (LRET) pathways via conserved potentially redox-active tryptophan and tyrosine residues have been proposed (Liers *et al.*, 2013; Strittmatter *et al.*, 2013; Linde *et al.*, 2015), as shown for BadDyP and AauDyP (Liers *et al.*, 2013). Recently, two possible LRET pathways were proposed for MscDyP1 (Figure 43) based on a homology model using the AauDyP crystal structure (Liers, 2014).

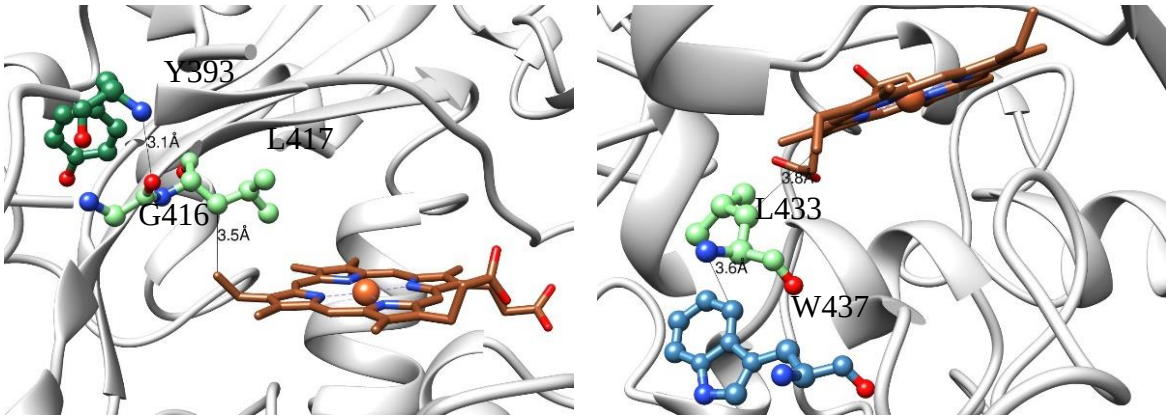

Figure 43: Possible LRET pathways in MscDyP1

Two hypothetical long-range electron transfer (LRET) pathways were proposed by (Liers, 2014), the participating residues are depicted as ball-and-stick models: **A:** via Tyr393, Gly 416, and Leu417 to heme. **B:** via Trp437 and Leu433 to heme. The heme molecule is colored brown, the protein backbone in light gray. This figure was prepared using UCSF Chimera.

The crystal structure of MscDyP1 confirmed the possibility of the first LRET pathway via Tyr393, Gln416, and Leu417 to Cβ of heme ring B since the distances are in a reasonable range (Figure 43 A). Unlike the homology model of MscDyP1 created by Liers *et al.*, the crystal structure of rMscDyP1 contained leucine at position 433 instead of isoleucine. However, this is a synonymous substitution of isosteric amino acids with similar functions and properties. Thus, the second proposed LRET pathway via Trp437 and Leu433 to Cβ heme ring C also appeared to be reasonable (Figure 43 B). Residues participating in these proposed LRET pathways are partly conserved in BadDyP, AauDyP, EglDyP, and MepDyP.

5.2.5 Conclusion and Outloook

In conclusion, the enzyme produced in *E. coli* exhibited structural differences to the enzyme produced in *A. niger* due to the lack of glycosylation. Therefore, overexpression of the mutants in a eukaryotic expression system and comparison with the enzmyes produced in *E. coli* or deglycosylation of (*A. niger*) MscDyP1 would be necessary to prove this hypothesis. Mutating the cysteine and methionine residues resulted in a partial loss of function that might be a result of an impaired structural integrity of the enzyme in response to mutation. The remaining residual activity upon deleting cysteine implied that the single conserved cysteine of MscDyP1 has a structural rather than catalytic function. Furthermore, the crystal structure of MscDyP1 indicated that oxidation of small molecular weight substrates might occur in three possible protein cavities: the classic heme cavity leading to the distal heme site, the second heme accession cavity leading to Cβ of heme ring C, and the Cys cavity at the proximal heme site. Furthermore, substrate oxidation on the protein surface at conserved potentially redox-active tryptophan and tyrosine residues, via LRET pathways to the central heme molecule, is likely. Additional mutational studies with Trp437 and Tyr393 as possible binding sites and might provide further insights into possibility of these LRET pathways. Altogether the crystal structure of MscDyP1 and the performed mutational, kinetic, crystallographic and docking studies indicated that as broad as the substrate versatility of MscDyP1 is, the catalytic properties appear to be equally versatile.

REFERENCES

Adams, P. D., Afonine, P. V., Bunkoczi, G., Chen, V. B., Echols, N., Headd, J. J., *et al.* (2011): The Phenix software for automated determination of macromolecular structures. *Methods* 55(1): 94-106.

Ainsworth, G. C., Sparrow, F. K., Sussman, A. S. (1973): A taxonomic review with keys: Basidiomycetes and lower fungi. The fungi, an advanced treatise. G. C. Ainsworth, Sparrow, F. K., Sussman, A. S, Academic Press, Orlando. 4B.

Assaraf, Y. G., Golenser, J., Spira, D. T. and Bachrach, U. (1984): Polyamine levels and the activity of their biosynthetic enzymes in human erythrocytes infected with the malarial parasite, Plasmodium falciparum. *Biochem J* 222(3): 815-819.

Atamna, H. and Ginsburg, H. (1993): Origin of reactive oxygen species in erythrocytes infected with Plasmodium falciparum. *Mol Biochem Parasitol* 61(2): 231-241.

Avila, M. A., Mingorance, J., Martinez-Chantar, M. L., Casado, M., Martin-Sanz, P., Bosca, L. and Mato, J. M. (1997): Regulation of rat liver S-adenosylmethionine synthetase during septic shock: role of nitric oxide. *Hepatology* 25(2): 391-396.

Ayala, E., Downey, J. S., Mashburn-Warren, L., Senadheera, D. B., Cvitkovitch, D. G. and Goodman, S. D. (2014): A biochemical characterization of the DNA binding activity of the response regulator VicR from Streptococcus mutans. *PLoS One* 9(9): e108027.

Banci, L. (1997): Structural properties of peroxidases. *J Biotechnol* 53(2-3): 253-263.

Barrett, W. C., DeGnore, J. P., Konig, S., Fales, H. M., Keng, Y. F., Zhang, Z. Y., *et al.* (1999): Regulation of PTP1B via glutathionylation of the active site cysteine 215. *Biochemistry* 38(20): 6699-6705.

Bateman, R. L., Rauh, D., Tavshanjian, B. and Shokat, K. M. (2008): Human carbonyl reductase 1 is an S-nitrosoglutathione reductase. *J Biol Chem* 283(51): 35756-35762.

Becker, K., Kanzok, S. M., Iozef, R., Fischer, M., Schirmer, R. H. and Rahlfs, S. (2003): Plasmoredoxin, a novel redox-active protein unique for malarial parasites. *Eur J Biochem* 270(6): 1057-1064.

Becker, K., Tilley, L., Vennerstrom, J. L., Roberts, D., Rogerson, S. and Ginsburg, H. (2004): Oxidative stress in malaria parasite-infected erythrocytes: host-parasite interactions. *Int J Parasitol* 34(2): 163-189.

Beckman, K. B. and Ames, B. N. (1997): Oxidative decay of DNA. *J Biol Chem* 272(32): 19633-19636.

Benhar, M., Forrester, M. T., Hess, D. T. and Stamler, J. S. (2008): Regulated protein denitrosylation by cytosolic and mitochondrial thioredoxins. *Science* 320(5879): 1050-1054.

Berger, B. J. and Knodel, M. H. (2003): Characterisation of methionine adenosyltransferase from Mycobacterium smegmatis and M. tuberculosis. *BMC Microbiol* 3: 12.

Berman, H. M., Westbrook, J., Feng, Z., Gilliland, G., Bhat, T. N., Weissig, H., *et al.* (2000): The Protein Data Bank. *Nucleic Acids Res* 28(1): 235-242.

Bernard, C. (1865): An Introduction to the Study of Experimental Medicine, Henry Schuman, Inc.

Bigelow, D. J. and Squier, T. C. (2011): Thioredoxin-dependent redox regulation of cellular signaling and stress response through reversible oxidation of methionines. *Mol Biosyst* 7(7): 2101-2109.

Biteau, B., Labarre, J. and Toledano, M. B. (2003): ATP-dependent reduction of cysteine-sulphinic acid by S. cerevisiae sulphiredoxin. *Nature* 425(6961): 980-984.

Bitonti, A. J., Dumont, J. A., Bush, T. L., Edwards, M. L., Stemerick, D. M., McCann, P. P. and Sjoerdsma, A. (1989): Bis(benzyl)polyamine analogs inhibit the growth of chloroquine-resistant human malaria parasites (Plasmodium falciparum) in vitro and

in combination with alpha-difluoromethylornithine cure murine malaria. *Proc Natl Acad Sci U S A* 86(2): 651-655.

Bradford, M. M. (1976): A rapid and sensitive method for the quantitation of microgram quantities of protein utilizing the principle of protein-dye binding. *Anal Biochem* 72: 248-254.

Broillet, M. C. (1999): S-nitrosylation of proteins. *Cell Mol Life Sci* 55(8-9): 1036-1042.

Brot, N. and Weissbach, H. (1983): Biochemistry and physiological role of methionine sulfoxide residues in proteins. *Arch Biochem Biophys* 223(1): 271-281.

Buttner, E., Ullrich, R., Strittmatter, E., Piontek, K., Plattner, D. A., Hofrichter, M. and Liers, C. (2015): Oxidation and nitration of mononitrophenols by a DyP-type peroxidase. *Arch Biochem Biophys* 574: 86-92.

Cabiscol, E. and Levine, R. L. (1996): The phosphatase activity of carbonic anhydrase III is reversibly regulated by glutathiolation. *Proc Natl Acad Sci U S A* 93(9): 4170-4174.

CDC (2015): Centers for Disease Control and Prevention. Retrieved July 5th, 2015, from www.cdc.gov/malaria.

Chamberlin, M. E., Ubagai, T., Mudd, S. H., Levy, H. L. and Chou, J. Y. (1997): Dominant inheritance of isolated hypermethioninemia is associated with a mutation in the human methionine adenosyltransferase 1A gene. *Am J Hum Genet* 60(3): 540-546.

Chamberlin, M. E., Ubagai, T., Pao, V. Y., Pearlstein, R. A. and Yang Chou, J. (2000): Structural requirements for catalysis and dimerization of human methionine adenosyltransferase I/III. *Arch Biochem Biophys* 373(1): 56-62.

Chao, C. C., Ma, Y. S. and Stadtman, E. R. (1997): Modification of protein surface hydrophobicity and methionine oxidation by oxidative systems. *Proc Natl Acad Sci U S A* 94(7): 2969-2974.

Chen, Q., Schlichtherle, M. and Wahlgren, M. (2000): Molecular aspects of severe malaria. *Clin Microbiol Rev* 13(3): 439-450.

Chiang, P. K., Chamberlin, M. E., Nicholson, D., Soubes, S., Su, X., Subramanian, G., *et al.* (1999): Molecular characterization of Plasmodium falciparum S-adenosylmethionine synthetase. *Biochem J* 344 Pt 2: 571-576.

Corrales, F., Cabrero, C., Pajares, M. A., Ortiz, P., Martin-Duce, A. and Mato, J. M. (1990): Inactivation and dissociation of S-adenosylmethionine synthetase by modification of sulfhydryl groups and its possible occurrence in cirrhosis. *Hepatology* 11(2): 216-222.

Corrales, F., Ochoa, P., Rivas, C., Martin-Lomas, M., Mato, J. M. and Pajares, M. A. (1991): Inhibition of glutathione synthesis in the liver leads to S-adenosyl-L-methionine synthetase reduction. *Hepatology* 14(3): 528-533.

Cowman, A. F., Berry, D. and Baum, J. (2012): The cellular and molecular basis for malaria parasite invasion of the human red blood cell. *J Cell Biol* 198(6): 961-971.

Cremers, C. M. and Jakob, U. (2013): Oxidant sensing by reversible disulfide bond formation. *J Biol Chem* 288(37): 26489-26496.

Czernik, A. J., Pang, D. T. and Greengard, P. (1987): Amino acid sequences surrounding the cAMP-dependent and calcium/calmodulin-dependent phosphorylation sites in rat and bovine synapsin I. *Proc Natl Acad Sci U S A* 84(21): 7518-7522.

Dafre, A. L., Sies, H. and Akerboom, T. (1996): Protein S-thiolation and regulation of microsomal glutathione transferase activity by the glutathione redox couple. *Arch Biochem Biophys* 332(2): 288-294.

Dalle-Donne, I., Rossi, R., Colombo, G., Giustarini, D. and Milzani, A. (2009): Protein S-glutathionylation: a regulatory device from bacteria to humans. *Trends Biochem Sci* 34(2): 85-96.

Dalle-Donne, I., Rossi, R., Colombo, R., Giustarini, D. and Milzani, A. (2006): Biomarkers of oxidative damage in human disease. *Clin Chem* 52(4): 601-623.

Dalle-Donne, I., Rossi, R., Giustarini, D., Colombo, R. and Milzani, A. (2007): S-glutathionylation in protein redox regulation. *Free Radic Biol Med* 43(6): 883-898.

Deigner, H. P., Mato, J. M. and Pajares, M. A. (1995): Study of the rat liver S-adenosylmethionine synthetase active site with 8-azido ATP. *Biochem J* 308 (Pt 2): 565-571.

Dekaney, C. M., Wu, G., Yin, Y. L. and Jaeger, L. A. (2008): Regulation of ornithine aminotransferase gene expression and activity by all-transretinoic acid in Caco-2 intestinal epithelial cells. *J Nutr Biochem* 19(10): 674-681.

Derakhshan, B., Hao, G. and Gross, S. S. (2007): Balancing reactivity against selectivity: the evolution of protein S-nitrosylation as an effector of cell signaling by nitric oxide. *Cardiovasc Res* 75(2): 210-219.

Eisenkolb, M. (2008): Masterarbeit: Charakterisierung der S-Adenosylmethionin-Synthetase (SAMS) des Malariaerregers *Plasmodium falciparum*. Department of Biochemistry and Molecular Biology, Justus-Liebig University Giessen.

Ekstrom, G. and Ingelman-Sundberg, M. (1989): Rat liver microsomal NADPH-supported oxidase activity and lipid peroxidation dependent on ethanol-inducible cytochrome P-450 (P-450IIE1). *Biochem Pharmacol* 38(8): 1313-1319.

Emsley, P. and Cowtan, K. (2004): Coot: model-building tools for molecular graphics. *Acta Crystallogr D Biol Crystallogr* 60(Pt 12 Pt 1): 2126-2132.

Fawal, N., Li, Q., Savelli, B., Brette, M., Passaia, G., Fabre, M., *et al.* (2013): PeroxiBase: a database for large-scale evolutionary analysis of peroxidases. *Nucleic Acids Res* 41(Database issue): D441-444.

Findlay, V. J., Townsend, D. M., Morris, T. E., Fraser, J. P., He, L. and Tew, K. D. (2006): A novel role for human sulfiredoxin in the reversal of glutathionylation. *Cancer Res* 66(13): 6800-6806.

Finkel, T. and Holbrook, N. J. (2000): Oxidants, oxidative stress and the biology of ageing. *Nature* 408(6809): 239-247.

Fomenko, D. E., Marino, S. M. and Gladyshev, V. N. (2008): Functional diversity of cysteine residues in proteins and unique features of catalytic redox-active cysteines in thiol oxidoreductases. *Mol Cells* 26(3): 228-235.

Fontecave, M., Atta, M. and Mulliez, E. (2004): S-adenosylmethionine: nothing goes to waste. *Trends Biochem Sci* 29(5): 243-249.

Foster, M. W., Hess, D. T. and Stamler, J. S. (2009): Protein S-nitrosylation in health and disease: a current perspective. *Trends Mol Med* 15(9): 391-404.

Fransen, M., Nordgren, M., Wang, B. and Apanasets, O. (2012): Role of peroxisomes in ROS/RNS-metabolism: implications for human disease. *Biochim Biophys Acta* 1822(9): 1363-1373.

Fruchter, R. G. and Crestfield, A. M. (1967): The specific alkylation by iodoacetamide of histidine-12 in the active site of ribonuclease. *J Biol Chem* 242(23): 5807-5812.

Gardner, M. J., Hall, N., Fung, E., White, O., Berriman, M., Hyman, R. W., *et al.* (2002): Genome sequence of the human malaria parasite Plasmodium falciparum. *Nature* 419(6906): 498-511.

Gardner, P. R., Gardner, A. M. and Hallstrom, C. K. (2004): Dioxygen-dependent metabolism of nitric oxide. *Methods Mol Biol* 279: 133-150.

Gawronski, J. D. and Benson, D. R. (2004): Microtiter assay for glutamine synthetase biosynthetic activity using inorganic phosphate detection. *Anal Biochem* 327(1): 114-118.

Gehr, M. (2014): Masterthesis: Redoxregulation der S-Adenosylmethioninsynthetase aus *Plasmodium falciparum*. Department of Biochemistry and Molecular Biology, Justus-Liebig University Giessen.

Geller, A. M., Kotb, M. Y., Jernigan, H. M., Jr. and Kredich, N. M. (1986): Purification and properties of rat lens methionine adenosyltransferase. *Exp Eye Res* 43(6): 997-1008.

Ginsburg, H., Atamna, H., Shalmiev, G., Kanaani, J. and Krugliak, M. (1996): Resistance of glucose-6-phosphate dehydrogenase deficiency to malaria: effects of fava bean hydroxypyrimidine glucosides on Plasmodium falciparum growth in culture and on the phagocytosis of infected cells. *Parasitology* 113 (Pt 1): 7-18.

Goldberg, B., Rattendi, D., Lloyd, D., Sufrin, J. R. and Bacchi, C. J. (1998): Effects of intermediates of methionine metabolism and nucleoside analogs on S-adenosylmethionine transport by Trypanosoma brucei brucei and a drug-resistant Trypanosoma brucei rhodesiense. *Biochem Pharmacol* 56(1): 95-103.

Gonzalez, B., Pajares, M. A., Hermoso, J. A., Alvarez, L., Garrido, F., Sufrin, J. R. and Sanz-Aparicio, J. (2000): The crystal structure of tetrameric methionine adenosyltransferase from rat liver reveals the methionine-binding site. *J Mol Biol* 300(2): 363-375.

Graham, D. E., Bock, C. L., Schalk-Hihi, C., Lu, Z. J. and Markham, G. D. (2000): Identification of a highly diverged class of S-adenosylmethionine synthetases in the archaea. *J Biol Chem* 275(6): 4055-4059.

Greene, R. C. (1969): Kinetic studies of the mechanism of S-adenosylmethionine synthetase from yeast. *Biochemistry* 8(6): 2255-2265.

Greetham, D., Vickerstaff, J., Shenton, D., Perrone, G. G., Dawes, I. W. and Grant, C. M. (2010): Thioredoxins function as deglutathionylase enzymes in the yeast Saccharomyces cerevisiae. *BMC Biochem* 11: 3.

Hara, M. R., Agrawal, N., Kim, S. F., Cascio, M. B., Fujimuro, M., Ozeki, Y., *et al.* (2005): S-nitrosylated GAPDH initiates apoptotic cell death by nuclear translocation following Siah1 binding. *Nat Cell Biol* 7(7): 665-674.

Hayashi, H. and Yamashita, Y. (2012): Role of N-glycosylation in cell surface expression and protection against proteolysis of the intestinal anion exchanger SLC26A3. *Am J Physiol Cell Physiol* 302(5): C781-795.

Hess, D. T., Matsumoto, A., Kim, S. O., Marshall, H. E. and Stamler, J. S. (2005): Protein S-nitrosylation: purview and parameters. *Nat Rev Mol Cell Biol* 6(2): 150-166.

Hiner, A. N., Hernandez-Ruiz, J., Rodriguez-Lopez, J. N., Arnao, M. B., Varon, R., Garcia-Canovas, F. and Acosta, M. (2001): The inactivation of horseradish peroxidase isoenzyme A2 by hydrogen peroxide: an example of partial resistance due to the formation of a stable enzyme intermediate. *J Biol Inorg Chem* 6(5-6): 504-516.

Hoffman, D. R., Marion, D. W., Cornatzer, W. E. and Duerre, J. A. (1980): S-Adenosylmethionine and S-adenosylhomocystein metabolism in isolated rat liver. Effects of L-methionine, L-homocystein, and adenosine. *J Biol Chem* 255(22): 10822-10827.

Hofrichter, M., Ullrich, R., Pecyna, M. J., Liers, C. and Lundell, T. (2010): New and classic families of secreted fungal heme peroxidases. *Appl Microbiol Biotechnol* 87(3): 871-897.

Hoshi, T. and Heinemann, S. (2001): Regulation of cell function by methionine oxidation and reduction. *J Physiol* 531(Pt 1): 1-11.

Huang, B. and Chen, C. (2010): Detection of protein S-nitrosation using irreversible biotinylation procedures (IBP). *Free Radic Biol Med* 49(3): 447-456.

Interpro (2015): Interpro: protein sequence analysis & classification. Retrieved September 5th, 2015, from http://www.ebi.ac.uk/interpro/.

Jacob, C., Battaglia, E., Burkholz, T., Peng, D., Bagrel, D. and Montenarh, M. (2012): Control of oxidative posttranslational cysteine modifications: from intricate chemistry to widespread biological and medical applications. *Chem Res Toxicol* 25(3): 588-604.

Jani, T. S., Gobejishvili, L., Hote, P. T., Barve, A. S., Joshi-Barve, S., Kharebava, G., *et al.* (2009): Inhibition of methionine adenosyltransferase II induces FasL expression, Fas-

DISC formation and caspase-8-dependent apoptotic death in T leukemic cells. *Cell Res* 19(3): 358-369.

Jensen, K. S., Pedersen, J. T., Winther, J. R. and Teilum, K. (2014): The pKa value and accessibility of cysteine residues are key determinants for protein substrate discrimination by glutaredoxin. *Biochemistry* 53(15): 2533-2540.

Jones, D. P. (2008): Radical-free biology of oxidative stress. *Am J Physiol Cell Physiol* 295(4): C849-868.

Jortzik, E., Fritz-Wolf, K., Sturm, N., Hipp, M., Rahlfs, S. and Becker, K. (2010): Redox regulation of Plasmodium falciparum ornithine delta-aminotransferase. *J Mol Biol* 402(2): 445-459.

Jortzik, E., Wang, L. and Becker, K. (2012): Thiol-based posttranslational modifications in parasites. *Antioxid Redox Signal* 17(4): 657-673.

Jourd'heuil, D., Laroux, F. S., Miles, A. M., Wink, D. A. and Grisham, M. B. (1999): Effect of superoxide dismutase on the stability of S-nitrosothiols. *Arch Biochem Biophys* 361(2): 323-330.

Kabsch, W. (2010): Xds. *Acta Crystallogr D Biol Crystallogr* 66(Pt 2): 125-132.

Kamarthapu, V., Rao, K. V., Srinivas, P. N., Reddy, G. B. and Reddy, V. D. (2008): Structural and kinetic properties of Bacillus subtilis S-adenosylmethionine synthetase expressed in Escherichia coli. *Biochim Biophys Acta* 1784(12): 1949-1958.

Kang, E. J., Campbell, R. E., Bastian, E. and Drake, M. A. (2010): Invited review: Annatto usage and bleaching in dairy foods. *J Dairy Sci* 93(9): 3891-3901.

Kanzok, S. M., Schirmer, R. H., Turbachova, I., Iozef, R. and Becker, K. (2000): The thioredoxin system of the malaria parasite Plasmodium falciparum. Glutathione reduction revisited. *J Biol Chem* 275(51): 40180-40186.

Kasozi, D., Mohring, F., Rahlfs, S., Meyer, A. J. and Becker, K. (2013): Real-time imaging of the intracellular glutathione redox potential in the malaria parasite Plasmodium falciparum. *PLoS Pathog* 9(12): e1003782.

Kaur, A., Van, P. T., Busch, C. R., Robinson, C. K., Pan, M., Pang, W. L., *et al.* (2010): Coordination of frontline defense mechanisms under severe oxidative stress. *Mol Syst Biol* 6: 393.

Kehr, S., Jortzik, E., Delahunty, C., Yates, J. R., 3rd, Rahlfs, S. and Becker, K. (2011): Protein S-glutathionylation in malaria parasites. *Antioxid Redox Signal* 15(11): 2855-2865.

Kehr, S., Sturm, N., Rahlfs, S., Przyborski, J. M. and Becker, K. (2010): Compartmentation of redox metabolism in malaria parasites. *PLoS Pathog* 6(12): e1001242.

Kim, S., Wing, S. S. and Ponka, P. (2004): S-nitrosylation of IRP2 regulates its stability via the ubiquitin-proteasome pathway. *Mol Cell Biol* 24(1): 330-337.

Kim, S. J. and Shoda, M. (1999): Purification and characterization of a novel peroxidase from Geotrichum candidum dec 1 involved in decolorization of dyes. *Appl Environ Microbiol* 65(3): 1029-1035.

Knott, A. B. and Bossy-Wetzel, E. (2010): Impact of nitric oxide on metabolism in health and age-related disease. *Diabetes Obes Metab* 12 Suppl 2: 126-133.

Komoto, J., Yamada, T., Takata, Y., Markham, G. D. and Takusagawa, F. (2004): Crystal structure of the S-adenosylmethionine synthetase ternary complex: a novel catalytic mechanism of S-adenosylmethionine synthesis from ATP and Met. *Biochemistry* 43(7): 1821-1831.

Kotb, M. and Kredich, N. M. (1985): S-Adenosylmethionine synthetase from human lymphocytes. Purification and characterization. *J Biol Chem* 260(7): 3923-3930.

Kotb, M., Mudd, S. H., Mato, J. M., Geller, A. M., Kredich, N. M., Chou, J. Y. and Cantoni, G. L. (1997): Consensus nomenclature for the mammalian methionine adenosyltransferase genes and gene products. *Trends Genet* 13(2): 51-52.

Kruger, R., Hung, C. W., Edelson-Averbukh, M. and Lehmann, W. D. (2005): Iodoacetamide-alkylated methionine can mimic neutral loss of phosphoric acid from phosphopeptides as exemplified by nano-electrospray ionization quadrupole time-of-flight parent ion scanning. *Rapid Commun Mass Spectrom* 19(12): 1709-1716.

Laemmli, U. K. (1970): Cleavage of structural proteins during the assembly of the head of bacteriophage T4. *Nature* 227(5259): 680-685.

Lee, C., Lee, S. M., Mukhopadhyay, P., Kim, S. J., Lee, S. C., Ahn, W. S., *et al.* (2004): Redox regulation of OxyR requires specific disulfide bond formation involving a rapid kinetic reaction path. *Nat Struct Mol Biol* 11(12): 1179-1185.

Lewis, D. F. L. (2002): Oxidative stress: the role of cytochromes P450 in oxygen activation. *J ournal of Chemical Technology and Biotechnology* 77: 1095.

Lieber, C. S. and Packer, L. (2002): S-Adenosylmethionine: molecular, biological, and clinical aspects--an introduction. *Am J Clin Nutr* 76(5): 1148S-1150S.

Liers, C., Aranda, E., Strittmatter, E., Piontek, K., Plattner, D., A., Zorn, H., Ullrich, R., Hofrichter, M. (2014): Phenol oxidation by DyP-type peroxidases in comparison to fungal andplant peroxidases. *Journal of Molecular Catalysis B: Enzymatic* 103: 41-46.

Liers, C., Bobeth, C., Pecyna, M., Ullrich, R. and Hofrichter, M. (2010): DyP-like peroxidases of the jelly fungus Auricularia auricula-judae oxidize nonphenolic lignin model compounds and high-redox potential dyes. *Appl Microbiol Biotechnol* 85(6): 1869-1879.

Liers, C., Pecyna, M. J., Kellner, H., Worrich, A., Zorn, H., Steffen, K. T., *et al.* (2013): Substrate oxidation by dye-decolorizing peroxidases (DyPs) from wood- and litter-degrading agaricomycetes compared to other fungal and plant heme-peroxidases. *Appl Microbiol Biotechnol* 97(13): 5839-5849.

Lind, C., Gerdes, R., Hamnell, Y., Schuppe-Koistinen, I., von Lowenhielm, H. B., Holmgren, A. and Cotgreave, I. A. (2002): Identification of S-glutathionylated cellular proteins during oxidative stress and constitutive metabolism by affinity purification and proteomic analysis. *Arch Biochem Biophys* 406(2): 229-240.

Lind, C., Gerdes, R., Schuppe-Koistinen, I. and Cotgreave, I. A. (1998): Studies on the mechanism of oxidative modification of human glyceraldehyde-3-phosphate dehydrogenase by glutathione: catalysis by glutaredoxin. *Biochem Biophys Res Commun* 247(2): 481-486.

Linde, D., Pogni, R., Canellas, M., Lucas, F., Guallar, V., Baratto, M. C., *et al.* (2015): Catalytic surface radical in dye-decolorizing peroxidase: a computational, spectroscopic and site-directed mutagenesis study. *Biochem J* 466(2): 253-262.

Liu, L., Hausladen, A., Zeng, M., Que, L., Heitman, J. and Stamler, J. S. (2001): A metabolic enzyme for S-nitrosothiol conserved from bacteria to humans. *Nature* 410(6827): 490-494.

Liu, X., Miller, M. J., Joshi, M. S., Thomas, D. D. and Lancaster, J. R., Jr. (1998): Accelerated reaction of nitric oxide with O2 within the hydrophobic interior of biological membranes. *Proc Natl Acad Sci U S A* 95(5): 2175-2179.

Loenen, W. A. (2006): S-adenosylmethionine: jack of all trades and master of everything? *Biochem Soc Trans* 34(Pt 2): 330-333.

Lombardini, J. B. and Sufrin, J. R. (1983): Chemotherapeutic potential of methionine analogue inhibitors of tumor-derived methionine adenosyltransferases. *Biochem Pharmacol* 32(3): 489-495.

Lu, S. C. (2000): S-Adenosylmethionine. *Int J Biochem Cell Biol* 32(4): 391-395.

Lu, S. C., Alvarez, L., Huang, Z. Z., Chen, L., An, W., Corrales, F. J., *et al.* (2001): Methionine adenosyltransferase 1A knockout mice are predisposed to liver injury and exhibit increased expression of genes involved in proliferation. *Proc Natl Acad Sci U S A* 98(10): 5560-5565.

Mackintosh, C. L., Beeson, J. G. and Marsh, K. (2004): Clinical features and pathogenesis of severe malaria. *Trends Parasitol* 20(12): 597-603.

Markham, G. D., Hafner, E. W., Tabor, C. W. and Tabor, H. (1980): S-Adenosylmethionine synthetase from Escherichia coli. *J Biol Chem* 255(19): 9082-9092.

Markham, G. D., Hafner, E. W., Tabor, C. W. and Tabor, H. (1983): S-adenosylmethionine synthetase (methionine adenosyltransferase) (Escherichia coli). *Methods Enzymol* 94: 219-222.

Markham, G. D. and Pajares, M. A. (2009): Structure-function relationships in methionine adenosyltransferases. *Cell Mol Life Sci* 66(4): 636-648.

Markham, G. D. and Satishchandran, C. (1988): Identification of the reactive sulfhydryl groups of S-adenosylmethionine synthetase. *J Biol Chem* 263(18): 8666-8670.

Martinez-Chantar, M. L. and Pajares, M. A. (1996): Role of thioltransferases on the modulation of rat liver S-adenosylmethionine synthetase activity by glutathione. *FEBS Lett* 397(2-3): 293-297.

Martinez-Ruiz, A., Villanueva, L., Gonzalez de Orduna, C., Lopez-Ferrer, D., Higueras, M. A., Tarin, C., *et al.* (2005): S-nitrosylation of Hsp90 promotes the inhibition of its ATPase and endothelial nitric oxide synthase regulatory activities. *Proc Natl Acad Sci U S A* 102(24): 8525-8530.

Martinez-Salgado, C., Eleno, N., Tavares, P., Rodriguez-Barbero, A., Garcia-Criado, J., Bolanos, J. P. and Lopez-Novoa, J. M. (2002): Involvement of reactive oxygen species on gentamicin-induced mesangial cell activation. *Kidney Int* 62(5): 1682-1692.

Mato, J. M., Alvarez, L., Ortiz, P. and Pajares, M. A. (1997): S-adenosylmethionine synthesis: molecular mechanisms and clinical implications. *Pharmacol Ther* 73(3): 265-280.

Mato, J. M., Camara, J., Fernandez de Paz, J., Caballeria, L., Coll, S., Caballero, A., *et al.* (1999): S-adenosylmethionine in alcoholic liver cirrhosis: a randomized, placebo-controlled, double-blind, multicenter clinical trial. *J Hepatol* 30(6): 1081-1089.

McCleverty, A. J. (1979): Reactions of nitric oxide coordinated to transition metals. *Chemical Reviews* 79(1): 53-76.

McQueney, M. S. and Markham, G. D. (1995): Investigation of monovalent cation activation of S-adenosylmethionine synthetase using mutagenesis and uranyl inhibition. *J Biol Chem* 270(31): 18277-18284.

Meister, A. and Anderson, M. E. (1983): Glutathione. *Annu Rev Biochem* 52: 711-760.

Merali, S. and Clarkson, A. B., Jr. (2004): S-adenosylmethionine and Pneumocystis. *FEMS Microbiol Lett* 237(2): 179-186.

Messika, E., Golenser, J., Abu-Elheiga, L., Robert-Gero, M., Lederer, E. and Bachrach, U. (1990): Effect of sinefungin on macromolecular biosynthesis and cell cycle of Plasmodium falciparum. *Trop Med Parasitol* 41(3): 273-278.

Mingorance, J., Alvarez, L., Sanchez-Gongora, E., Mato, J. M. and Pajares, M. A. (1996): Site-directed mutagenesis of rat liver S-adenosylmethionine synthetase. Identification of a cysteine residue critical for the oligomeric state. *Biochem J* 315 (Pt 3): 761-766.

Miseta, A. and Csutora, P. (2000): Relationship between the occurrence of cysteine in proteins and the complexity of organisms. *Mol Biol Evol* 17(8): 1232-1239.

Mitchell, A., Chang, H. Y., Daugherty, L., Fraser, M., Hunter, S., Lopez, R., *et al.* (2015): The InterPro protein families database: the classification resource after 15 years. *Nucleic Acids Res* 43(Database issue): D213-221.

MMV (2015): Medicines for Malaria Venture. Retrieved November 20th, 2015, from www.mmv.org.

Mohring, F., Pretzel, J., Jortzik, E. and Becker, K. (2014): The redox systems of Plasmodium falciparum and Plasmodium vivax: comparison, in silico analyses and inhibitor studies. *Curr Med Chem* 21(15): 1728-1756.

Moncada, S., Palmer, R. M. and Higgs, E. A. (1991): Nitric oxide: physiology, pathophysiology, and pharmacology. *Pharmacol Rev* 43(2): 109-142.

Morgan, B., Ezerina, D., Amoako, T. N., Riemer, J., Seedorf, M. and Dick, T. P. (2013): Multiple glutathione disulfide removal pathways mediate cytosolic redox homeostasis. *Nat Chem Biol* 9(2): 119-125.

Mudd, S. H. (1963): Activation of methionine for transmethylation. VI. Enzyme-bound tripolyphosphate as an intermediate in the reaction catalyzed by the methionine-activating enzyme of Baker's yeast. *J Biol Chem* 238: 2156-2163.

Muller, I. B., Das Gupta, R., Luersen, K., Wrenger, C. and Walter, R. D. (2008): Assessing the polyamine metabolism of Plasmodium falciparum as chemotherapeutic target. *Mol Biochem Parasitol* 160(1): 1-7.

Muller, S. (2004): Redox and antioxidant systems of the malaria parasite Plasmodium falciparum. *Mol Microbiol* 53(5): 1291-1305.

Muller, S. (2015): Role and Regulation of Glutathione Metabolism in Plasmodium falciparum. *Molecules* 20(6): 10511-10534.

Mun, K. C., Lee, K. T., Choi, H. J., Jin, K. B., Han, S. Y., Park, S. B., *et al.* (2008): Effects of cyclosporine on the production of the reactive oxygen species in the glial cells. *Transplant Proc* 40(8): 2742-2743.

Murzin A. G., B. S. E., Hubbard T., Chothia C. (1995): SCOP: a structural classification of proteins database for the investigation of sequences and structures. *JOurnal of Molecular Biology* 247: 536-540.

Nagahara, N. (2011): Intermolecular disulfide bond to modulate protein function as a redox-sensing switch. *Amino Acids* 41(1): 59-72.

Nakajima, M., Takeuchi, T. and Morimoto, K. (1996): Determination of 8-hydroxydeoxyguanosine in human cells under oxygen-free conditions. *Carcinogenesis* 17(4): 787-791.

NCBI National Center for Biotechnology Information. Retrieved 29.06.2016, from http://www.ncbi.nlm.nih.gov/.

Nickel, C., Rahlfs, S., Deponte, M., Koncarevic, S. and Becker, K. (2006): Thioredoxin networks in the malarial parasite Plasmodium falciparum. *Antioxid Redox Signal* 8(7-8): 1227-1239.

Nie, G., Reading, N. S. and Aust, S. D. (1999): Relative stability of recombinant versus native peroxidases from Phanerochaete chrysosporium. *Arch Biochem Biophys* 365(2): 328-334.

Oden, K. L. and Clarke, S. (1983): S-adenosyl-L-methionine synthetase from human erythrocytes: role in the regulation of cellular S-adenosylmethionine levels. *Biochemistry* 22(12): 2978-2986.

Ogola, H. J., Hashimoto, N., Miyabe, S., Ashida, H., Ishikawa, T., Shibata, H. and Sawa, Y. (2010): Enhancement of hydrogen peroxide stability of a novel Anabaena sp. DyP-type peroxidase by site-directed mutagenesis of methionine residues. *Appl Microbiol Biotechnol* 87(5): 1727-1736.

Okamoto, T., Akaike, T., Sawa, T., Miyamoto, Y., van der Vliet, A. and Maeda, H. (2001): Activation of matrix metalloproteinases by peroxynitrite-induced protein S-glutathiolation via disulfide S-oxide formation. *J Biol Chem* 276(31): 29596-29602.

Ostergaard, H., Tachibana, C. and Winther, J. R. (2004): Monitoring disulfide bond formation in the eukaryotic cytosol. *J Cell Biol* 166(3): 337-345.

Ostman, A., Frijhoff, J., Sandin, A. and Bohmer, F. D. (2011): Regulation of protein tyrosine phosphatases by reversible oxidation. *J Biochem* 150(4): 345-356.

Pajares, M. A., Alvarez, L. and Perez-Sala, D. (2013): How are mammalian methionine adenosyltransferases regulated in the liver? A focus on redox stress. *FEBS Lett* 587(12): 1711-1716.

Pajares, M. A., Corrales, F. J., Ochoa, P. and Mato, J. M. (1991): The role of cysteine-150 in the structure and activity of rat liver S-adenosyl-L-methionine synthetase. *Biochem J* 274 (Pt 1): 225-229.

Pajares, M. A., Duran, C., Corrales, F., Pliego, M. M. and Mato, J. M. (1992): Modulation of rat liver S-adenosylmethionine synthetase activity by glutathione. *J Biol Chem* 267(25): 17598-17605.

Pajares, M. A. and Markham, G. D. (2011): Methionine adenosyltransferase (s-adenosylmethionine synthetase). *Adv Enzymol Relat Areas Mol Biol* 78: 449-521.

Pal, C. and Bandyopadhyay, U. (2012): Redox-active antiparasitic drugs. *Antioxid Redox Signal* 17(4): 555-582.

Passardi, F., Cosio, C., Penel, C. and Dunand, C. (2005): Peroxidases have more functions than a Swiss army knife. *Plant Cell Rep* 24(5): 255-265.

PATH (2015): MVI PATH Malaria Vaccine Initiative. Retrieved November 20th, 2015, from http://www.malariavaccine.org.

PDB, R. (2015): RSCB PDB Protein Data Bank. Retrieved July 30th, 2015, from http://www.rcsb.org.

Perez-Mato, I., Castro, C., Ruiz, F. A., Corrales, F. J. and Mato, J. M. (1999): Methionine adenosyltransferase S-nitrosylation is regulated by the basic and acidic amino acids surrounding the target thiol. *J Biol Chem* 274(24): 17075-17079.

Perez-Pertejo, Y., Reguera, R. M., Ordonez, D. and Balana-Fouce, R. (2006): Characterization of a methionine adenosyltransferase over-expressing strain in the trypanosomatid Leishmania donovani. *Biochim Biophys Acta* 1760(1): 10-19.

Perez-Pertejo, Y., Reguera, R. M., Villa, H., Garcia-Estrada, C., Balana-Fouce, R., Pajares, M. A. and Ordonez, D. (2003): Leishmania donovani methionine adenosyltransferase. Role of cysteine residues in the recombinant enzyme. *Eur J Biochem* 270(1): 28-35.

PeroxiBase (2015): PeroxiBase: The peroxidase database. Retrieved April 2nd, 2015, from http://peroxibase.toulouse.inra.fr.

Pham-Huy, L. A., He, H. and Pham-Huy, C. (2008): Free radicals, antioxidants in disease and health. *Int J Biomed Sci* 4(2): 89-96.

Pineda-Molina, E., Klatt, P., Vazquez, J., Marina, A., Garcia de Lacoba, M., Perez-Sala, D. and Lamas, S. (2001): Glutathionylation of the p50 subunit of NF-kappaB: a mechanism for redox-induced inhibition of DNA binding. *Biochemistry* 40(47): 14134-14142.

Pop, S. M., Kolarik, R. J. and Ragsdale, S. W. (2004): Regulation of anaerobic dehalorespiration by the transcriptional activator CprK. *J Biol Chem* 279(48): 49910-49918.

Porcelli, M., Ilisso, C. P., De Leo, E. and Cacciapuoti, G. (2015): Biochemical characterization of a thermostable adenosylmethionine synthetase from the archaeon Pyrococcus furiosus with high catalytic power. *Appl Biochem Biotechnol* 175(6): 2916-2933.

Powis, G. and Montfort, W. R. (2001): Properties and biological activities of thioredoxins. *Annu Rev Biophys Biomol Struct* 30: 421-455.

Pretzel, J. (2011): Masterthesis: S-Adenosylmathioninsynthetase aus *Plasmodium falciparum*. Department of Biochemistry and Molecular Biology, Justus-Liebig University Giessen.

Priora, R., Coppo, L., Salzano, S., Di Simplicio, P. and Ghezzi, P. (2010): Measurement of mixed disulfides including glutathionylated proteins. *Methods Enzymol* 473: 149-159.

Puhse, M., Szweda, R. T., Ma, Y., Jeworrek, C., Winter, R. and Zorn, H. (2009): Marasmius scorodonius extracellular dimeric peroxidase - exploring its temperature and pressure stability. *Biochim Biophys Acta* 1794(7): 1091-1098.

Rahlfs, S. and Becker, K. (2001): Thioredoxin peroxidases of the malarial parasite Plasmodium falciparum. *Eur J Biochem* 268(5): 1404-1409.

Rao, R., Xu, D., Thelen, J. J. and Miernyk, J. A. (2013): Circles within circles: crosstalk between protein Ser/Thr/Tyr-phosphorylation and Met oxidation. *BMC Bioinformatics* 14 Suppl 14: S14.

Rao, R. S., Moller, I. M., Thelen, J. J. and Miernyk, J. A. (2015): Convergent signaling pathways--interaction between methionine oxidation and serine/threonine/tyrosine O-phosphorylation. *Cell Stress Chaperones* 20(1): 15-21.

Reczkowski, R. S. and Markham, G. D. (1995): Structural and functional roles of cysteine 90 and cysteine 240 in S-adenosylmethionine synthetase. *J Biol Chem* 270(31): 18484-18490.

Reczkowski, R. S. and Markham, G. D. (1999): Slow binding inhibition of S-adenosylmethionine synthetase by imidophosphate analogues of an intermediate and product. *Biochemistry* 38(28): 9063-9068.

Reguera, R. M., Balana-Fouce, R., Perez-Pertejo, Y., Fernandez, F. J., Garcia-Estrada, C., Cubria, J. C., *et al.* (2002): Cloning expression and characterization of methionine adenosyltransferase in Leishmania infantum promastigotes. *J Biol Chem* 277(5): 3158-3167.

Reguera, R. M., Perez-Pertejo, Y., Ordonez, C., Cubria, J. C., Tekwani, B. L., Balana-Fouce, R. and Ordonez, D. (1999): S-adenosylmethionine synthesis in Leishmania infantum promastigotes. *Cell Biol Int* 23(8): 579-583.

Reynaert, N. L., Ckless, K., Korn, S. H., Vos, N., Guala, A. S., Wouters, E. F., *et al.* (2004): Nitric oxide represses inhibitory kappaB kinase through S-nitrosylation. *Proc Natl Acad Sci U S A* 101(24): 8945-8950.

Reytor, E., Perez-Miguelsanz, J., Alvarez, L., Perez-Sala, D. and Pajares, M. A. (2009): Conformational signals in the C-terminal domain of methionine adenosyltransferase I/III determine its nucleocytoplasmic distribution. *FASEB J* 23(10): 3347-3360.

Roos, G., Foloppe, N. and Messens, J. (2013): Understanding the pK(a) of redox cysteines: the key role of hydrogen bonding. *Antioxid Redox Signal* 18(1): 94-127.

Ruiz-Duenas, F. J., Fernandez, E., Martinez, M. J. and Martinez, A. T. (2011): Pleurotus ostreatus heme peroxidases: an in silico analysis from the genome sequence to the enzyme molecular structure. *C R Biol* 334(11): 795-805.

Ruiz, F., Corrales, F. J., Miqueo, C. and Mato, J. M. (1998): Nitric oxide inactivates rat hepatic methionine adenosyltransferase In vivo by S-nitrosylation. *Hepatology* 28(4): 1051-1057.

Sanchez-Gongora, E., Pastorino, J. G., Alvarez, L., Pajares, M. A., Garcia, C., Vina, J. R., *et al.* (1996): Increased sensitivity to oxidative injury in chinese hamster ovary cells stably transfected with rat liver S-adenosylmethionine synthetase cDNA. *Biochem J* 319 (Pt 3): 767-773.

Sanchez-Gongora, E., Ruiz, F., Mingorance, J., An, W., Corrales, F. J. and Mato, J. M. (1997): Interaction of liver methionine adenosyltransferase with hydroxyl radical. *FASEB J* 11(12): 1013-1019.

Sanchez-Perez, G. F., Bautista, J. M. and Pajares, M. A. (2004): Methionine adenosyltransferase as a useful molecular systematics tool revealed by phylogenetic and structural analyses. *J Mol Biol* 335(3): 693-706.

Sanchez del Pino, M. M., Perez-Mato, I., Sanz, J. M., Mato, J. M. and Corrales, F. J. (2002): Folding of dimeric methionine adenosyltransferase III: identification of two folding intermediates. *J Biol Chem* 277(14): 12061-12066.

Sato, T., Hara, S., Matsui, T., Sazaki, G., Saijo, S., Ganbe, T., *et al.* (2004): A unique dye-decolorizing peroxidase, DyP, from Thanatephorus cucumeris Dec 1: heterologous

expression, crystallization and preliminary X-ray analysis. *Acta Crystallogr D Biol Crystallogr* 60(Pt 1): 149-152.

Scheibner, M., Hulsdau, B., Zelena, K., Nimtz, M., de Boer, L., Berger, R. G. and Zorn, H. (2008): Novel peroxidases of Marasmius scorodonius degrade beta-carotene. *Appl Microbiol Biotechnol* 77(6): 1241-1250.

Schlesier, J., Siegrist, J., Gerhardt, S., Erb, A., Blaesi, S., Richter, M., *et al.* (2013): Structural and functional characterisation of the methionine adenosyltransferase from Thermococcus kodakarensis. *BMC Struct Biol* 13: 22.

Schwede, T., Kopp, J., Guex, N. and Peitsch, M. C. (2003): SWISS-MODEL: An automated protein homology-modeling server. *Nucleic Acids Res* 31(13): 3381-3385.

SCOP (2009): SCOP: Structural Classification of Proteins. Retrieved July 5th, 2015, from http://scop.mrc-lmb.cam.ac.uk/scop/.

Shelton, M. D., Chock, P. B. and Mieyal, J. J. (2005): Glutaredoxin: role in reversible protein s-glutathionylation and regulation of redox signal transduction and protein translocation. *Antioxid Redox Signal* 7(3-4): 348-366.

Sies, H. and Akerboom, T. P. (1984): Glutathione disulfide (GSSG) efflux from cells and tissues. *Methods Enzymol* 105: 445-451.

Simo, G., Herder, S., Cuny, G. and Hoheisel, J. (2010): Identification of subspecies specific genes differentially expressed in procyclic forms of Trypanosoma brucei subspecies. *Infect Genet Evol* 10(2): 229-237.

Singh, R. and Eltis, L. D. (2015): The multihued palette of dye-decolorizing peroxidases. *Arch Biochem Biophys* 574: 56-65.

Sliskovic, I., Raturi, A. and Mutus, B. (2005): Characterization of the S-denitrosation activity of protein disulfide isomerase. *J Biol Chem* 280(10): 8733-8741.

Spangenberg, T., Burrows, J. N., Kowalczyk, P., McDonald, S., Wells, T. N. and Willis, P. (2013): The open access malaria box: a drug discovery catalyst for neglected diseases. *PLoS One* 8(6): e62906.

Stadtman, E. R., Moskovitz, J. and Levine, R. L. (2003): Oxidation of methionine residues of proteins: biological consequences. *Antioxid Redox Signal* 5(5): 577-582.

Stamler, J. S., Toone, E. J., Lipton, S. A. and Sucher, N. J. (1997): (S)NO signals: translocation, regulation, and a consensus motif. *Neuron* 18(5): 691-696.

Stocker, R. and Keaney, J. F., Jr. (2004): Role of oxidative modifications in atherosclerosis. *Physiol Rev* 84(4): 1381-1478.

Strittmatter, E., Liers, C., Ullrich, R., Wachter, S., Hofrichter, M., Plattner, D. A. and Piontek, K. (2013): First crystal structure of a fungal high-redox potential dye-decolorizing peroxidase: substrate interaction sites and long-range electron transfer. *J Biol Chem* 288(6): 4095-4102.

Strittmatter, E., Serrer, K., Liers, C., Ullrich, R., Hofrichter, M., Piontek, K., *et al.* (2015): The toolbox of Auricularia auricula-judae dye-decolorizing peroxidase - Identification of three new potential substrate-interaction sites. *Arch Biochem Biophys* 574: 75-85.

Sturm, N., Jortzik, E., Mailu, B. M., Koncarevic, S., Deponte, M., Forchhammer, K., *et al.* (2009): Identification of proteins targeted by the thioredoxin superfamily in Plasmodium falciparum. *PLoS Pathog* 5(4): e1000383.

Sufrin, J. R., Lombardini, J. B. and Alks, V. (1993): Differential kinetic properties of L-2-amino-4-methylthio-cis-but-3-enoic acid, a methionine analog inhibitor of S-adenosylmethionine synthetase. *Biochim Biophys Acta* 1202(1): 87-91.

Sugano, Y. (2009): DyP-type peroxidases comprise a novel heme peroxidase family. *Cell Mol Life Sci* 66(8): 1387-1403.

Sugano, Y., Muramatsu, R., Ichiyanagi, A., Sato, T. and Shoda, M. (2007): DyP, a unique dye-decolorizing peroxidase, represents a novel heme peroxidase family: ASP171

replaces the distal histidine of classical peroxidases. *J Biol Chem* 282(50): 36652-36658.

Sugano, Y., Nakano, R., Sasaki, K. and Shoda, M. (2000): Efficient heterologous expression in Aspergillus oryzae of a unique dye-decolorizing peroxidase, DyP, of Geotrichum candidum Dec 1. *Appl Environ Microbiol* 66(4): 1754-1758.

Sun, J., Steenbergen, C. and Murphy, E. (2006): S-nitrosylation: NO-related redox signaling to protect against oxidative stress. *Antioxid Redox Signal* 8(9-10): 1693-1705.

Tabor, C. W. and Tabor, H. (1984): Polyamines. *Annu Rev Biochem* 53: 749-790.

Takusagawa, F., Kamitori, S., Misaki, S. and Markham, G. D. (1996): Crystal structure of S-adenosylmethionine synthetase. *J Biol Chem* 271(1): 136-147.

Tamir, S., Burney, S. and Tannenbaum, S. R. (1996): DNA damage by nitric oxide. *Chem Res Toxicol* 9(5): 821-827.

Taylor, J. C. and Markham, G. D. (2003): Conformational dynamics of the active site loop of S-adenosylmethionine synthetase illuminated by site-directed spin labeling. *Arch Biochem Biophys* 415(2): 164-171.

Taylor, J. C., Takusagawa, F. and Markham, G. D. (2002): The active site loop of S-adenosylmethionine synthetase modulates catalytic efficiency. *Biochemistry* 41(30): 9358-9369.

Teng, R., Junankar, P. R., Bubb, W. A., Rae, C., Mercier, P. and Kirk, K. (2009): Metabolite profiling of the intraerythrocytic malaria parasite Plasmodium falciparum by (1)H NMR spectroscopy. *NMR Biomed* 22(3): 292-302.

Theorell, H. (1950): [Research on peroxidases and catalases]. *Rend Ist Sup Sanit* 13(11-12): 876-893.

Thomas, T. and Thomas, T. J. (2001): Polyamines in cell growth and cell death: molecular mechanisms and therapeutic applications. *Cell Mol Life Sci* 58(2): 244-258.

Toledo, J. C., Jr. and Augusto, O. (2012): Connecting the chemical and biological properties of nitric oxide. *Chem Res Toxicol* 25(5): 975-989.

Tomasi, M. L., Ryoo, M., Skay, A., Tomasi, I., Giordano, P., Mato, J. M. and Lu, S. C. (2013): Polyamine and methionine adenosyltransferase 2A crosstalk in human colon and liver cancer. *Exp Cell Res* 319(12): 1902-1911.

Townsend, D. M., Manevich, Y., He, L., Hutchens, S., Pazoles, C. J. and Tew, K. D. (2009): Novel role for glutathione S-transferase pi. Regulator of protein S-Glutathionylation following oxidative and nitrosative stress. *J Biol Chem* 284(1): 436-445.

Trager, W., Tershakovec, M., Chiang, P. K. and Cantoni, G. L. (1980): Plasmodium falciparum: antimalarial activity in culture of sinefungin and other methylation inhibitors. *Exp Parasitol* 50(1): 83-89.

Trujillo, M., Alvarez, M. N., Peluffo, G., Freeman, B. A. and Radi, R. (1998): Xanthine oxidase-mediated decomposition of S-nitrosothiols. *J Biol Chem* 273(14): 7828-7834.

Turrens, J. F., Alexandre, A. and Lehninger, A. L. (1985): Ubisemiquinone is the electron donor for superoxide formation by complex III of heart mitochondria. *Arch Biochem Biophys* 237(2): 408-414.

Turrens, J. F. and Boveris, A. (1980): Generation of superoxide anion by the NADH dehydrogenase of bovine heart mitochondria. *Biochem J* 191(2): 421-427.

Tuteja, R. (2007): Malaria - an overview. *FEBS J* 274(18): 4670-4679.

Valderrama, B., Ayala, M. and Vazquez-Duhalt, R. (2002): Suicide inactivation of peroxidases and the challenge of engineering more robust enzymes. *Chem Biol* 9(5): 555-565.

Valko, M., Leibfritz, D., Moncol, J., Cronin, M. T., Mazur, M. and Telser, J. (2007): Free radicals and antioxidants in normal physiological functions and human disease. *Int J Biochem Cell Biol* 39(1): 44-84.

Valko, M., Rhodes, C. J., Moncol, J., Izakovic, M. and Mazur, M. (2006): Free radicals, metals and antioxidants in oxidative stress-induced cancer. *Chem Biol Interact* 160(1): 1-40.

van Schalkwyk, D. A., Priebe, W. and Saliba, K. J. (2008): The inhibitory effect of 2-halo derivatives of D-glucose on glycolysis and on the proliferation of the human malaria parasite Plasmodium falciparum. *J Pharmacol Exp Ther* 327(2): 511-517.

Villegas, J. A., Mauk, A. G. and Vazquez-Duhalt, R. (2000): A cytochrome c variant resistant to heme degradation by hydrogen peroxide. *Chem Biol* 7(4): 237-244.

von Eckardstein, A., Walter, M., Holz, H., Benninghoven, A. and Assmann, G. (1991): Site-specific methionine sulfoxide formation is the structural basis of chromatographic heterogeneity of apolipoproteins A-I, C-II, and C-III. *J Lipid Res* 32(9): 1465-1476.

Wang, L., Delahunty, C., Prieto, J. H., Rahlfs, S., Jortzik, E., Yates, J. R., 3rd and Becker, K. (2014): Protein S-nitrosylation in Plasmodium falciparum. *Antioxid Redox Signal* 20(18): 2923-2935.

Wani, R., Nagata, A. and Murray, B. W. (2014): Protein redox chemistry: post-translational cysteine modifications that regulate signal transduction and drug pharmacology. *Front Pharmacol* 5: 224.

Wariishi, H., Akileswaran, L. and Gold, M. H. (1988): Manganese peroxidase from the basidiomycete Phanerochaete chrysosporium: spectral characterization of the oxidized states and the catalytic cycle. *Biochemistry* 27(14): 5365-5370.

Wariishi, H. and Gold, M. H. (1990): Lignin peroxidase compound III. Mechanism of formation and decomposition. *J Biol Chem* 265(4): 2070-2077.

WHO (2008): World Malaria Report 2008.

WHO (2010): World Malaria Report 2010.

WHO (2012): World Malaria Report 2012.

WHO (2015): Wold Health Organisation. Retrieved August 14th, 2015, from http://www.who.int.

Wink, D. A. and Mitchell, J. B. (1998): Chemical biology of nitric oxide: Insights into regulatory, cytotoxic, and cytoprotective mechanisms of nitric oxide. *Free Radic Biol Med* 25(4-5): 434-456.

Woo, H. A., Chae, H. Z., Hwang, S. C., Yang, K. S., Kang, S. W., Kim, K. and Rhee, S. G. (2003): Reversing the inactivation of peroxiredoxins caused by cysteine sulfinic acid formation. *Science* 300(5619): 653-656.

Xiong, Y., Uys, J. D., Tew, K. D. and Townsend, D. M. (2011): S-glutathionylation: from molecular mechanisms to health outcomes. *Antioxid Redox Signal* 15(1): 233-270.

Yarlett, N., Garofalo, J., Goldberg, B., Ciminelli, M. A., Ruggiero, V., Sufrin, J. R. and Bacchi, C. J. (1993): S-adenosylmethionine synthetase in bloodstream Trypanosoma brucei. *Biochim Biophys Acta* 1181(1): 68-76.

Yoshida, T. and Sugano, Y. (2015): A structural and functional perspective of DyP-type peroxidase family. *Arch Biochem Biophys* 574: 49-55.

Yoshida, T., Tsuge, H., Hisabori, T. and Sugano, Y. (2012): Crystal structures of dye-decolorizing peroxidase with ascorbic acid and 2,6-dimethoxyphenol. *FEBS Lett* 586(24): 4351-4356.

Yoshida, T., Tsuge, H., Konno, H., Hisabori, T. and Sugano, Y. (2011): The catalytic mechanism of dye-decolorizing peroxidase DyP may require the swinging movement of an aspartic acid residue. *FEBS J* 278(13): 2387-2394.

Yoshitake, S., Nanri, H., Fernando, M. R. and Minakami, S. (1994): Possible differences in the regenerative roles played by thioltransferase and thioredoxin for oxidatively damaged proteins. *J Biochem* 116(1): 42-46.

Zaffagnini, M., Morisse, S., Bedhomme, M., Marchand, C. H., Festa, M., Rouhier, N., *et al.* (2013): Mechanisms of nitrosylation and denitrosylation of cytoplasmic

glyceraldehyde-3-phosphate dehydrogenase from Arabidopsis thaliana. *J Biol Chem* 288(31): 22777-22789.

Zelena, K., Zorn, H., Nimtz, M. and Berger, R. G. (2009): Heterologous expression of the msp2 gene from Marasmius scorodonius. *Arch Microbiol* 191(5): 397-402.

Zorn, H., Langhoff, S., Scheibner, M. and Berger, R. G. (2003): Cleavage of beta,beta-carotene to flavor compounds by fungi. *Appl Microbiol Biotechnol* 62(4): 331-336.

Zubieta, C., Joseph, R., Krishna, S. S., McMullan, D., Kapoor, M., Axelrod, H. L., *et al.* (2007): Identification and structural characterization of heme binding in a novel dye-decolorizing peroxidase, TyrA. *Proteins* 69(2): 234-243.